Multiple-scattering approach with complex potential in the interpretation of electron and photon spectroscopies

2006 J. Phys.: Condens. Matter 18 R175

(http://iopscience.iop.org/0953-8984/18/9/R01)

INSTITUTE OF PHYSICS PUBLISHING JOURNAL OF PHYSICS: CONDENSED MATTER

J. Phys.: Condens. Matter **18** (2006) R175–R230 doi:10.1088/0953-8984/18/9/R01

TOPICAL REVIEW

Multiple-scattering approach with complex potential in the interpretation of electron and photon spectroscopies

D Sébilleau[1], R Gunnella[2], Z-Y Wu[3], S Di Matteo[4] and C R Natoli[4]

[1] Laboratoire de Physique des Atomes, Lasers, Molécules et Surfaces, UMR CNRS-Université 6627, Université de Rennes-1, 35042 Rennes-Cédex, France
[2] Dipartimento di Fisica, Universitá di Camerino, via Madonna delle Carceri, 62032 Camerino, Italy
[3] Beijing Synchrotron Radiation Facility, Institute of High Energy Physics, The Chinese Academy of Sciences, Beijing 100049, People's Republic of China
[4] LNF-INFN, CP 13, via Enrico Fermi, I-00044 Frascati, Italy

E-mail: didier.sebilleau@univ-rennes1.fr

Received 4 July 2005, in final form 23 January 2006
Published 17 February 2006
Online at stacks.iop.org/JPhysCM/18/R175

Abstract

We present a unitary cluster approach to the calculation of several electron and photon spectroscopies, ranging from core and valence level photoelectron diffraction and absorption to electron, Auger and anomalous diffraction. Electron energy loss and Auger–photoelectron coincidence spectroscopies can also be treated in the same frame. This approach is based on multiple-scattering theory with a complex optical potential of the Hedin–Lundqvist type and is valid for all electron kinetic energies. Similarities and differences between these diffraction techniques are examined and cluster size convergence is discussed in connection with the electron mean free path. Applications to selected problems are presented to illustrate the method, both for structural and electronic analysis.

Contents

1. Introduction

We propose in the present paper to develop a unitary cluster approach for a variety of structural techniques, like core and valence state photoelectron diffraction (PED), low and medium energy electron diffraction (LEED/MEED), Auger electron diffraction (AED), diffraction anomalous fine structure (DAFS), resonant elastic x-ray scattering (REXS), Auger photoelectron coincidence spectroscopy (APECS) or electron energy loss spectroscopy (EELS) based on multiple-scattering (MS) theory with effective optical (complex) potential, in analogy with similar developments in the theory of x-ray absorption fine structure (XAFS) [1].

The rather good success of this theory in describing both amplitudes and phases of the fine structure oscillations in absorption spectra ([2–5] and references therein) makes one fairly confident that one can also reach the same level of accuracy in PED, LEED, MEED, AED, APECS, DAFS, REXS and EELS. In fact, all these techniques share with XAFS the fact of having the same continuum wavefunction for the probe electron in the elastic channel either in the intermediate or in the final state. This scattering wavefunction obeys an effective Schrödinger equation with an optical potential that describes the effects of the elimination of the inelastic channels from the diffraction problem.

One of the advantages of this unitary approach is that it makes possible a comparison among the various diffraction techniques and allows the discussion of their similarities and differences in a rather direct way. Another advantage is the use of a complex optical potential of the Hedin–Lundqvist type on the basis of the GW approximation for the electron self-energy [6–8], whose imaginary part is able to describe the extrinsic inelastic losses of the electron in the final continuum state and gives rise to a finite mean free path of the electron probe. Therefore, the amplitude reduction in the elastic diffraction channel consequent to this loss phenomenon is taken automatically into account.

This fact in turn makes a cluster approach to the diffraction problem very natural since only atoms within a sphere with a radius roughly equal to twice the mean free path around the emitter in the case of PED and AED are expected to contribute to the diffraction patterns (we will show how a LEED/MEED process, where there is no emitter, can be reduced to this case). This finding is at variance with what is found in XAS where only atoms within a sphere with

radius equal to the mean free path contribute to the fine oscillations. In an MS picture, such as the one we will adopt in this paper, the difference comes from the fact that in absorption spectra only closed paths that return to the emitter are allowed whereas in all the other cases both closed and open paths are allowed, due to the detection of the final state electron. Apart from this difference, all the above structural techniques share the property of probing the local environment of the emitter due to the final lifetime of the probe.

Actually, it is through this concept (or its equivalent counterpart, the finite mean free path) that it is possible to reconcile the seemingly opposite points of view of the short-range order and the long-range order theories in the description of diffraction processes in periodic systems, as pointed out by Schaich [9] and shown explicitly to all orders of MS by Natoli and Benfatto [10] for the absorption case. Therefore, the use of a complex potential introduces automatically in the calculations a built-in size effect and eliminates the need for adding 'by hand' a mean free path parameter [11, 12]. This correlation between size effect and mean free path will be used to discuss cluster size convergence in relation to mean free path length.

In this review, we shall sketch a derivation of the effective Schrödinger equation (SE) from the many-body formulation of the multichannel scattering problem given by Natoli *et al* [13], along the lines described by Natoli *et al* [1]. In this way we shall derive an expression for the cross-section of PED (or for the decay rate in the case of AED), LEED/MEED, APECS, DAFS, REXS and EELS valid for all kinetic energies of the electron in the continuum final state with no approximation for the geometrical shape of the cluster potential. This approach will allow a realistic description of the surface potential and is currently under progress. However, due to its simplicity, a specialization of the theory to the muffin-tin case will be given and used.

We shall adopt throughout this paper a non-relativistic approach, so that in the expansion of the electron wavefunction we shall use the l, m, σ basis. In atomic calculations this is not a limitation, since relativistic effects can be taken into account by solving explicitly for the upper component of the Dirac equation, along the lines described in [14]. The resulting pseudo-Schrödinger equation (PSE) is closely akin to the Pauli equation, which can be easily solved in the spin–orbit coupled basis j, j_z. The only small price to pay is the modification of the atomic potential appearing in the Dirac equation, as detailed in the reference above. As soon as this is done, relativistic effects can be easily incorporated in the calculation of atomic t-matrices[5] and in the formulation of the MS theory, which can be written without difficulty in the j, j_z basis. Recourse to a mixed basis (spin–orbit coupled for the initial core states, where spin–orbit effects are relevant, and uncoupled for the final states, when spin–orbit effects are negligible) is also possible and has been used. However, the use of the l, m, σ basis in the final state becomes again relevant in presence of spin-polarized potentials, when treating magnetic effects. This is because j is no longer a good quantum number at the atomic level and MS theory becomes a two-channel problem connected by the spin-flip terms of the spin–orbit interaction. Work along this line is in progress by the authors of the present review, which however concerns only non-magnetic effects. In any case, a completely relativistic formulation of MS theory can be found even in textbooks [15], and programs are available to calculate in this approach the electronic properties of matter ([16] and references therein).

Many-particle relativistic effects also play an important role, e.g. in Auger electron emission and core level photoemission, but their inclusion in the respective transition amplitudes is not considered in this review. The emphasis here is rather on how to incorporate realistically diffraction effects in the wavefunction of the continuum electrons and for these electrons relativistic effects are not so important.

[5] Notice that in this approximation the relativistic transition matrix element of an external electromagnetic perturbation reduces to the non-relativistic expression.

The general derivation described above is used for discussing both the low and high energy limits of the theory in the attempt to establish rules for the convergence of the MS series. At the same time we show that the reduction procedure from the many-body formulation to the description of the completely relaxed (elastic) channel can also in principle be applied to the description of any channel, in particular the one describing Kikuchi electrons, for which one can establish an effective Schrödinger equation analogous to the elastic case. Physical considerations can indeed be given whereby the effective potential in this case should be very similar to the one relative to the elastic channel. As a consequence, the diffraction mechanism of these electrons is described by the same theory, thus substantiating the conclusion put forward by Osterwalder *et al* [17]. Applications to selected problems will be presented to illustrate the method, both for structural and electronic analysis.

2. Calculation of cross-sections

2.1. General expression of the cross-section

In this review we are interested in spectroscopies in which the probe particle is an electron, the source of which can be either external to the sample under investigation (as in the case of an electron beam scattering off the sample) or internal (created e.g. by a real or virtual photoemission process). Therefore we shall restrict ourselves to the cases in which the impinging and detected particles are either photons or electrons. For the convenience of the reader and to fix the notations we derive here the general expressions for the cross-sections for such spectroscopies and discuss in the following their interpretation within a unified framework, namely multiple-scattering theory.

We assume that the matter sample (atoms and/or molecules in gaseous or condensed phase) is described by states labelled by $|\varphi\rangle$, with a suitable index to characterize their type. Similarly, we denote by $|\phi\rangle$ the states of a given particle in the incoming beam. The states of the total interacting system (incoming particle + matter sample) are labelled $|\Psi\rangle$. The potential describing the interaction of the incident particles with the sample is denoted by V_I.

If the Hamiltonians of the incoming particle and the matter alone are noted respectively as H_P and H_M, then the total Hamiltonian of the system is

$$H = H_P + H_M + V_I = H_o + V_I$$

where H_o describes the system without interaction. The eigenstates of the unperturbed Hamiltonian H_o are then simply

$$|\Phi\rangle = |\varphi\rangle|\phi\rangle.$$

If V_I is sufficiently 'small', under conditions to be conveniently specified, we can treat it as a perturbation of the system described by H_o. In this case, standard perturbation theory tells us that we can approximate the eigenstates $|\Psi\rangle$ of the total Hamiltonian H in terms of the eigensolutions $|\Phi\rangle$ of the unperturbed Hamiltonian $H_o = H_P + H_M$. These eigensolutions can be written as

$$\begin{aligned} H_o|\Phi_i\rangle &= \mathcal{E}_i|\Phi_i\rangle \qquad \text{with } \mathcal{E}_i = \mathsf{E}_i + E_i \\ H_o|\Phi_f\rangle &= \mathcal{E}_f|\Phi_f\rangle \qquad \text{with } \mathcal{E}_f = \mathsf{E}_f + E_f \end{aligned} \tag{1}$$

E and E are the eigenvalues associated with $|\varphi\rangle$ and $|\phi\rangle$ respectively for the corresponding Hamiltonian. We are interested here in transitions from an initial state $|\Phi_i\rangle$ of H_o to a final state $|\Phi_f\rangle$ of the same Hamiltonian that can result from the action of the interaction term V_I.

From time-dependent perturbation theory [18], we know that the transition probability per unit time from state $|\Phi_i\rangle$ to state $|\Phi_f\rangle$ under the effect of the perturbation V_I is given by

$$W_{i\to f} = \frac{2\pi}{\hbar}\left|\langle\Phi_f|T_I|\Phi_i\rangle\right|^2 \rho(\mathcal{E}_f). \tag{2}$$

Here $\rho(\mathcal{E}_f)$ is the density of final states of the detected particle and T_I is the transition operator associated with the interaction potential V_I. Transition operators are introduced in scattering theory as a convenient way to describe the effect of a given perturbation on the eigenstates of the unperturbed system. Following their usual definition, T_I can be expressed by the relation [19]

$$T_I = V_I + V_I G(\mathcal{E}_i) V_I \tag{3}$$

where $G(\mathcal{E}_i)$ is the resolvent of the total Hamiltonian H at the energy of the initial state (or of the final state as the energy $\mathcal{E}$ of the total system is conserved). This resolvent is defined by

$$G(\mathcal{E}_i) = \lim_{\epsilon\to 0^+} \frac{1}{\mathcal{E}_i - H \pm \mathrm{i}\epsilon}. \tag{4}$$

An infinitesimal imaginary part is introduced in order to impose appropriate boundary conditions when required. The action of $G(\mathcal{E}_i)$ on any eigenstate $|\Psi_n\rangle$ of H gives

$$G(\mathcal{E}_i)|\Psi_n\rangle = \frac{|\Psi_n\rangle}{\mathcal{E}_i - \mathcal{E}_n}. \tag{5}$$

At the lowest order in V_I, the transition operator can be approximated by the perturbation V_I. When inserted in (2), this gives Fermi's golden rule No 2 [18]. To second order in V_I, it can be replaced by

$$T_I \approx V_I + V_I G_o(\mathcal{E}_i) V_I \tag{6}$$

which gives Fermi's golden rule No 1 [20]. $G_o(\mathcal{E}_i)$ is the unperturbed resolvent and is obtained from (4) by replacing H by H_o.

The cross-section is then obtained from (2) by dividing by the flux I_0 of incoming particles.

2.2. *Cross-section for incoming photons*

If we neglect the magnetic terms, the interaction potential describing the interaction of a photon beam with an electron can be written, in the non-relativistic limit, as

$$V_I = \frac{e}{m}\boldsymbol{A}\cdot\boldsymbol{p} + \frac{e^2}{2m}\boldsymbol{A}^2 \tag{7}$$

where $\boldsymbol{p}$ is the electron momentum and $\boldsymbol{A}$ the vector potential of the electromagnetic field, which is given by

$$\boldsymbol{A}(\boldsymbol{r}) = \sum_{\boldsymbol{q},\hat{e}_q} \sqrt{\frac{\hbar}{2\epsilon_0\omega_q\mathcal{V}}}\left[a_{\boldsymbol{q},\hat{e}_q}\mathrm{e}^{\mathrm{i}\boldsymbol{q}\cdot\boldsymbol{r}}\hat{\boldsymbol{e}}_q + a^{\dagger}_{\boldsymbol{q},\hat{e}_q}\mathrm{e}^{-\mathrm{i}\boldsymbol{q}\cdot\boldsymbol{r}}\hat{\boldsymbol{e}}^*_q\right]. \tag{8}$$

Here $a_{\boldsymbol{q},\hat{e}_q}$ is the annihilation operator for photons and $a^{\dagger}_{\boldsymbol{q},\hat{e}_q}$ is the corresponding creation operator. The sum is over the wavevector $\boldsymbol{q}$ and the two polarizations $\hat{\boldsymbol{e}}_q$ of the incoming wave field. $\mathcal{V}$ is the normalization volume. For x-ray radiation, the inverse of q (Å) $= 0.5\times 10^{-3}\hbar\omega_q(eV)$ can be large compared to the extension of the core orbitals involved in the transition. In this case, $\boldsymbol{q}\cdot\boldsymbol{r} \ll 1$ and the exponential can be replaced either by 1 (dipole approximation) or by $1+\mathrm{i}\boldsymbol{q}\cdot\boldsymbol{r}$ (quadrupole approximation).

In order to simplify the notations, we have written equation (7) in the one-electron case. In the more general case of many-electron systems, the term $e/m\boldsymbol{A}\cdot\boldsymbol{p}$ has to be replaced by

$\sum_i q_i/m_i \boldsymbol{p}_i \cdot \boldsymbol{A}$, where the sum runs on all the particles composing the system. In this case the Coulomb term that describes the interaction between the particles in the system is actually part of the unperturbed Hamiltonian H_M and therefore will not appear in the expression of the interaction potential. Due to the $1/m_i$ scaling of the matter–radiation interaction potential, we will restrict ourselves here to the case of electrons, as nucleons will contribute much less. Except for EELS, we shall continue to use for simplicity the one-electron notation for the derivation of the various cross-sections. The extension to the many-body case will then be straightforward.

If we introduce the expression (7) of the interaction potential in (6), we obtain to the second order in e/m

$$T_I^{(2)} = \frac{e}{m}\boldsymbol{A}\cdot\boldsymbol{p} + \left(\frac{e}{m}\right)^2\left[\frac{m}{2}\boldsymbol{A}\cdot\boldsymbol{A} + \boldsymbol{A}\cdot\boldsymbol{p}G_o(\mathcal{E}_i)\boldsymbol{A}\cdot\boldsymbol{p}\right] + \mathrm{O}\left(\frac{e^3}{m^3}\right). \tag{9}$$

The term linear in e/m describes first order processes in which only one photon at a time is created or absorbed, while the second term in $(e/m)^2$ describes second order processes in which two photons are involved, as in photon scattering. Therefore, the transition operator $T_I^{(2)}$ expressed in (9) can describe three kinds of processes: emission, absorption or scattering of photons.

We shall not consider in this work the case of emission but we focus instead on the processes of absorption and scattering of photons, which many spectroscopies we review here rely on. In the case of absorption, if the final state photoelectron is detected, the spectroscopy is called photoemission spectroscopy. One speaks instead of photoabsorption spectroscopy when one counts only the number of absorbed photons per second out of a flux of incident photons. In transmission spectroscopy for example, calling the transmitted and incident photon flux I and I_0, the absorption coefficient as a function of the incident photon energy $\hbar\omega$ is given by $\mu(\hbar\omega) = \ln(I_0/I)$. However, an alternative way to measure the number of absorbed photons is to count the number of holes created in the photoemission process either through the decay products of the excited atoms of the substance under investigation or by counting the total number of emitted photoelectrons. It is then clear that the photoabsorption cross-section is obtained by the photoemission cross-section by integrating over all final state photoelectrons compatible with total energy conservation.

The cross-section $\mathrm{d}\sigma/\mathrm{d}\hat{\boldsymbol{k}}$ for emission of an electron in the element of solid angle around the direction $\hat{\boldsymbol{k}}$ is given by

$$\frac{\mathrm{d}\sigma}{\mathrm{d}\hat{\boldsymbol{k}}} I_0 = \frac{\mathrm{d}W}{\mathrm{d}\hat{\boldsymbol{k}}} \tag{10}$$

where $I_0 = c/\mathcal{V}$ [21] is the incident photon flux and $\mathrm{d}W/\mathrm{d}\hat{\boldsymbol{k}}$ is the transition probability per unit time and solid angle given by equation (2), in which $\rho(E_f)$ is now the density of free final states for an electron ejected along $\hat{\boldsymbol{k}}$ at the energy E_f. This latter is given by the Einstein relation $E_f = \hbar\omega - E_{\mathrm{exc}}$, where E_{exc} is the total excitation energy left in the system under study. Moreover, $|\Phi_i\rangle$ is the system initial state, the tensor product of a photon state $a_{\boldsymbol{q}}^\dagger|0\rangle$ times a matter electronic ground state $|\phi_{\mathrm{g}}^e\rangle$, whereas $|\Phi_f\rangle$ is the product of the photon vacuum state $|0\rangle$ times an electronic final state $|\phi_{\boldsymbol{k}}^-\rangle$, the time-reversed solution of the Schrödinger equation with scattering boundary conditions at infinity. This condition will be better specified later on in section 3.

For the transition operator in the case of one-photon absorption, after replacing the vector potential $\boldsymbol{A}$ by its expression (8), we obtain

$$T_{I,\mathrm{abs}} = \frac{e}{m}\sum_{\boldsymbol{q},\hat{\boldsymbol{e}}_{\boldsymbol{q}}}\sqrt{\frac{\hbar}{2\epsilon_o\omega_{\boldsymbol{q}}\mathcal{V}}}(\hat{\boldsymbol{e}}_{\boldsymbol{q}}\cdot\boldsymbol{p})a_{\boldsymbol{q},\hat{\boldsymbol{e}}_{\boldsymbol{q}}}\mathrm{e}^{\mathrm{i}\boldsymbol{q}\cdot\boldsymbol{r}} \tag{11}$$

so that the photoemission cross-section becomes

$$\frac{\mathrm{d}\sigma}{\mathrm{d}\hat{\boldsymbol{k}}} = 4\pi^2\alpha\frac{\hbar}{m^2\omega_q}\rho(E_f)\left|\langle\phi_{\boldsymbol{k}}^-|\hat{\boldsymbol{e}}_q\cdot\boldsymbol{p}\mathrm{e}^{\mathrm{i}\boldsymbol{q}\cdot\boldsymbol{r}}|\phi_i\rangle\right|^2 \tag{12}$$

where $\alpha = e^2/(4\pi\epsilon_0\hbar c)$ is the fine structure constant, a dimensionless coefficient whose numerical value is $\alpha \sim 1/137$.

Likewise, the photoabsorption cross-section is obtained by dividing the transition probability $W_{i\to f}$ summed over all possible final states consistent with energy conservation by the incoming flux I_0 of photons:

$$\sigma_{\mathrm{abs}} = 4\pi^2\alpha\frac{\hbar}{m^2\omega_q}\sum_f\left|\langle\phi_f|\hat{\boldsymbol{e}}_q\cdot\boldsymbol{p}\mathrm{e}^{\mathrm{i}\boldsymbol{q}\cdot\boldsymbol{r}}|\phi_i\rangle\right|^2\delta(E_i - E_f + \hbar\omega_q). \tag{13}$$

Equations (12) and (13) simplify in the dipole approximation. In this case, the exponential term can be dropped and making use of the relation

$$\langle\phi_n|\hat{\boldsymbol{e}}_q\cdot\boldsymbol{p}|\phi_m\rangle = \mathrm{i}m\omega_q\langle\phi_n|\hat{\boldsymbol{e}}_q\cdot\boldsymbol{r}|\phi_m\rangle$$

we obtain for the photoemission cross-section

$$\frac{\mathrm{d}\sigma}{\mathrm{d}\hat{\mathbf{k}}} = 4\pi^2\alpha\hbar\omega_q\rho(E_f)\left|\langle\phi_{\hat{\boldsymbol{k}}}^-|\hat{\boldsymbol{e}}_q\cdot\boldsymbol{r}|\phi_i\rangle\right|^2 \tag{14}$$

and for the photoabsorption cross-section

$$\sigma_{\mathrm{abs}} = 4\pi^2\alpha\hbar\omega_q\sum_f\left|\langle\phi_f|\hat{\boldsymbol{e}}_q\cdot\boldsymbol{r}|\phi_i\rangle\right|^2\delta(E_i - E_f + \hbar\omega_q) \tag{15}$$

which are the standard formulae in the dipole approximation. The replacement of $\boldsymbol{r}$ by $\sum_i^N \boldsymbol{r}_i$ gives the corresponding N-electron formulae, $|\phi_i\rangle$ and $|\phi_f\rangle$ now being N-electron states.

The density of free photoelectron final states per unit energy and solid angle is easily seen to be

$$\rho(E_f) = \frac{\mathcal{V}}{(2\pi)^3}\frac{\mathrm{d}^3k}{\mathrm{d}E_f\mathrm{d}\hat{\boldsymbol{k}}} = \frac{\mathcal{V}}{(2\pi\hbar)^3}\hbar km. \tag{16}$$

It is customary to incorporate this factor into the normalization of the photoelectron wavefunction passing from a plane wave normalization

$$\int \mathrm{d}\boldsymbol{r}\,\phi_{\boldsymbol{k}}^*(\boldsymbol{r})\phi_{\boldsymbol{k}'}(\boldsymbol{r}) = \frac{(2\pi)^3}{\mathcal{V}}\delta(\boldsymbol{k}-\boldsymbol{k}')$$

to a normalization to one state per unit energy interval

$$\int \mathrm{d}\boldsymbol{r}\,\phi_k^*(\boldsymbol{r})\phi_{k'}(\boldsymbol{r}) = \frac{2m}{\hbar^2}\delta(k^2-k'^2).$$

In fact, calling $\mathcal{N}$ the normalization factor such that $\sqrt{\mathcal{N}}\phi_k = \phi_k$, we find

$$\frac{2m}{\hbar^2}\delta(k^2-k'^2) = \mathcal{N}\frac{(2\pi)^3}{\mathcal{V}}\delta(\boldsymbol{k}-\boldsymbol{k}') = \mathcal{N}\frac{(2\pi)^3}{\mathcal{V}}\frac{2k}{k^2}\delta(k^2-k'^2)\delta(\hat{\boldsymbol{k}}-\hat{\boldsymbol{k}}')$$

so that

$$\mathcal{N} = \frac{\mathcal{V}}{(2\pi)^3}\frac{k}{2}\frac{2m}{\hbar^2} = \frac{k}{16\pi^3} \tag{17}$$

which is identical to $\rho(E_f)$, the last equality holding in atomic units of lengths and Rydberg units of energy ($2m/\hbar^2 \to 1$).

The second order term in the expression (9) of $T_I^{(2)}$, which is the scattering term, involves two photons, one created and one absorbed. There are obviously three possibilities for such a

process in a time-dependent scheme. The first one, which corresponds to the term in $\boldsymbol{A}\cdot\boldsymbol{A}$, describes a situation in which the incoming photon is absorbed at the same time as the outgoing photon is created. We label this process (a). The second possibility, often termed the direct process, is when the outgoing photon is created after the absorption of the incoming one. We call it (b). In this case, an electron is excited in the time between the two processes. Finally, the exchange process (c) is associated with the creation of the outgoing photon before the absorption of the incoming one. Both processes (b) and (c) differ only by the nature of the intermediate state. For (b), it corresponds to the matter system in an excited state $|n\rangle$ with no photons. In contrast, in case (c), the system is in state $|n\rangle$ plus two photons.

We can now calculate the transition operators that will allow the computation of the cross-section of these processes. Taking the matrix elements between the initial and final states, we find [22] for case (a)

$$\langle\Phi_f|T^{(2)}_{I(a)}|\Phi_i\rangle = \frac{e^2}{2m}\frac{\hbar}{2\epsilon_o\mathcal{V}}\frac{1}{\sqrt{\omega_{q_f}\omega_{q_i}}}\langle\Phi_f|(\hat{e}^*_{q_f}\cdot\hat{e}_{q_i})\mathrm{e}^{\mathrm{i}(q_i-q_f)\cdot r} \times\left[a_{q_i\hat{e}_{q_i}}a^\dagger_{q_f\hat{e}_{q_f}}+a^\dagger_{q_f\hat{e}_{q_f}}a_{q_i\hat{e}_{q_i}}\right]|\Phi_i\rangle. \tag{18}$$

For elastic scattering, the initial and final states of the matter system are the same and this matrix element becomes

$$f_T(\boldsymbol{Q}) = \int|\phi(\boldsymbol{r})|^2\mathrm{e}^{-\mathrm{i}\boldsymbol{Q}\cdot\boldsymbol{r}}\,\mathrm{d}\boldsymbol{r} \tag{19}$$

$\boldsymbol{Q}$ is the momentum transfer vector given by $\boldsymbol{Q}=\boldsymbol{q}_f-\boldsymbol{q}_i$. In the case of an atom the quantity $f_T(\boldsymbol{Q})$ is called the atomic form factor and it is the Fourier transform of the atomic charge density.

The contributions of the two other terms (b) and (c) can be worked out similarly. They give [22–24]

$$\begin{aligned}\langle\Phi_f|T^{(2)}_{I(b)}|\Phi_i\rangle &= N\sum_n\frac{\langle\phi_f|\hat{e}^*_{q_f}\cdot\boldsymbol{p}\mathrm{e}^{-\mathrm{i}q_f\cdot r}|\phi_n\rangle\langle\phi_n|\hat{e}_{q_i}\cdot\boldsymbol{p}\mathrm{e}^{\mathrm{i}q_i\cdot r}|\phi_i\rangle}{E_i-E_n+\hbar\omega_{q_i}-\mathrm{i}\epsilon}\\ \langle\Phi_f|T^{(2)}_{I(c)}|\Phi_i\rangle &= N\sum_n\frac{\langle\phi_f|\hat{e}_{q_i}\cdot\boldsymbol{p}\mathrm{e}^{\mathrm{i}q_i\cdot r}|\phi_n\rangle\langle\phi_n|\hat{e}^*_{q_f}\cdot\boldsymbol{p}\mathrm{e}^{-\mathrm{i}q_f\cdot r}|\phi_i\rangle}{E_i-E_n-\hbar\omega_{q_f}-\mathrm{i}\epsilon}.\end{aligned} \tag{20}$$

In the independent particle picture the sum is over all the unoccupied states $|\phi_n\rangle$; in the many-body approach it is over all states. The prefactor N is given by

$$N=\left(\frac{e}{m}\right)^2\frac{\hbar}{2\epsilon_o\mathcal{V}}\frac{1}{\sqrt{\omega_{q_f}\omega_{q_i}}}.$$

Adding the three terms together, dividing by the incoming flux $c/\mathcal{V}$ and multiplying by the density of photons in the final state (according to (2)) given by [21]

$$\frac{\mathcal{V}}{(2\pi)^3}\frac{(\hbar\omega_{q_f})^2}{\hbar^3c^3}$$

the cross-section for the scattering case becomes

$$\begin{aligned}\frac{\mathrm{d}\sigma}{\mathrm{d}\Omega} = r_o^2\frac{\omega_{q_f}}{\omega_{q_i}}\Bigg|&\hat{e}^*_{q_f}\cdot\hat{e}_{q_i}\langle\phi_f|\mathrm{e}^{-\mathrm{i}\boldsymbol{Q}\cdot r}|\phi_i\rangle\\ &+\frac{1}{m}\Bigg[\sum_n\frac{\langle\phi_f|\hat{e}^*_{q_f}\cdot\boldsymbol{p}\mathrm{e}^{-\mathrm{i}q_f\cdot r}|\phi_n\rangle\langle\phi_n|\hat{e}_{q_i}\cdot\boldsymbol{p}\mathrm{e}^{\mathrm{i}q_i\cdot r}|\phi_i\rangle}{E_i-E_n+\hbar\omega_{q_i}-\mathrm{i}\epsilon}\\ &+\frac{\langle\phi_f|\hat{e}_{q_i}\cdot\boldsymbol{p}\mathrm{e}^{\mathrm{i}q_i\cdot r}|\phi_n\rangle\langle\phi_n|\hat{e}^*_{q_f}\cdot\boldsymbol{p}\mathrm{e}^{-\mathrm{i}q_f\cdot r}|\phi_i\rangle}{E_i-E_n-\hbar\omega_{q_f}-\mathrm{i}\epsilon}\Bigg]\Bigg|^2.\end{aligned} \tag{21}$$

Here $d\Omega$ is the element of solid angle about $\boldsymbol{q}_f$ and $r_o = e^2/(4\pi\epsilon_0 mc^2)$ is the classical radius of the electron. This result is known as the Kramers–Heisenberg cross-section for the scattering of light by atomic electrons.

When the kinetic energy of the incoming photons is very large compared to the relevant excitation energies of the system $(E_n - E_i)$, the second and third terms in the above equation are negligible compared to the first. Due to the particular polarization dependence this term is called the Thomson term and the corresponding process Thomson scattering. However, when the photon energy is of the order of some excitation energy of the system, the second term becomes singular. Actually, the singularity is avoided by considering that the intermediate state $|\phi_n\rangle$ is short lived and so it has a finite lifetime Γ_n that should replace ϵ in the denominator of (21). Nevertheless, a strong enhancement of the cross-section still results when the energy of the incoming photon goes through an absorption edge, since usually $\Gamma_n \ll (E_n - E_i)$. This phenomenon is called resonance (or anomalous) scattering. For this reason, the direct term in the Kramers–Heisenberg cross-section is often called the resonant term while the third term, which cannot be singular, is called the non-resonant one.

Under resonance conditions, the non-resonant term in expression (21) of the cross-section, i.e. the second dispersive term, can usually be neglected. If we consider furthermore the case of elastic coherent scattering (corresponding to the DAFS or REXS spectroscopies), this cross-section further simplifies as

$$\frac{d\sigma}{d\Omega} = r_o^2 \left| \hat{e}^*_{q_f} \cdot \hat{e}_{q_i} f_T(\boldsymbol{Q}) + \frac{1}{m} \sum_n \frac{\langle \phi_i | \hat{e}^*_{q_f} \cdot \boldsymbol{p} e^{-i q_f \cdot r} | \phi_n \rangle \langle \phi_n | \hat{e}_{q_i} \cdot \boldsymbol{p} e^{i q_i \cdot r} | \phi_i \rangle}{E_i - E_n + \hbar\omega_{q_i} - i\epsilon} \right|^2 \tag{22}$$

since in this case $|\phi_i\rangle = |\phi_f\rangle$.

It is then customary to decompose the resonant term, the only complex term remaining as the Thomson term is real, into its real and imaginary part, noted respectively $f'(\hbar\omega_{q_i})$ and $f''(\hbar\omega_{q_i})$. The cross-section is then rewritten as

$$\frac{d\sigma}{d\Omega} = r_o^2 \left| \hat{e}^*_{q_f} \cdot \hat{e}_{q_i} f_T(\boldsymbol{Q}) + f'(\hbar\omega_{q_i}) + i f''(\hbar\omega_{q_i}) \right|^2$$

$f'(\hbar\omega_{q_i})$ is a dispersion correction to the Thomson amplitude $f_T(\boldsymbol{Q})$ while $f''(\hbar\omega)$ is an absorption correction.

Using the well known relation [25]

$$\frac{1}{x - x_o + i\epsilon} = \mathcal{P}\left(\frac{1}{x - x_o}\right) - i\pi\delta(x - x_o)$$

where the symbol $\mathcal{P}$ stands for Cauchy's principal value, we obtain for the imaginary part

$$f''(\hbar\omega_{q_i}) = \frac{\pi}{m} \sum_n \langle \phi_i | \hat{e}^*_{q_f} \cdot \boldsymbol{p} e^{-i q_f \cdot r} | \phi_n \rangle \langle \phi_n | \hat{e}_{q_i} \cdot \boldsymbol{p} e^{i q_i \cdot r} | \phi_i \rangle \delta(E_i - E_n + \hbar\omega_{q_i}). \tag{23}$$

In the dipole approximation, the factors $e^{-i q_f \cdot r}$ and $e^{i q_i \cdot r}$ disappear in the matrix elements. In the case of forward scattering ($\boldsymbol{q}_f = \boldsymbol{q}_i$ and $\hat{e}_{q_i} = \hat{e}_{q_f}$), this expression simplifies as

$$f''(\hbar\omega_{q_i}) = \frac{\pi}{m} \sum_n \left| \langle \phi_n | \hat{e}_{q_i} \cdot \boldsymbol{p} e^{i q_i \cdot r} | \phi_i \rangle \right|^2 \delta(E_i - E_n + \hbar\omega). \tag{24}$$

We see clearly here that $f''(\hbar\omega_{q_i})$ is proportional to the absorption cross-section (13). $f'(\hbar\omega_{q_i})$ can then be obtained from $f''(\hbar\omega_{q_i})$ by making use of the Kramers–Kronig relations.

2.3. Cross-section for incoming electrons

Similar processes as for photons can occur when focusing a beam of electrons on a sample. We can have elastic scattering (as in the case of LEED), inelastic scattering (EELS for instance) or

absorption, when one counts only the number of electrons removed from the incoming beam. In the case of elastic scattering, the incoming electrons only interact with the sample potential V_S through an elastic process. In contrast, when they suffer energy loss within the sample, there is an additional interaction potential, called V_L, responsible for it. This is the case of EELS, where an electron of the sample is excited via the Coulomb interaction. In this case, the total interaction potential will be written as $V_I = V_S + V_L$.

The calculation of the scattering cross-section is similar to the one we have outlined in the previous subsection. Let us call H_o the Hamiltonian of the free electron incident onto the sample. The eigenstates can be taken as plane wave states represented respectively by $|\boldsymbol{k}_i\rangle$ and $|\boldsymbol{k}_f\rangle$ in the initial and the final state. The total Hamiltonian is then

$$H = H_o + V_I = H_o + V_S + V_L.$$

Following (2), the cross-section can be written as

$$\frac{\mathrm{d}\sigma}{\mathrm{d}\hat{\boldsymbol{k}}_f} = \frac{2\pi}{\hbar I_i} \left|\langle \boldsymbol{k}_f | T_I | \boldsymbol{k}_i \rangle\right|^2 \rho(E_f).$$

Here, I_i the flux of incoming electrons and T_I the transition operator related to the interaction potential V_I by an equation similar to (3).

With plane waves normalized at one state in a box of volume $\mathcal{V}$, i.e.

$$\langle \boldsymbol{r} | \boldsymbol{k} \rangle = \frac{1}{\sqrt{\mathcal{V}}} \mathrm{e}^{\mathrm{i}\boldsymbol{k}\cdot\boldsymbol{r}}$$

the flux of incoming electrons can be shown to be [21]

$$I_i = \frac{1}{\mathcal{V}} \frac{\hbar k_i}{m}$$

and as before the density of final states

$$\rho(E_f) = \frac{\mathcal{V}}{(2\pi)^3} \frac{m k_f}{\hbar^2}.$$

Replacing in the expression of the cross-section above, we obtain

$$\frac{\mathrm{d}\sigma}{\mathrm{d}\hat{\boldsymbol{k}}_f} = \mathcal{V}^2 \left(\frac{m}{2\pi\hbar^2}\right)^2 \frac{k_f}{k_i} \left|\langle \boldsymbol{k}_f | T_I | \boldsymbol{k}_i \rangle\right|^2.$$

Note that this cross-section does not depend on the normalization volume $\mathcal{V}$ as the prefactor $\mathcal{V}^2$ will cancel with the volume terms coming from $|\boldsymbol{k}_i\rangle$ and $|\boldsymbol{k}_f\rangle$.

If we take the standard condition of normalization to the continuum

$$\langle \boldsymbol{k}_f | \boldsymbol{k}_i \rangle = \delta(\boldsymbol{k}_i - \boldsymbol{k}_f)$$

then the volume $\mathcal{V}$ in the expression of the cross-section, and in the expression of the plane waves, should be replaced by $(2\pi)^3$. Making this replacement leads to

$$\frac{\mathrm{d}\sigma}{\mathrm{d}\hat{\boldsymbol{k}}_f} = 4\pi^4 \left(\frac{2m}{\hbar^2}\right)^2 \frac{k_f}{k_i} \left|\langle \boldsymbol{k}_f | T_I | \boldsymbol{k}_i \rangle\right|^2. \tag{25}$$

For elastic scattering, i.e. $V_L = 0$, this simplifies to

$$\frac{\mathrm{d}\sigma}{\mathrm{d}\hat{\boldsymbol{k}}_f} = 4\pi^4 \left(\frac{2m}{\hbar^2}\right)^2 \left|\langle \boldsymbol{k}_f | T_S | \boldsymbol{k}_i \rangle\right|^2$$

with now $k_f = k_i = k$. The term $(2m/\hbar^2)^2$ can be incorporated into the square modulus so as to express the energies in Rydberg. Remembering the continuum normalization condition

this leads to a matrix element $\langle \boldsymbol{k}_f|(2m/\hbar^2)T_S|\boldsymbol{k}_i\rangle$ proportional to $1/k$ with dimension [L] of a length, which is the customary normalization for T-matrix elements.

In the case of inelastic scattering we need to calculate the transition operator T_I from the knowledge of T_S and T_L. This problem has been addressed by many authors and can be solved conveniently within the distorted-wave Born approximation. The basic idea in this approach is to partition the Hamiltonian $H = H_o + V_S + V_L$ into $H = H_S + V_L$ with $H_S = H_o + V_S$. H_S is solved first, and then the solutions of H can be expressed in terms of the solutions of H_S using standard scattering theory. Since inelastic scattering involves at least two-particle states, let us indicate by $|\phi\rangle$ the solutions of H_o, by $|\Phi^{\pm}\rangle$ the scattering solutions of H_S and by $|\Psi^{\pm}\rangle$ those of H considered as multiparticle Hamiltonians. The sign $+$ represents an outgoing state and the sign $-$ an incoming one. Then, according to the result given by Bethe and Jackiw [26], one has

$$\langle \phi_f|T_I|\phi_i\rangle = \langle \phi_f|T_S|\phi_i\rangle + \langle \Phi_f^-|V_L|\Psi_i^+\rangle. \tag{26}$$

This expression is exact. If we expand $|\Psi_i^+\rangle$ in terms of the solutions $|\Phi_i^+\rangle$ of H_S and keep only the first term (this amounts to identifying $|\Psi_i^+\rangle$ with $|\Phi_i^+\rangle$), we have the distorted wave Born approximation (DWBA), which gives for the cross-section

$$\frac{\mathrm{d}\sigma}{\mathrm{d}\hat{\boldsymbol{k}}_f} = 4\pi^4\left(\frac{2m}{\hbar^2}\right)^2\frac{k_f}{k_i}|\langle \Phi_f^-|V_L|\Phi_i^+\rangle|^2. \tag{27}$$

The matrix element $\langle \phi_f|T_S|\phi_i\rangle$ in (26) is zero because V_S, which describes elastic scattering, cannot induce transitions with energy change.

2.4. Doubly differential ionization cross-section

We consider now the case where two electrons are excited from a sample resulting from the same ionization process and later measured by two analysers. The second electron may result either from the decay of the core hole created by the ejection of the first electron (Auger decay) or from a loss of this latter. Hence we only consider the case where the two electrons are excited at a different time but with a causal relationship. Excitation by a single photon of a quasiparticle formed by an electron pair as in one of the double photoemission processes [27–29] will not be treated here. We shall write as V_{I1} and V_{I2} the two ionization potentials to remain as general as possible and specialize them later according to the process investigated. Here again, we have a multiparticle problem and therefore we will keep the notations we introduced for inelastic scattering.

The total Hamiltonian is written as $H = H_S + V_{I1} + V_{I2}$, where H_S is the sample Hamiltonian in the absence of any ionization. The transition operator associated with this Hamiltonian can be written exactly as

$$T = (V_{I1} + V_{I2}) + (V_{I1} + V_{I2})G(V_{I1} + V_{I2}).$$

Here, G is the propagator of the full system defined as $(z - H)^{-1}$. It can be expanded in terms of the sample propagator $G_S = (z - H_S)^{-1}$ using Dyson's equation. Truncating this expansion to first order gives

$$T^{(1)} = (V_{I1} + V_{I2}) + (V_{I1} + V_{I2})G_S(V_{I1} + V_{I2}).$$

This expression is still relatively general. Let us specialize it to the process we consider now. The zeroth-order term $(V_{I1} + V_{I2})$ vanishes, as V_{I1} and V_{I2} do not act simultaneously. Furthermore, the first ionization precedes the second ionization process in time so that we are left with

$$T_{DDI}^{(1)} = V_{I2}G_SV_{I1}.$$

As before, we write the ground state of the system described by H_S as $|\Phi_i\rangle = |\Phi_N\rangle$, with the index N indicating the number of electrons. We represent the final state by $|\Phi_f\rangle = |\Phi_{N-2}\rangle|\boldsymbol{k}_1\rangle|\boldsymbol{k}_2\rangle$, with $|\boldsymbol{k}_1\rangle$ and $|\boldsymbol{k}_2\rangle$ representing the two escaping electrons. Following equation (2), we can write the doubly differential cross-section as

$$\frac{\mathrm{d}^2\sigma}{\mathrm{d}\hat{\boldsymbol{k}}_1\,\mathrm{d}\hat{\boldsymbol{k}}_2} = \frac{2\pi}{\hbar I_o}\left|\langle\Phi_f|T^{(1)}_{DDI}|\Phi_i\rangle\right|^2 \rho(\mathcal{E}_f)$$

where I_o is the flux of the incoming particle (electron, photon, ...) that results in the ionization of the system through V_{I1}. $\rho(\mathcal{E}_f)$ is the density of final states of the detected particles.

We can introduce a sum over intermediate states $|\Phi_n\rangle$ which we will characterize later. We choose the $\{|\Phi_n\rangle\}$ to be eigenstates of H_S of eigenenergy $\mathcal{E}_n$, suitably normalized so that no normalization coefficient appears in the closure relation of the basis they form. Then

$$\frac{\mathrm{d}^2\sigma}{\mathrm{d}\hat{\boldsymbol{k}}_1\,\mathrm{d}\hat{\boldsymbol{k}}_2} = \frac{2\pi}{\hbar I_o}\left|\sum_n \langle\Phi_f|V_{I2}G_S|\Phi_n\rangle\langle\Phi_n|V_{I1}|\Phi_i\rangle\right|^2 \rho(\mathcal{E}_f). \tag{28}$$

As before, due to energy conservation, G_S can be taken either at the energy of the initial state $\mathcal{E}_i$ or at that of the final state $\mathcal{E}_f$. It should be noted however that this energy conservation relation does not put constraints on the energy $\mathcal{E}_n$ of the intermediate states, since these latter involve virtual transitions.

Furthermore,

$$G_s(\mathcal{E}_i)|\Phi_n\rangle = (\mathcal{E}_i - H_S)^{-1}|\Phi_n\rangle = \frac{|\Phi_n\rangle}{\mathcal{E}_i - \mathcal{E}_n + \mathrm{i}\epsilon}$$

as $|\Phi_n\rangle$ is an eigenstate of H_S. We replace now into the expression (28) of the cross-section and make use of the value (16) of the density of states of free electrons to obtain

$$\frac{\mathrm{d}^2\sigma}{\mathrm{d}\hat{\boldsymbol{k}}_1\,\mathrm{d}\hat{\boldsymbol{k}}_2} = \frac{2\pi}{\hbar I_o}\frac{\mathcal{V}^2}{(2\pi)^6}\frac{m^2}{\hbar^4}k_1k_2\left|\sum_n \frac{\langle\Phi_f|V_{I2}|\Phi_n\rangle\langle\Phi_n|V_{I1}|\Phi_i\rangle}{\mathcal{E}_i - \mathcal{E}_n + \mathrm{i}\Gamma_n}\right|^2 \delta(\mathcal{E}_i - \mathcal{E}_f). \tag{29}$$

We have added here an energy broadening to account for the fact that the intermediate state $|\Phi_n\rangle$ is short lived, its lifetime being that of the core hole created by the effect of V_{I1}.

3. Reduction of the many-body problem to an effective one-particle problem for photoemission and photoabsorption

In the remainder of this article, we shall use atomic units of lengths ($a_0 = \hbar^2/me^2 = 0.529$ Å) and Rydberg units of energy (1 Ryd $= \hbar^2/(2me^2a_0^2) = 13.6$ eV), and drop the index $\boldsymbol{q}$ from all the wavefield quantities to simplify the notations.

In section 2.2, we have derived a general expression for the photoemission and photoabsorption cross-sections. The two processes are closely related inasmuch as the absorption of a photon by an atom results primarily in the ejection of a photoelectron, when its energy is greater than the ionization potential. Indeed, the photoabsorption cross-section is nothing more than the integration of the photoemission cross-section over all emission angles and all the final channels (elastic plus inelastic) with the same final energy. The reason we treat both cases together is duplex. Firstly, the mathematical formalism is the same, as is the reduction process to an effective one-particle problem; secondly, and more importantly, on purely physical grounds we can think of photoabsorption as a photoemission process with the same electron source (the photoabsorber), in which the detector, instead of being outside the sample, coincides with the source. This analogy will be apparent from the mathematical formalism elaborated below.

Both processes are complicated many-body problems which still challenge an exhaustive theoretical treatment. Since we are mainly interested in their structural applications, we shall present in this section a many-body derivation of their cross-section and illustrate the reduction of this problem to an effective single-particle problem with complex energy-dependent optical potential. This process of reduction will help us to understand the validity and the limits of application of the resulting theoretical scheme as well as to choose an appropriate optical potential.

By treating photoabsorption and photoemission together, we shall thus be able to assess the sensitivity of a particular potential in absorption by looking at its performance in photoelectron diffraction and vice versa.

3.1. The photoemission case

In an angular-resolved photoemission experiment, the photoelectrons of energy E_k larger than the work function of the sample are detected along a direction $\hat{\boldsymbol{k}}$ determined by the user. We can therefore infer that the differential cross-section for such a photoemission experiment will be similar to the photoabsorption one (see subsection 2.2) but with two essential differences:

(a) no summation is required on the final states because the detector selects only the particular states of interest;
(b) the outgoing wavefunction of the photoelectron should exhibit some specific boundary conditions to account for the fact that no electron was present in the continuum in the distant past.

Taking these points into account, the photoemission cross-section in the many-body case for the ejection of a photoelectron of final momentum $\boldsymbol{k}$ and kinetic energy k^2 along the direction $\hat{\boldsymbol{k}}$ can be written as

$$\frac{\mathrm{d}\sigma(\omega)}{\mathrm{d}\hat{\boldsymbol{k}}} = 4\pi^2\alpha\hbar\omega \left| \langle \Theta\Psi_{\boldsymbol{k}}^N | \hat{\boldsymbol{e}} \cdot \sum_{i=1}^{n} \boldsymbol{r}_i | \Psi_{\mathrm{g}}^N \rangle \right|^2 \tag{30}$$

where $\Psi_{\boldsymbol{k}}^N$ is the many-body final scattering state, normalized to one state per energy interval unit, for the N-electron system with one electron of momentum $\boldsymbol{k}$ travelling to infinity, and Ψ_{g}^N its ground state, with respective energies E_k^N and E_{g}^N. As in the previous section, $\hbar\omega$ is the incoming photon energy and $\hat{\boldsymbol{e}}$ its polarization. Energy conservation imposes that $\hbar\omega = E_k^N - E_{\mathrm{g}}^N$. According to Breit and Bethe [30], in order to satisfy the correct boundary conditions for the ejected photoelectron (no electron in a continuum state in the remote past), we must take the time-reversed scattering state by application of the time-reversal operator Θ. A similar boundary condition has been implicitly imposed in the expression (27) of the inelastic cross-section of electron scattering.

In the case of photoemission from a deep core state $\phi_{L_0}^c$ of angular momentum $L_0 = (l_0, m_0)$, we assume that, to a good approximation,

$$\begin{aligned}\Psi_{\mathrm{g}}^N(\boldsymbol{r}, \boldsymbol{r}_1, \ldots, \boldsymbol{r}_{N-1}) &= (N!)^{1/2} A \phi_{L_0}^c(\boldsymbol{r}) \sum_n c_n \Phi_n^{N-1}(\boldsymbol{r}_1, \ldots, \boldsymbol{r}_{N-1}) \\ &= (N!)^{1/2} A \phi_{L_0}^c(\boldsymbol{r}) \Psi_{\mathrm{g}}^{N-1}(\boldsymbol{r}_1, \ldots, \boldsymbol{r}_{N-1})\end{aligned} \tag{31}$$

where A is the usual anti-symmetrization operator ($A = 1/N! \sum_P (-1)^P P$, with $A^2 = A$, P being the permutation operator) and $\Phi_n^{N-1}(\boldsymbol{r}_1, \ldots, \boldsymbol{r}_{N-1})$ are Slater determinants describing the configurations present in the ground state of the system. Normalization imposes $\sum_n |c_n|^2 =$

1 if $\langle\phi_c|\phi^c\rangle = 1$ and for simplicity we shall omit spin variables, since we will not consider here magnetic systems. In a similar way we can write without loss of generality

$$\Psi_f^N(\boldsymbol{r}, \boldsymbol{r}_1, \ldots, \boldsymbol{r}_{N-1}) = (N!)^{1/2} A \sum_\alpha \phi_\alpha^f(\boldsymbol{r}) \tilde{\Psi}_\alpha^{N-1}(\boldsymbol{r}_1, \ldots, \boldsymbol{r}_{N-1}) \tag{32}$$

where α labels any complete basis set and where the functions ϕ_α^f, ignoring exchange effects, can be thought to describe the excited photoelectron while the $\tilde{\Psi}_\alpha^{N-1}$ states are eigenstates of the Hamiltonian H^{N-1} describing the remaining $(N-1)$-electron system with eigenvalues E_α^{N-1}:

$$H^{N-1}\tilde{\Psi}_\alpha^{N-1} = E_\alpha^{N-1}\tilde{\Psi}_\alpha^{N-1}. \tag{33}$$

The tilde over them stands as a reminder that in the expansion (31) the relaxed states around the core hole are dominant. If needed, they can be in turn expanded in terms of Slater determinants describing the intervening configurations in the final state. Borrowing the term from many-particle scattering theory, we can call the states $\tilde{\Psi}_\alpha^{N-1}$ final state channels. Here and henceforth the lower index f in the final state Ψ_f^N can be replaced by $\boldsymbol{k}$ whenever we deal specifically with the scattering state $\Psi_{\boldsymbol{k}}^N$.

The wavefunction Ψ_f^N is an eigenstate of the total Hamiltonian H^N with eigenvalue $E_f^N = E_g^N + \hbar\omega$, i.e.

$$H^N\Psi_f^N = E_f^N\Psi_f^N. \tag{34}$$

Moreover,

$$H^N = -\nabla_{\boldsymbol{r}}^2 + \sum_i V(\boldsymbol{r}, \boldsymbol{r}_i) + H^{N-1} \tag{35}$$

where $V(\boldsymbol{r}, \boldsymbol{r}_i)$ is the interaction potential of the excited photoelectron with the rest of the system.

By inserting (32) into (34), projecting onto the states $\tilde{\Psi}_\alpha^{N-1}$ and using (33), one obtains for the amplitude functions ϕ_α^f the set of coupled equations

$$(\nabla^2 + k_\alpha^2)\phi_\alpha^f(\boldsymbol{r}) = \sum_\beta \int V_{\alpha\beta}(\boldsymbol{r}, \boldsymbol{r}')\phi_\beta^f(\boldsymbol{r}')\,\mathrm{d}\boldsymbol{r}' \tag{36}$$

where

$$k_\alpha^2 = \hbar\omega - (E_g^{N-1} - E_g^N) - (E_\alpha^{N-1} - E_g^{N-1}) = \hbar\omega - I_c - \Delta E_\alpha \tag{37}$$

I_c being the ionization potential for the core state and ΔE_α the excitation energy left behind in the $(N-1)$-particle system. The non-local interchannel potentials $V_{\alpha\beta}(\boldsymbol{r}, \boldsymbol{r}')$ are the matrix elements between states $\tilde{\Psi}_\alpha^{N-1}$ and $\tilde{\Psi}_\beta^{N-1}$ of the interaction potential $V(\boldsymbol{r}, \boldsymbol{r}_i)$ and include local terms coming from the Coulomb interaction as well as non-local exchange terms originating from the exchange interaction. The set of equations (36) is to be supplemented with the boundary conditions related to the behaviour of the photoelectron at infinity and to the state of the $(N-1)$-electron system according to the partition of the total energy $E_f^N = E_g^N + \hbar\omega$ between them. To each different partition there corresponds a different set of boundary conditions leading to a different solution of the set of (36). For example, if we are interested in a particular photoemission channel β with kinetic energy k_β^2 leaving behind the energy ΔE_β in the system, in the limit $r \longrightarrow +\infty$ we should impose the scattering conditions

$$\phi_\alpha(\boldsymbol{r}; \boldsymbol{k}_\beta) \simeq \left(\frac{k_\alpha}{16\pi^3}\right)^{\frac{1}{2}} \left[\mathrm{e}^{\mathrm{i}\boldsymbol{k}_\beta\cdot\boldsymbol{r}}\delta_{\alpha\beta} + f_\alpha(\hat{\boldsymbol{r}}, \boldsymbol{k}_\beta)\frac{\mathrm{e}^{\mathrm{i}k_\alpha r}}{r}\right] \tag{38}$$

where we have made explicit the dependence of ϕ_α on k_β as an argument rather than an upper index. Here, as usual, $\delta_{\alpha\beta}$ is the Kronecker symbol, and f_α is the scattering amplitude. The

factor $\left(k_\alpha/16\pi^3\right)^{1/2}$ takes care of the normalization of the photoelectronic plane wave at the detector to one state per Rydberg. In the case of double electron transitions with two electrons in the continuum, equation (38) can easily be changed accordingly. For more details we refer the reader to Natoli *et al* [13], where a formal solution of these equations is given in the framework of the multichannel multiple-scattering theory. For the sake of the argument developed here, we need only the expression for photoemission cross-section, which is obtained from (30)–(32) as

$$\frac{\mathrm{d}\sigma(\omega)}{\mathrm{d}\hat{\boldsymbol{k}}} = 8\pi^2\alpha\hbar\omega\sum_{m_0}\left|\sum_\alpha\langle S_\alpha^*\phi_\alpha^-(\boldsymbol{r};\boldsymbol{k}_\beta)|\hat{\boldsymbol{e}}\cdot\boldsymbol{r}|\phi^c_{l_0m_0}(\boldsymbol{r})\rangle\right|^2 \tag{39}$$

which is valid if we orthogonalize the excited channels ϕ_α^- to all the one-particle states belonging to the configurations Φ_n present in the ground state Ψ_{g}^N. Here we have introduced the overlap integrals $S_\alpha = \langle\tilde{\Psi}_\alpha^{N-1}|\Psi_{\mathrm{g}}^{N-1}\rangle$ of the passive electrons and indicated by ϕ_α^- the time-reversal of ϕ_α (in practice the complex conjugate, if spin is neglected). Spin–orbit splitting in the initial core state has been ignored, since it is not relevant for our argument, and spin degeneracy has been taken into account by an extra factor of two.

The set of equations in (36) contains the complete description of all the outcomes of the photoemission process, be it of intrinsic origin (i.e. consequent to the relaxation of the system around the core hole) or extrinsic (excitations created by the photoelectron in its way out of the system). Their complete solution is out of the question; however, one can analyse their consequence in particular cases. Since we are mainly interested in structural analysis, both in photoemission and photoabsorption, we need only to consider the completely relaxed or elastic channel (i.e. the one for which $\Delta E_\beta = 0$), because it carries most of the weight and is usually used for structural analysis. Indeed, as a typical value, $|S_0|^2 = |\langle\tilde{\Psi}_0^{N-1}|\Psi_{\mathrm{g}}^{N-1}\rangle|^2 \sim 0.8$–$0.9$ [31]. For simplicity, we shall attribute to this channel here and in the following the index $\alpha = 0$. However, any other channel can in principle be capable of carrying structural information, provided the photoelectron in the chosen channel remains in the same energy state after the loss event. This is the case of the Kikuchi electrons (coming from plasmon-loss peaks) considered by Osterwalder *et al* [17], who observed the same diffraction patterns from a (001) single-crystal surface of aluminium independently from the number of losses n suffered by the photoelectron. In this case it is reasonable to assume that in all these channels the effective potential will be substantially the same for photoelectrons with a kinetic energy more than 1000 eV, since the plasmon oscillations involve only valence electrons and at these energies atomic scattering is due mainly to core electrons.

With this in mind, we can then think of solving the set of coupled Schrödinger equations (36) by eliminating all unwanted channels in favour of the elastic one. The result is a single equation for the channel function $\phi_0(\boldsymbol{r})$ with an effective complex energy-dependent non-local optical potential of the kind

$$\left[\nabla^2 + k_0^2 - V_c(\boldsymbol{r})\right]\phi_0(\boldsymbol{r}) = \int \Sigma^{\mathrm{opt}}(\boldsymbol{r},\boldsymbol{r}';\hbar\omega)\phi_0(\boldsymbol{r}')\,\mathrm{d}\boldsymbol{r}' \tag{40}$$

where we have isolated its local Coulomb part (V_c) and indicated the energy dependence coming from the eliminated channels by the argument $\hbar\omega$ in Σ^{opt}. Once this equation is solved we can write each $\phi_\alpha(\boldsymbol{r})$ in terms of $\phi_0(\boldsymbol{r})$ through a relation of the type $\phi_\alpha(\boldsymbol{r}) = \int A_\alpha(\boldsymbol{r},\boldsymbol{r}';\hbar\omega)\phi_0(\boldsymbol{r}')\,\mathrm{d}\boldsymbol{r}'$, involving complicated inversions of the operators $\left[\nabla^2 + k_\alpha^2 - V_\alpha(\boldsymbol{r},\boldsymbol{r}')\right]$ in (36). We can therefore write (39) as

$$\frac{\mathrm{d}\sigma(\omega)}{\mathrm{d}\hat{\boldsymbol{k}}_0} = 8\pi^2\alpha\hbar\omega\sum_{m_0}\left|\sum_\alpha\left\langle S_\alpha^*\int A_\alpha^-(\boldsymbol{r},\boldsymbol{r}';\hbar\omega)\phi_0^-(\boldsymbol{r}';\boldsymbol{k}_0)\,\mathrm{d}\boldsymbol{r}'|\times\hat{\boldsymbol{e}}\cdot\boldsymbol{r}|\phi^c_{l_0m_0}(\boldsymbol{r})\right\rangle\right|^2 \tag{41}$$

so that everything is expressed in terms of $\phi_0^-(\boldsymbol{r})$. Notice that in the summation over α the most important term is $S_0^*\phi_0^-(\boldsymbol{r})$, since by definition $A_0^-(\boldsymbol{r},\boldsymbol{r}';\hbar\omega) = \delta(r-r')$. Our task is then to solve (40) with the asymptotic boundary conditions given by (38). This can be done in the framework of MST by transforming this integro-differential equation (40) into a Lippman–Schwinger equation with non-local potential, following the method illustrated by Natoli, Benfatto and Doniach [32] and Natoli *et al* [13]. In these papers the derivation of the MS equations is given for local potentials, but it is clear that the same derivation is valid for non-local potentials as well. Indeed, the essence of the method rests on the partition of the space into Voronoi polyhedrons (equivalent to Wigner–Seitz cells for periodic systems) such that their diameter is always smaller than the nearest distance between their centres. In each such polyhedron a local solution $\Psi_L(\boldsymbol{r})$ of (40) is obtained behaving like $J_L(\boldsymbol{r}) = j_l(k_0 r)Y_L(\hat{\boldsymbol{r}})$ near the origin, where $j_l(kr)$ is the usual spherical Bessel function of order l and $Y_L(\hat{\boldsymbol{r}})$ the spherical harmonics of type $L \equiv (l,m)$ (unless explicitly stated, we shall use throughout the paper a real basis). These functions are used to expand locally in the ith cell the overall solution of class C^1 (continuous together with first derivatives) in the whole space, satisfying the boundary condition (38), as

$$\Phi^i(\boldsymbol{r}_i;\boldsymbol{k}_0) = \sum_L A_L^i(\boldsymbol{k}_0)\Phi_L^i(\boldsymbol{r}_i) \tag{42}$$

provided that the amplitudes $A_L^i(\boldsymbol{k}_0)$ satisfy the compatibility equations

$$\sum_{L'} C_{LL'}^i A_{L'}^i(\boldsymbol{k}_0) = A_L^0(\boldsymbol{k}_0) - \sum_{j,L',L''}(1-\delta_{ij})G_{LL'}^{ij}S_{L'L''}^i A_{L''}^j(\boldsymbol{k}_0) \tag{43}$$

where

$$A_L^0(\boldsymbol{k}_0) = Y_L(\hat{\boldsymbol{k}}_0)\mathrm{e}^{\mathrm{i}\boldsymbol{k}_0\cdot\boldsymbol{R}_{i0}}(k_0/\pi)^{1/2} \tag{44}$$

is the exciting amplitude originating from the plane wave in (38). A derivation is provided in appendix A for the convenience of the reader. Here $C_{LL'}^i$ and $S_{LL'}^i$ are surface integrals over the surface S_i of the ith cell given by

$$C_{LL'}^i = \int_{S_i}\left[\tilde{H}_L^+(\boldsymbol{r})\nabla\Phi_{L'}^i(\boldsymbol{r}) - \Phi_{L'}^i(\boldsymbol{r})\nabla\tilde{H}_L^+(\boldsymbol{r})\right]\cdot\boldsymbol{n}_i\,\mathrm{d}\sigma_i \tag{45}$$

$$S_{LL'}^i = \int_{S_i}\left[J_L^+(\boldsymbol{r})\nabla\Phi_{L'}^i(\boldsymbol{r}) - \Phi_{L'}^i(\boldsymbol{r})\nabla J_L^+(\boldsymbol{r})\right]\cdot\boldsymbol{n}_i\,\mathrm{d}\sigma_i \tag{46}$$

and $G_{LL'}^{ij}$ are the KKR structure factors having the well known expression

$$G_{LL'}^{ij} = 4\pi\sum_{L''}\mathrm{i}^{l-l'+l''}C_{LL'}^{L''}\tilde{H}_{L''}^+(\boldsymbol{R}_{ij}) \tag{47}$$

where $\tilde{H}_L^+(\boldsymbol{r}) = -\mathrm{i}kh_l^+(k_0 r)Y_L(\hat{\boldsymbol{r}})$, h_l^+ being the Hankel function with outgoing spherical wave behaviour, $\boldsymbol{R}_{ij} = \boldsymbol{R}_i - \boldsymbol{R}_j$ is the vector connecting the origins of the two cells centred at $\boldsymbol{R}_i$ and $\boldsymbol{R}_j$, and $\boldsymbol{R}_{io} = \boldsymbol{R}_i - \boldsymbol{R}_o$ connects site i with the origin of the coordinates o, assumed to coincide with the photoabsorber. The quantities $C_{LL'}^{L''} = \int Y_L(\hat{\boldsymbol{r}})Y_{L'}(\hat{\boldsymbol{r}})Y_{L''}^*(\hat{\boldsymbol{r}})$ are known as Gaunt coefficients. In order to be able to use the physical language of MST we introduce the quantities

$$B_L^i(\boldsymbol{k}_0) = \sum_{L'} S_{LL'}^i A_{L'}^i(\boldsymbol{k}_0) \tag{48}$$

and define the suitably normalized local basis solutions $\tilde{\Phi}_L^i = \sum_{L'}\Phi_{L'}^i(S^i)_{LL'}^{-1}$, so that

$$\Phi^i(\boldsymbol{r}_i;\boldsymbol{k}_0) = \sum_L \tilde{\Phi}_L^i(\boldsymbol{r}_i)B_L^i(\boldsymbol{k}_0). \tag{49}$$

The coefficients $B^i_L(\boldsymbol{k}_0)$ are easily seen to satisfy the MS equations

$$\sum_{L'}(T^i)^{-1}_{LL'}B^i_{L'}(\boldsymbol{k}_0) = A^0_L(\boldsymbol{k}_0) - \sum_{j,L'}(1-\delta_{ij})G^{ij}_{LL'}B^j_{L'}(\boldsymbol{k}_0) \tag{50}$$

where we have formally introduced the quantity $T^i_{LL'} = \sum_{L''} S^i_{LL''}(C^i)^{-1}_{L''L'}$. Under certain conditions or in the case of cells with spherical shape it can be shown [13] that $T^i_{LL'}$ is the scattering matrix of the non-spherical potential located inside the ith cell and $B^i_L(\boldsymbol{k}_0)$ is a total scattering amplitude impinging on it in response to a plane wave excitation of momentum $\boldsymbol{k}_0$. Indeed, (50) are nothing else but the self-consistent equations for these amplitudes. We shall assume in the following that this is the case, in order to make the discussion more physical. Otherwise, it is easy to pass from this representation to the other. For convenience we define the cell T-matrix $T_c = [T^i_{LL'}\delta_{ij}]$ and the matrix $G = [(1-\delta_{ij})G^{ij}_{LL'}]$ of the free spherical wave propagator. Then (50) are easily solved for the amplitudes $B^i_L(\boldsymbol{k}_0)$ to give

$$B^i_L(\boldsymbol{k}_0) = \left(\frac{k_0}{\pi}\right)^{\frac{1}{2}} \sum_{j,L'} \tau^{ij}_{LL'} \mathrm{i}^{l'} Y_{L'}(\hat{\boldsymbol{k}}_0)\mathrm{e}^{\mathrm{i}\boldsymbol{k}_0\cdot\boldsymbol{R}_{j0}} \tag{51}$$

where we have introduced the inverse $\boldsymbol{\tau}$ of the MS matrix

$$\tau^{ij}_{LL'} = \left[(T_c^{-1}+G)^{-1}\right]^{ij}_{LL'} \tag{52}$$

known as the full scattering path operator, giving the total amplitude of propagation from site i to site j, starting with angular momentum L and arriving with angular momentum L'. We now have all the ingredients to calculate the photoemission cross-section. Introducing the energy-dependent matrix element for the creation of the photoelectron

$$M^c_{L_0L}(\hbar\omega) = \sum_{\alpha}\left\langle S^*_\alpha \int A^-_\alpha(\boldsymbol{r},\boldsymbol{r}';\hbar\omega)\tilde{\Phi}^-_L(\boldsymbol{r}')\,\mathrm{d}\boldsymbol{r}'|\hat{e}\cdot\boldsymbol{r}|\phi^c_{L_0}\right\rangle \tag{53}$$

we easily find that our quantity of interest takes the simple form

$$\frac{\mathrm{d}\sigma(\omega)}{\mathrm{d}\hat{\boldsymbol{k}}_0} = 8\pi^2\alpha\hbar\omega\sum_{m_0}\left|\sum_L M^c_{L_0L}(\hbar\omega)B^o_L(\boldsymbol{k}_0)\right|^2. \tag{54}$$

Remembering (51), we then see that the photoemission current along direction $\hat{\boldsymbol{k}}_0$ is the square modulus of the sum of all possible composite amplitudes obtained as products of an amplitude $M^c_{L_0L}$ for exciting a core electron at site o (the origin) with angular momentum L, times the amplitude of propagation $\tau^{oj}_{LL'}$ from this site to any other site (cell) j with final angular momentum L', times the amplitude $Y_{L'}(\hat{\boldsymbol{k}}_0)$ for emission along $\hat{\boldsymbol{k}}_0$, times the phase factor $\mathrm{e}^{\mathrm{i}\boldsymbol{k}_0\cdot\boldsymbol{R}_{j0}}$ that takes into account the phase relation of the electronic wave between sites o and j. It is therefore the result of a complicated interference process with heavy demand on the reliability of the optical potential. The expression (54) has constituted the basis for the interpretation of photoelectron diffraction data at low photoelectron kinetic energies with good success [33]. A computer program in the MT approximation is also available [34] and currently used [35]. The emitted current depends on three variables, the photon energy and the two angles of the direction $\hat{\boldsymbol{k}}_0$. Therefore, as anticipated at the beginning of this section, by fixing the energy one can test the performance of a particular model optical potential in reproducing polar and azimuthal diffraction scans.

Before finishing this section, we want to quote an interesting relation connecting the square modulus of the scattering amplitude $B^o_L(\boldsymbol{k}_0)$ with the imaginary part of the scattering path operator τ^{oo}_{LL}. More generally, in the case of a real potential one can show [32] that as a consequence of the MS equations (50) the following relation holds:

$$\int \mathrm{d}\hat{\boldsymbol{k}}_0\left[B^i_L(\boldsymbol{k}_0)\right]^* B^j_{L'}(\boldsymbol{k}_0) = -\frac{1}{\pi}\,\mathrm{Im}\left[\tau^{ij}_{LL'}\right]. \tag{55}$$

This relation is a consequence of the conservation of the particle flux and is not valid in the case of losses (complex potential). It can be used to connect the integrated photoemission cross-section with the photoabsorption cross-section derived from the Green's function expression. Indeed, indicating by $M_{L_0L}(\hbar\omega)$ the atomic transition matrix element in the case of a single channel and real potential, from expression (54) we obtain

$$\int \mathrm{d}\hat{\boldsymbol{k}}_0 \frac{\mathrm{d}\sigma(\omega)}{\mathrm{d}\hat{\boldsymbol{k}}_0} = -8\pi\alpha\hbar\omega \sum_{m_0}\sum_{LL'} M_{L_0L}(\hbar\omega)\,\mathrm{Im}\left[\tau^{oo}_{LL'}\right] M_{L_0L'}(\hbar\omega) \tag{56}$$

which is identical to the photoabsorption cross-section derived below.

3.2. The photoabsorption case

Turning now to absorption, we need to integrate (39) over $\hat{\boldsymbol{k}}$ and sum over all final channels with the same total energy $E_{\mathrm{tot}} = \hbar\omega + E_{\mathrm{g}}$. To this purpose it is expedient to make explicit the energy conservation condition and label the final state with f. By defining the Green's function matrix with outgoing wave boundary conditions

$$G^{+}_{\alpha\alpha'} = \sum_f \frac{\phi^f_\alpha(\boldsymbol{r})\phi^f_{\alpha'}(\boldsymbol{r}')^*}{E - \Delta E_f - k_f^2 + \mathrm{i}\epsilon}$$

the photoabsorption cross-section is easily seen to be

$$\sigma_{\mathrm{abs}}(\omega) = -8\pi\alpha\hbar\omega\,\mathrm{Im}\sum_{m_0}\left[\int\int \mathrm{d}\boldsymbol{r}\phi^c_{L_0}(\boldsymbol{r})\hat{\boldsymbol{e}}\cdot\boldsymbol{r} \times \sum_{\alpha,\alpha'} S^*_\alpha S_{\alpha'} G^{+}_{\alpha\alpha'}(\boldsymbol{r},\boldsymbol{r}';\hbar\omega - I_c)\hat{\boldsymbol{e}}\cdot\boldsymbol{r}'\phi^c_{L_0}(\boldsymbol{r}')\,\mathrm{d}\boldsymbol{r}'\right] \tag{57}$$

which is the same expression we would have obtained starting from (30), (31) and (32). In appendix C-4 of Natoli *et al* [13] it is shown that this matrix satisfies the set of coupled equations, writing E for $\hbar\omega - I_c$,

$$(\boldsymbol{\nabla}^2 + k^2_\alpha)G^{+}_{\alpha\beta}(\boldsymbol{r},\boldsymbol{r}';E) - \sum_\gamma \int V_{\alpha\gamma}(\boldsymbol{r},\boldsymbol{r}'')G^{+}_{\gamma\beta}(\boldsymbol{r}'',\boldsymbol{r}';E)\,\mathrm{d}\boldsymbol{r}'' = \delta_{\alpha\beta}\delta(\boldsymbol{r}-\boldsymbol{r}').$$

Following the same steps as in the photoemission case, the elimination of all channels in favour of the relaxed one ($\alpha = 0$) leads to the following expression:

$$\sum_{\alpha,\alpha'} S^*_\alpha S_{\alpha'} G^{+}_{\alpha\alpha'}(\boldsymbol{r},\boldsymbol{r}';E) = \sum_{\alpha,\alpha'} S^*_\alpha S_{\alpha'} \int\int A^*_\alpha(\boldsymbol{r},\boldsymbol{x};E)G^{+}_{00}(\boldsymbol{x},\boldsymbol{x}';E)A_{\alpha'}(\boldsymbol{x}',\boldsymbol{r}';E)\,\mathrm{d}\boldsymbol{x}\,\mathrm{d}\boldsymbol{x}' \tag{58}$$

where the non-local operator $A_\alpha(\boldsymbol{r},\boldsymbol{r}';E)$ is the same as before and G_{00} obeys the analogous equation corresponding to (40) with the same optical potential

$$[\boldsymbol{\nabla}^2 + k_0^2 - V_c(\boldsymbol{r})]G^{+}_{00}(\boldsymbol{r},\boldsymbol{r}';E) - \int \Sigma^{\mathrm{opt}}(\boldsymbol{r},\boldsymbol{x};E)G^{+}_{00}(\boldsymbol{x},\boldsymbol{r}';E)\,\mathrm{d}\boldsymbol{x} = \delta(\boldsymbol{r}-\boldsymbol{r}'). \tag{59}$$

The solution to this equation within MST, for $\boldsymbol{r}$ in cell i and $\boldsymbol{r}'$ in cell j, can be written as [81]

$$G^{+}_{00}(\boldsymbol{r},\boldsymbol{r}';E) = \sum_{L,L'}\tilde{\Phi}_L(\boldsymbol{r})\left(\tau^{ij}_{LL'} - \delta_{ij}T^i_{LL'}\right)\tilde{\Phi}_{L'}(\boldsymbol{r}') + \delta_{ij}\sum_{L,L'}\tilde{\Phi}_L(\boldsymbol{r}_<)T^i_{LL'}\tilde{\Psi}^{+}_{L'}(\boldsymbol{r}_>) \tag{60}$$

with the same meaning of the symbols already introduced and remembering that the functions $\tilde{\Phi}_L(\boldsymbol{r})$ do not carry the normalization to one state per Rydberg. The second term on the rhs

is the singular part of the Green's function, $r_<(r_>)$ is the lesser (greater) of r, r' and $\tilde{\Psi}^+_{L'}(r)$ that solution of (59) inside cell i irregular at the origin that matches smoothly to $\tilde{H}^+_L(r)$ at the boundary. Making the reasonable assumption that the range of the functions $A_\alpha(r, r'; E)$ is of the order of the atomic dimensions (this is obviously true for A_0) and using (58), (60) in the expression (57), we finally obtain for the photoabsorption cross-section

$$\sigma_{\rm abs}(\omega) = -8\pi\alpha\hbar\omega\,{\rm Im}\sum_{m_0} M^{c*}_{L_0L}(\omega)\left(\tau^{oo}_{LL'} - T^o_{LL'}\right)M^c_{L_0L'}(\omega) + \sigma_{\rm at}(\omega) \tag{61}$$

due to the localization of the core initial state, with $M^c_{L_0L}$ given by (53) and defining an atomic absorption given by

$$\sigma_{\rm at}(\omega) = -8\pi\alpha\hbar\omega\,{\rm Im}\sum_{m_0}\int\int {\rm d}r\phi^c_{L_0}(r)\hat{e}\cdot r M(r, r'; \omega)\hat{e}\cdot r'\phi^c_{L_0}(r')\,{\rm d}r' \tag{62}$$

where

$$M(r, r'; \omega) = \sum_{\alpha,\alpha'} S^*_\alpha S_{\alpha'}\sum_{L,L'}\int\int A^*_\alpha(r, x; \omega)\tilde{\Phi}_L(x_<)T^o_{LL'}\tilde{\Psi}_{L'}(x_>)A_{\alpha'}(x', r'; \omega)\,{\rm d}x\,{\rm d}x'. \tag{63}$$

Equation (61) is the final expression we wanted to arrive at. It is valid under quite general conditions, as apparent from our derivation, and shows the natural partition into an atomic contribution and a MS one. By removing all cells of the cluster except the one containing the photo-absorber, $\tau^{oo}_{LL'}$ reduces to $T^o_{LL'}$ so that the MS contribution is zero. Even though in a multi-atom system one cannot define precisely an atomic entity, we shall continue to use the term atom as a useful reminder for the central cell and because it is after all a reasonable approximation to the isolated atom. The fact that the second site index is equal to the first means that electron source and detector coincide, as already anticipated. Indeed equation (61) tells us that the structural part of the photoabsorption cross-section $\sigma_{\rm str}(\omega)$ is proportional to the imaginary part of the product of the amplitude M for emitting the photoelectron, times the full scattering amplitude of propagation τ from the photoemitter site and back, times another amplitude M for detecting it.

Since the escape direction of the photoelectron has been integrated out, the only variable left is the energy and we can only test energy-dependent diffraction patterns. Compared to photoelectron diffraction, this means that these patterns might be distorted by the energy dependence of the matrix elements necessary to create and detect the photoelectron at the absorption site. However in all those cases where this dependence turns out to be smooth, we can hope to recover the structural information we are interested in. This condition requires that one can neglect electronic correlations in the final state and that only one configuration (Slater determinant) is predominant in the expansion (31). This happens with good approximation in the K-edge spectra of many materials where the final photoelectron states, being of p symmetry around the photoabsorber, are usually sufficiently delocalized not to suffer correlation effects with the electrons of the system. For example, this is the case of transition metal ions of the first series in the periodic table in many compounds and in particular in materials of biological interest. Moreover very often the spin-restricted (unrestricted) Hartree–Fock approximation for the initial state provides a reasonably good description to the ground state for closed (open) shell configurations. Only in special cases do we have examples of configuration mixing in the ground state, as in the case of Cu^{2+} ion in the La_2CuO_4 compound [36] or valence fluctuating compounds. In such instances a better strategy is to solve the multichannel equations for the configurations that enter in the ground state, eliminating all the other channels by expressing them as a function of the configurations of interest. This approach is currently in progress [37].

As we saw in section 3.1, the predominance of one configuration implies to a reasonable approximation that we can make the ansatz of locality and neglect the spatial dependence of $A_\alpha(\boldsymbol{r}-\boldsymbol{r}';\hbar\omega)$. Therefore, using the same kind of derivation as that of equation (80), we obtain for (58)

$$\sum_{\alpha,\alpha'} S_\alpha^* S_{\alpha'} G^+_{\alpha\alpha'}(\boldsymbol{r},\boldsymbol{r}';E) = |S_0(\omega)|^2 G^+_{00}(\boldsymbol{r},\boldsymbol{r}';E). \tag{64}$$

This equation, together with (57), tells us that the effect of the eliminated channels results in a shape function $|S_0(\omega)|^2$ that modulates the absorption coefficient originating from the primary channel

$$\sigma_{\rm abs}(\omega) = |S_0(\omega)|^2 \sigma^0_{\rm abs}(\omega). \tag{65}$$

The expression for $\sigma^0_{\rm abs}(\omega)$ is easily obtained by observing that in the same approximation (63) gives

$$M(\boldsymbol{r},\boldsymbol{r}';\omega) = |S_0(\omega)|^2 \sum_{L,L'} \tilde{\Phi}_L(\boldsymbol{r}_<) T^o_{LL'} \tilde{\Psi}_{L'}(\boldsymbol{r}_>) = |S_0(\omega)|^2 \tilde{M}(\boldsymbol{r},\boldsymbol{r}';\omega) \tag{66}$$

whereas (53) becomes, dropping $\hbar$,

$$M^c_{L_0L}(\omega) = \langle \bar{\Phi}_L(\boldsymbol{r})|\hat{\boldsymbol{e}}\cdot\boldsymbol{r}|\phi^c_{L_0}(\boldsymbol{r})\rangle \sum_\alpha S_\alpha A_\alpha(\omega) = \tilde{M}^c_{L_0L}(\omega) \sum_\alpha S_\alpha A_\alpha(\omega) \tag{67}$$

so that insertion in (61) and (62) provides the wanted result, simply by replacing the transition matrix elements M with $\tilde{M}$.

$$\begin{aligned}\sigma^0_{\rm abs}(\omega) &= -8\pi\alpha\hbar\omega {\rm Im} \sum_{m_0,L,L'} \tilde{M}^{c*}_{L_0L}(\omega)\left(\tau^{oo}_{LL'} - T^o_{LL'}\right)\tilde{M}^c_{L_0L'}(\omega) + \sigma^0_{\rm at}(\omega)\\ &= \sigma^0_{\rm str}(\omega) + \sigma^0_{\rm at}(\omega).\end{aligned} \tag{68}$$

Even with these approximations the first principle calculation of $|S_0(\omega)|^2$ is not an easy task. The most noticeable effect is provided by double electron transitions (that are included in our scheme), since they show up as a change of slope in the atomic background component of the cross-section [38], occurring at definite energies that depend on the photoabsorber. An analytical or numerical modelling of these effects would be highly desirable, although for our purposes it is sufficient to know that such kinks can be factorized into this shape function.

Before proceeding, we notice that in the case of real potential the terms proportional to the Kronecker symbol δ_{ij} in equation (60) differ by a real quantity [47], so that the absorption cross-section reduces to expression (56). In this case the atomic absorption $\sigma^0_{\rm at}(\omega)$ can also be written as

$$\sigma^0_{\rm at}(\omega) = -8\pi\alpha\hbar\omega\, {\rm Im} \sum_{m_0,L,L'} \tilde{M}^{c*}_{L_0L}(\omega) T^0_{LL'} \tilde{M}^c_{L_0L'}(\omega). \tag{69}$$

At this point we are left with the problem of determining the nature of the optical potential $\Sigma^{\rm opt}(\boldsymbol{r},\boldsymbol{r}';E)$ in (59). This potential contains both the effect of the intrinsic channels (excitations induced in the system by the sudden creation of the core hole) and of the extrinsic channels (excitations created by the photoelectron in its way out of the system). Model systems to describe both types of processes and their interference have been studied by some authors [40, 41]. However, a practical scheme for realistic calculations has not been devised yet. The only optical potentials currently in use are those based on the Dyson self-energy of the photoelectron propagation in the system. This clearly accounts only for the extrinsic losses. Depending on the systems, various reasonable approximations have been devised.

It is well known, for example, that for metals we can obtain very good agreement with the observed absorption spectra by using a one-particle approach with an X–α potential and

convoluting the calculated spectrum with a Lorentzian broadening function, which has an energy-dependent width related to the mean free path of the photoelectron in the system by the relation [42, 43]

$$\Gamma(E) = \frac{\hbar}{\lambda(E)}\left(\frac{2E}{m}\right)^{\frac{1}{2}}$$

where $\Gamma(E)$ is the full width at half maximum. Here conventional units are used.

In the framework of the above multi-channel approach this finding can be rationalized by observing that in a metal the completely relaxed channel together with the plasmon excitation channels (whether intrinsic or extrinsic) almost completely exhaust the sum rule

$$\sum_{\alpha} |S_\alpha|^2 = \sum_{\alpha} \langle \Psi_{\rm g}^{N-1} | \tilde{\Psi}_\alpha^{N-1} \rangle \langle \tilde{\Psi}_\alpha^{N-1} | \Psi_{\rm g}^{N-1} \rangle = \langle \Psi_{\rm g}^{N-1} | \Psi_{\rm g}^{N-1} \rangle = 1$$

which holds because of the completeness of the intermediate relaxed states $\tilde{\Psi}_\alpha^{N-1}$. Indeed, the intensity of the double-electron excitation channels is of the order of 10^{-2}–10^{-3} times that of the main relaxed channel [39]. Therefore, an optical potential given by $V_{X-\alpha} + {\rm i}\Gamma(E)$ is able to give a satisfactory picture of the absorption process for metals. The only discrepancy with experiments lies in the calculated absorption maxima falling short of the observed ones due to the energy independence of the X–α exchange.

A better approximation is provided by the Hedin–Lundqvist (H–L) potential [6, 7], owing to its energy-dependent exchange and its imaginary part that is able to reproduce rather accurately the observed mean free path in metals [44]. This is the self-energy, based on the GW approximation, of an electron propagating in a homogeneous interacting electron gas, calculated at the local density of the system under study. Although initially devised to describe exchange and correlation corrections to the Coulomb potential due to the valence charge, Lee and Beni [45] have extended its validity in the atomic core region as well.

By neglecting the effect of the intrinsic processes, one can indeed approximate $\Sigma^{\rm opt}(\boldsymbol{r}, \boldsymbol{r}'; E)$ as the Dyson self-energy of the photoelectron in the final state. This approximation is consistent with the physical picture of the photoabsorption process, in which we add an electron to the ground state of the $(Z+1)$-equivalent atom. From this point of view $G_{00}(\boldsymbol{r}, \boldsymbol{r}'; E)$ describes the propagation amplitude of the excited photoelectron from point $\boldsymbol{r}$ to point $\boldsymbol{r}'$. This is the probability amplitude that the added electron remains in the same original state in which it was added to the system. Its imaginary part gives the total probability amplitude for scattering out of this initial state. In this scheme the self-energy $\Sigma_D(\boldsymbol{r}, \boldsymbol{r}'; E)$ acts as a complex optical potential that describes the reduction of the wavefunction amplitude of the elastic channel, due to the transitions to all the other channels. The localization of the initial core state has the consequence that the optical paths of the photoelectron in the final state begin and end at the photoabsorbing site. We expect that neglecting the effects of the intrinsic processes on $\Sigma^{\rm opt}(\boldsymbol{r}, \boldsymbol{r}'; E)$ is a reasonably good approximation, since their main effect is already incorporated in the shape function $|S_0(\omega)|^2$.

One can therefore interpret the H–L potential as an effective optical potential that controls the propagation and damping of the excited photoelectron everywhere in the system. In this approach it can be viewed as a local density approximation to the self-energy of the photoelectron in real systems. Nowadays it is the potential most widely used in the calculation of the absorption and photoelectron diffraction cross-sections of many systems, ranging from metals and semiconductors to ionic and covalent systems with varied success.

Finally, Fujikawa *et al* [8] have improved on the H–L potential by restricting its validity to the valence charge, as originally devised. They relied on the GW approximation for the photoelectron self-energy $\Sigma_{GW} = GW$ in the solid, where $W = \epsilon^{-1}V$, V is the bare Coulomb interaction and $\epsilon = 1 - VP$ is the dielectric response function of the system, and

split both the polarization propagator $P = P^v + P^c$ and the one-electron Green's function $G = G^v + G^c$ into core and valence parts. Since the core polarization was assumed to be much smaller than the valence polarization, they obtain an expansion in powers of P^c for $\Sigma_{GW} = G^v W^v + V^c_{\rm ex} + G^v W^v P^c W^v + \cdots$. Here $G^v W^v$ is the self-energy for the valence electrons, which, when calculated via the plasmon-pole approximation for the dielectric function, is equivalent to the H–L potential, $V^c_{\rm ex} = G^c V$ is the bare Hartree–Fock exchange and $G^v W^v P^c W^v$ is the screened polarization potential for the ion cores. Details of this latter are given in appendix C of [1]. Preliminary calculations for a photoelectron with kinetic energy greater than about 100 eV show that this non-local potential gives the same scattering amplitude as the total H–L potential at large scattering angles, whereas it provides a better description of the small-angle scattering. More work is however needed to establish its performance at low photoelectron energies.

Once the optical potential has been specified, one can proceed to the calculation of the key ingredients in (68), namely the cell functions $\tilde{\Phi}_L(\boldsymbol{r})$ and $\tilde{\Psi}^+_L(\boldsymbol{r})$ in the absorbing sphere, needed to calculate the atomic absorption $\sigma^0_{\rm at}(\omega)$ and the transition matrix elements $\tilde{M}$ creating the photoelectron, and the scattering path operator $\tau^{ij}_{LL'} = [(T_c^{-1} + G)^{-1}]^{ij}_{LL'}$. The inversion of the MS matrix $(T_c^{-1} + G)$ becomes time consuming at energies greater than about 50–150 eV, depending on the number of cells in the cluster. Fortunately, in the majority of cases, above ~50 eV one can invert the MS matrix by series expansion

$$\begin{aligned} \boldsymbol{\tau} &= (T_c^{-1} + G)^{-1} = (I + T_c G)^{-1} T_c \\ &= \sum_n (-1)^n (T_c G)^n T_c = \sum_n (-1)^n T_c (G T_c)^n \end{aligned} \tag{70}$$

so that the total absorption is seen to be made up of an atomic smooth contribution plus an infinite series of oscillatory signals [46, 47]. This observation has been the basis for the development of computer codes for analysing the EXAFS signal and based on the empirical extraction of a structural signal from the experimental data to compare with the theoretical signal (GNXAS [2, 3], FEFF [5] and EXCURVE [4] packages).

A major ingredient in the extraction procedure is the definition of a background atomic absorption coefficient $\mu_{\rm at}(\omega)$ such that the structural signal is defined as

$$\chi(\omega) = \frac{\mu(\omega) - \mu_{\rm at}(\omega)}{\mu_{\rm at}(\omega)}.$$

By identifying $\mu_{\rm at}(\omega)$ with $\sigma_{\rm at}(\omega)$ (ignoring the usual proportionality factor $N\rho/A$, where N is the Avogadro number) one is led by (68) to the identification

$$\chi(\omega) = \frac{\sigma^0_{\rm str}(\omega)}{\sigma^0_{\rm at}(\omega)}. \tag{71}$$

In this formula the shape function $|S_0(\omega)|^2$ seems to have dropped out from the ratio. However, this is a consequence of the identification of $\mu_{\rm at}(\omega)$ with $\sigma_{\rm at}(\omega)$, which is only approximate due to the empirical definition of $\mu_{\rm at}(\omega)$, that does not take into account the exact form of $|S_0(\omega)|^2$. The nearer is $\mu_{\rm at}(\omega)$ to $\sigma_{\rm at}(\omega)$, the more exact is the independence of $\chi(\omega)$ from the shape function. This is the reason why in many instances of EXAFS analysis $|S_0(\omega)|^2$ seems to be constant and very near to unity. Also notice that the atomic absorption $\sigma^0_{\rm at}(\omega)$ does not factorize from the structural signal $\sigma^0_{\rm str}(\omega)$. Indeed, only if the optical potential is real is the structural signal proportional to the atomic absorption, which in this case takes the form (69). However, due to the presence of inelastic processes, the potential is complex and this different behaviour of $\sigma^0_{\rm at}(\omega)$ and $\sigma^0_{\rm str}(\omega)$ should be taken into account in a refined treatment of the experimental data.

Therefore, in order to extract structural and electronic information on the system under study, rather than relying on an empirical definition of $\mu_{\rm at}(\omega)$, which becomes more and more difficult to define in the XANES part of the absorption spectrum, one should naturally try to fit the entire experimental spectrum, all the more since the relevant information is confined in the first 100–150 eV from the edge and consequently well within the energy range where a complete inversion of the MS matrix is possible for a wide variety of systems. Indeed, from the photoelectron diffraction studies one already knows that the coherent diffraction process carrying the structural information is well described by an optical potential of the H–L type [48, 33]. Regarding the matrix elements for the creation of the photoelectron and its energy dependence, past and present experience indicate that the smoothing action of the complex part of the potential helps us in reproducing the correct behaviour. Remaining discrepancies can be rather easily absorbed into a redefinition of this complex part. Even the effect of the shape function $|S_0(\omega)|^2$ on the absorption spectrum, under the assumptions described above, can be mimicked via an additional damping. These statements have been substantiated by the applications of the method to particular systems [49].

3.3. The mean free path

In this section we shall show explicitly that the mathematical structure of the theory, in both spectroscopies, contains the intuitive picture of the photoelectron damping in the expected way, by making contact with existing expressions for the mean free path λ. Since the optical potential is complex, one expects that the coherent part of the propagation, which only carries the structural information, be attenuated by a damping factor related to the mean free path of the photoelectron in the system, whereas incoherent terms should appear describing the effects of scattering out of the coherent channel due to the presence of inelastic processes, described by the complex part of the potential.

Indeed, we shall find out how the incoherent terms due to the presence of inelastic processes find their place into the theory and, as a by-product, how we can mimic their effects when we ignore the details of their manifestation.

For sake of illustration we shall assume that the MS series for $\boldsymbol{\tau}$ in (70) converges and that the optical potential is local and of the muffin-tin form. The general n th term of the series, dropping one factor T_c^o that factorizes into the amplitude for emitting and detecting the photoelectron, has the form

$$\left[(T_c G)^n\right]^{of}_{LL'} = \sum_{i,j,\ldots,k} \sum_{L_1,L_2,\ldots,L_n} t^o_l G^{oi}_{LL_1} t^i_{l_1} G^{ij}_{L_1L_2} t^j_{l_2} \cdots G^{kf}_{L_nL'} \tag{72}$$

where $t^i_l = k^{-1} e^{i\delta^i_l} \sin\delta^i_l$ is the atomic scattering matrix for the atom at site i and angular momentum l in terms of the corresponding phase shift δ^i_l and $G^{ij}_{LL'}$ the spherical wave propagators already introduced in appendix A. Without loss of generality, for simplicity we shall consider in (72) a closed path with three sites o, i and j, so that $j = k$, $f = o$ and $L_n = L_2$. The extension of the argument to the most general case will then be straightforward.

Since the potential is complex, the generic atomic phase shift δ is also complex so that we can write $\delta = \delta_1 + i\delta_2$. Therefore,

$$\begin{aligned} kt &= e^{i\delta}\sin\delta \\ &= e^{-2\delta_2} e^{i\delta_1}\sin\delta_1 + i\frac{1-e^{-2\delta_2}}{2} \end{aligned} \tag{73}$$

which reduces to the known expression with real δ in the limit $\delta_2 \longrightarrow 0$. In an electron–atom scattering process with complex potential [50] it is known that, within a factor k^{-2}, $\mathrm{Im}[kt]$ represents the total scattering cross-section (elastic plus inelastic), whereas $|kt|^2$ gives

the elastic cross-section (without energy loss for the impinging electron). On the basis of the definition (73) the relation

$$\mathrm{Im}[kt] = |kt|^2 + \frac{1 - \mathrm{e}^{-4\delta_2}}{4}$$

holds, so that $(1 - \mathrm{e}^{-4\delta_2})/4$ is the inelastic cross-section. For convenience we shall work henceforth in terms of the dimensionless quantity kt, since the propagator G in (72) is proportional to k, the photoelectron momentum.

From (73) it is clear that the coherent signal is obtained by choosing for all the kt factors appearing in (72) the term $\mathrm{e}^{-2\delta_2}\mathrm{e}^{\mathrm{i}\delta_1}\sin\delta_1$. All the other terms containing at least one factor $\mathrm{i}(1-\mathrm{e}^{-2\delta_2})/2$ describe inelastic processes with loss of coherence for the photoelectronic wave. Indeed we have $(1 - \mathrm{e}^{-2\delta_2})/2 \simeq (1 - \mathrm{e}^{-4\delta_2})/4 \simeq \delta_2$ for sufficiently small δ_2, which is usually the case.

Concerning the coherent signal of interest, we see that it has the same form and value as the structural signal obtained for a real potential, except for a damping factor coming from each kt and each propagator G. To proceed further we need to find an expression for this latter. Again for illustrative purposes we shall work in the so-called plane wave approximation (PWA), but it can be shown that all the following considerations are valid even when spherical wave corrections for the photoelectron propagating wave are taken into account. In the PWA we can write [32]

$$G^{ij}_{LL'} \simeq \frac{\mathrm{e}^{\mathrm{i}\kappa^I R_{ij}}}{\kappa^I R_{ij}} Y_L(\hat{\boldsymbol{R}}_{ij}) Y_{L'}(\hat{\boldsymbol{R}}_{ij})$$

where R_{ij} is the distance between sites i and j, and $\kappa^I = [E - V_I]^{1/2} = \kappa^I_1 + \mathrm{i}\kappa^I_2$ is the photoelectron momentum in the interstitial region, where the potential V_I is constant and can be complex.

Calling R_i the sphere radius of the potential at site i, it is easily seen that in the case of the three sites o, i and j the damping is represented by an exponential factor with exponent

$$-2\delta^o_2 - \kappa^I_2 R_{oi} - 2\delta^i_2 - \kappa^I_2 R_{ij} - 2\delta^j_2 - \kappa^I_2 R_{jo}. \tag{74}$$

We now need an expression for the phase shift δ^i, which in the WKB approximation is given by [51]

$$\delta^i = \int_0^{R_i} [E - V_i(r)]^{\frac{1}{2}}\,\mathrm{d}r - \kappa^I R_i \tag{75}$$

where the potential $V_i(r)$ inside the sphere R_i is assumed to be complex. Notice that, in keeping with the plane wave approximation for the propagator G, we have dropped the centrifugal term in the WKB expression, so that in this case the phase shifts are independent of the angular momentum l. However, as already emphasized, the argument remains valid even when spherical wave corrections are taken into account.

Considering now that in the path going from site o, the photoabsorbing site, to site i and j and back to o, each atom is traversed for a length $2R$, if R is the radius of the corresponding sphere, writing $R_{\mathrm{path}} = R_{oi} + R_{ij} + R_{jo}$ for the total length of the path we see that the damping factor is given by $\exp(-\kappa_2 R_{\mathrm{tot}})$, where

$$\kappa_2 = R^{-1}_{\mathrm{path}}\,\mathrm{Im}\int_{\mathrm{path}} [E - V(r)]^{\frac{1}{2}}\,\mathrm{d}r \tag{76}$$

since in the interstitial region $V(r) \equiv V_I$ and e.g. inside sphere j, $V(r) \equiv V_j(r)$. This is exactly the same expression we would have obtained had we studied the propagation of an

electronic wave in the potential $V(r)$, by solving the problem in the WKB approximation. The mean free path is accordingly given by

$$\lambda = (2\kappa_2)^{-1} \tag{77}$$

consistent with the fact that $\exp(-\kappa_2 R_{\text{tot}})$ is an attenuation factor for an amplitude of propagation. This finding substantiates what was anticipated in the introduction, namely that in absorption spectra only atoms within a sphere centred on the emitter with radius equal to the mean free path contribute to the absorption structure, since the cross-section is given by the imaginary part of a scattering amplitude and only closed paths are possible. In contrast, in PED, AED and, as we shall see, LEED/MEED this radius equals twice the mean free path, since the cross-section is proportional to the square of a scattering amplitude with interference between different contributions (direct atomic versus propagation processes).

Starting from equation (76), a further simplification is achieved if we take into account that everywhere in the system $E - V_1(r) \gg V_2(r)$, $V_1(r)$ and $V_2(r)$ being the real and imaginary parts of the potential. Then, expanding the square root in (76) as

$$[E - V(r)]^{\frac{1}{2}} \simeq [E - V_1(r)]^{\frac{1}{2}} + \frac{\mathrm{i}}{2} V_2(r)[E - V_1(r)]^{\frac{1}{2}}$$

we obtain

$$\kappa_2 = 2R_{\text{path}}^{-1} \int_{\text{path}} V_2(r)[E - V_1(r)]^{\frac{1}{2}}\,\mathrm{d}r \leqslant (2kR_{\text{path}})^{-1} \int_{\text{path}} V_2(r)\,\mathrm{d}r$$

remembering that $k = E^{1/2}$. Therefore, from (77) we finally get in atomic units

$$\lambda(\text{au}) = \frac{k(\text{au}^{-1})}{\bar{\Sigma}_2(\text{Ryd})} \tag{78}$$

defining $\bar{\Sigma}_2 = R_{\text{path}}^{-1} \int_{\text{path}} V_2(r)\,\mathrm{d}r$, since $V_2(r)$ is actually a self-energy. This expression is the same as that given by Penn [44], who has in conventional units

$$\lambda = \frac{\hbar^2 k^2}{2mk\bar{\Sigma}_2} = \frac{E_k}{k\bar{\Sigma}_2}$$

taking into account that $E_k = k^2$ (Ryd), with the only difference that $\bar{\Sigma}_2$ is defined as a volume average of the imaginary part of the H–L self-energy instead of a line average as here.

From the above discussion we see that what actually determines the photoelectron damping is a line average of the various MS paths. If the system is homogeneous enough this average will not sensibly depend on the path, so that we can ignore in practice the position dependence of the self-energy and replace it by a function of only the energy of the photoelectron: $E = \hbar\omega - I_c$. Since the cross section is analytical in the energy E, neglecting the cut at the Fermi energy, we can approximately take into account the effect of the absorptive part of the potential on the cross-section $\sigma^r_{\text{abs}}(E)$, calculated with the real part of the potential, by performing the following convolution:

$$\begin{aligned}\sigma^r_{\text{abs}}(E) &= \pi^{-1} \int_{\epsilon_F}^{\infty} \bar{\Sigma}_2(E')\sigma^r_{\text{abs}}(E')\left[(E - E')^2 + \bar{\Sigma}_2^2(E')\right]^{-1}\,\mathrm{d}E' \\ &\simeq \sigma^r_{\text{abs}}[E - \mathrm{i}\bar{\Sigma}_2(E)]\end{aligned}$$

which holds if we are away from the edge, so that we can extend the integral to $-\infty$ and provided $\bar{\Sigma}_2(E)$ does not vary too rapidly with E. Explicit calculations via both methods substantiate this statement.

From this point of view, the effect of the core-hole lifetime can be easily incorporated in the theory by adding $\Gamma_h/2$ to $\bar{\Sigma}_2(E)$, where Γ_h is the full width at half maximum of the core

hole and related to its lifetime by the relation $\tau = \hbar/\Gamma_h$. We assume here an exponential decay of the core hole, which is true in the vast majority of the cases of our interest. To estimate the effect of this added damping on the mean free path one has simply to evaluate equation (78) by replacing $\bar{\Sigma}_2(E)$ with $\Gamma_h/2 + \bar{\Sigma}_2(E)$, so that

$$\lambda_{\rm tot} = \frac{E_k}{k(\bar{\Sigma}_2 + \Gamma_h/2)} \longrightarrow \lambda_{\rm tot}^{-1} = \frac{\bar{\Sigma}_2}{k} + \frac{\Gamma_h}{2k} = \lambda_{in}^{-1} + \lambda_h^{-1} \tag{79}$$

with obvious meaning for λ_{in} (inelastic mean free path) and λ_h (mean free path corresponding to the finite lifetime of the core hole).

In the H–L approximation for the self-energy, at energies lower than the plasmon energy the mean free path would be infinite if it were not limited by the core-hole lifetime. This is due to the plasmon pole approximation that we have retained in the expression for the dielectric function of Σ_h (see appendix B of [1]). Damping originating from channels other than plasmon excitations (creation of electron–hole pairs) cannot be calculated in this approximation. These latter have however been evaluated [6] and found negligible compared to the core-hole lifetime and the experimental resolution. They can be introduced back in using the formula given by Quinn and Ferrell [52], as implemented in the *FEFF* code [5]. After the photoelectron reaches the plasmon energy, it interacts with the electron gas by creating plasmon excitations and suffering a reduction in the coherent wavefunction amplitude. This fact would entail a rather sharp decrease in the photoelectron mean free path, which should show up as a localized feature in photoabsorption spectra. In reality, the setting in of the plasmon damping is not so sharp due to the quantum interference between intrinsic and extrinsic losses at the plasmon edge [40, 41]. Therefore, we introduce an empirical modelling of this fact in our fitting analysis that takes into account both this smooth opening of the plasmon loss channel and the effect of the electron–hole excitations.

4. Probe electron detected

As we have seen previously in the case of photoabsorption and photoemission (see sections 3.1 and 3.2), whether the photoelectron is detected or not changes the expression of the cross-section. Indeed, in the latter case, a sum has to be made on all the possible final states due to the probe electron not being detected. We will therefore make the distinction between the two cases now, and focus in the present section on the spectroscopies involving the detection of the probe electron.

4.1. Core level photoelectron diffraction

Photoelectron diffraction is just a particular case of photoemission. It consists in monitoring a photoemission feature corresponding to a particular excitation channel (usually a core level peak but it can be any other structure) as a function either of the energy of the photoelectron or its escape direction (polar and azimuthal angles). Therefore, the case of core level photelectron diffraction is described by expression (54) of the differential cross-section.

We shall now consider the case where we can neglect electronic correlations in the final state and where only one configuration, i.e. one Slater determinant, is predominant in the expansion (31) of the ground state wavefunction. The predominance of one particular configuration implies that the spectral shape of the excited channels is rather featureless and similar to the ground state, since most of them consist in particle-hole or plasmon-like excitations which do not change drastically the ground state potential. This means that to a reasonable approximation we can put $A_\alpha(\boldsymbol{r}, \boldsymbol{r}'; \hbar\omega) = A_\alpha(\hbar\omega)\delta(\boldsymbol{r} - \boldsymbol{r}')$. Inserting this

approximation in (53) leads to

$$M^c_{L_0L}(\hbar\omega) = \langle\tilde{\Phi}_L(\boldsymbol{r})|\hat{e}\cdot\boldsymbol{r}|\phi^c_{L_0}(\boldsymbol{r})\rangle \sum_\alpha S_\alpha A_\alpha(\hbar\omega)$$
$$= \tilde{M}^c_{L_0L}(\hbar\omega)\sum_\alpha S_\alpha A_\alpha(\hbar\omega). \tag{80}$$

Writing $|\sum_\alpha S_\alpha A_\alpha(\omega)|^2 = |S_0(\omega)|^2$ due to the fact that $|S_0|^2$ is the preponderant term of the series (by definition $A_0(\omega) = 1$), we obtain for the cross-section

$$\frac{\mathrm{d}\sigma}{\mathrm{d}\hat{\boldsymbol{k}}_0} = 8\pi^2\alpha\hbar\omega\,|S_0(\hbar\omega)|^2\sum_{m_0}\left|\sum_L \tilde{M}^c_{L_0L}(\hbar\omega)B^o_L(\boldsymbol{k}_0)\right|^2. \tag{81}$$

The prefactor $|S_\alpha(\hbar\omega)|^2$ in the previous equation (we resume for the moment the general channel index as similar expressions as (81) can be worked out for the other non-elastic channels $\alpha \neq 0$) gives the fraction of photoelectrons that go in the particular channel under consideration. Its $\hbar\omega$ dependence describes the effect of the opening of the various channels and in the limit $\hbar\omega \to \infty$ it equals the asymptotic value S_α of the sudden approximation.

Using definition (51) of the amplitudes $B^o_L(\boldsymbol{k}_0)$, the cross-section for core photoelectron diffraction in the elastic channel $\alpha = 0$ can be written as

$$\frac{\mathrm{d}\sigma}{\mathrm{d}\hat{\boldsymbol{k}}_0} = 8\pi^2\alpha\hbar\omega\frac{k_0}{\pi}\,|S_0(\hbar\omega)|^2\sum_{m_0}\left|\sum_j\sum_{L,L'}\tilde{M}^c_{L_0L}(\hbar\omega)\tau^{oj}_{LL'}\mathrm{i}^{l'}Y_{L'}(\hat{\boldsymbol{k}}_0)\mathrm{e}^{\mathrm{i}\boldsymbol{k}_0\cdot\boldsymbol{R}_{jo}}\right|^2. \tag{82}$$

Use of such an expression is particularly rewarding as it permits us to realistically calculate photoemission intensity at low kinetic emission energy. This spectroscopy allows us, in a peculiar way, to keep track of the individual single emitters on the surface with respect to other atomic emitters in the bulk due to their core level energy shifts [53]. At this energy the photoelectron current in semiconductors and insulators shows high angular anisotropy [54, 55], which greatly increases the sensitivity of photoemission to the very first atomic layers. A variety of physical effects related to the structural origin of the core levels are disclosed by PED experiments: namely core level shifts due to initial versus final state electronic effects, chemical reactions (heterogrowth for instance) versus structural phase transitions, adsorption mechanisms and vibronic coupling in small chemisorbed molecules. The first example of such a study of a core level shift analysis on Si [56] was the high anisotropy PED data measured on the single-domain Si(001)-2 × 1 surface, which was mainly due to the static (i.e. not flipping) nature of the buckled Si dimers (in marked contrast with more or less recent assertions about the average symmetric configuration due to a rapidly flipping Si dimer, claimed to explain controversial microscopy and photoemission data). Another important study which is still far from being complete is the origin of the core level shifts in semiconductors, where a competition between initial state effects (due to static screening) and final state effects (due to dynamical screening) adds significant insight into the many-body theory of the shift.

In the case of the Ge(001) surface (figure 1) this kind of study has led to a picture of the Ge surface somewhat less affected by screening effects than expected from the *ab initio* theory. Finally, we have recently adapted the method to the study of adsorption geometry of cyclic molecules on Si surfaces. Organic chemistry on surfaces is still an open field of investigation that can have a great impulse from techniques like photoelectron diffraction. The geometry of small cyclic molecules on the Si surface, used to functionalize the Si surface for further chemical manipulations, has been investigated on the basis of a large data set of angle resolved measurements [57] of the photoemission intensity on the basis of equation (82) and suitable analysis programs [34].

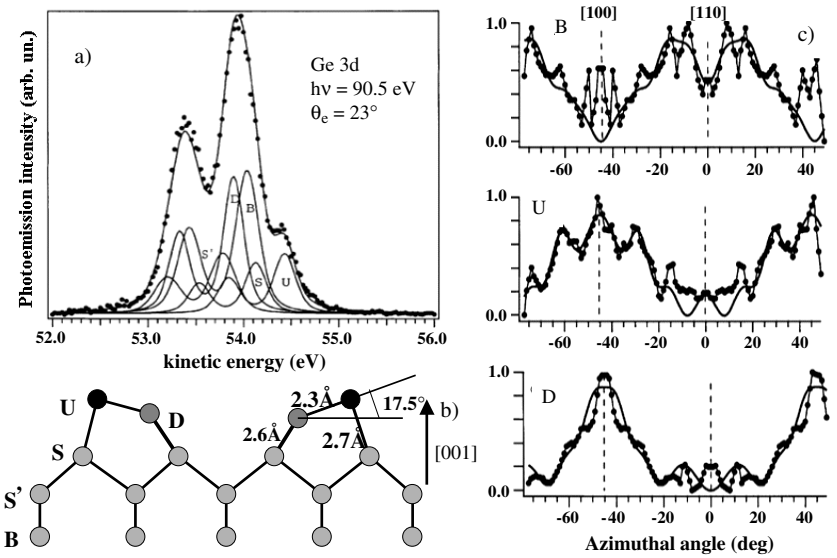

Figure 1. (a) Photoemission intensity of the Ge 3d core level at high resolution and liquid nitrogen temperature on the c(4 × 2)-Ge(001) surface. The structural origin of the peaks is labelled as sketched in panel (b). (c) Comparison of azimuthal dependence of MS theory with the deconvoluted experimental intensity of the three main components of the core level [53].

4.2. Valence level photoelectron diffraction

Let us now compare equation (82) to the photoemission cross-section from a valence state in order to discuss the relation between these two spectroscopies. We shall deal again with the simple case of weak electronic correlation, where one can safely assume that the initial state wavefunction $\Psi_G^N(\boldsymbol{r}_i)$ can be factorized as a properly antisymmetrized product $\phi_v(\boldsymbol{r})\Psi_G^{N-1}(\boldsymbol{r}_i)$, where $\phi_v(\boldsymbol{r})$ is the valence state.

Under this assumption, if we partition the muffin-tin space in cells around the spheres that cover the whole space (e.g. Wigner–Seitz cells for periodic systems), we obtain for the photoemission cross-section in the elastic channel

$$\begin{aligned}\frac{\mathrm{d}\sigma}{\mathrm{d}\hat{\boldsymbol{k}}_0} &= 8\pi^2\alpha\hbar\omega\frac{k_0}{\pi}|S_0(\hbar\omega)|^2\left|\sum_i\sum_L \tilde{M}_L^{vi}B_L^i(\boldsymbol{k}_0)\right|^2 \\ &= 8\pi^2\alpha\hbar\omega\frac{k_0}{\pi}|S_0(\hbar\omega)|^2\left|\sum_{i,j}\sum_{L,L'}\tilde{M}_L^{vi}(\boldsymbol{k}_{\mathrm{BZ}})\tau_{LL'}^{ij}i^{l'}Y_{L'}(\hat{\boldsymbol{k}}_0)\mathrm{e}^{\mathrm{i}\boldsymbol{k}_0\cdot\boldsymbol{R}_{jo}}\right|^2 \end{aligned} \tag{83}$$

where now the cell matrix element

$$\tilde{M}_L^{vi} = \langle\tilde{\Phi}_L(\boldsymbol{r})|\hat{e}\cdot\boldsymbol{r}_i|\phi_v^i(\boldsymbol{r}_i)\rangle$$

bears the index i of the cell which the space integral is referred to.

For periodic systems with one atom per unit cell we can write, neglecting surface effects,

$$\tilde{M}_L^{vi} = \tilde{M}_L^{vo}(\boldsymbol{k}_{\mathrm{BZ}})\mathrm{e}^{-\mathrm{i}\boldsymbol{k}_{\mathrm{BZ}}\cdot\boldsymbol{R}_{io}} \tag{84}$$

where we have made explicit the dependence of the matrix element on the Brillouin zone (BZ) vector $\boldsymbol{k}_{\mathrm{BZ}}$ of the valence band state. In this case the expression for the cross-section becomes

$$\frac{\mathrm{d}\sigma}{\mathrm{d}\hat{\boldsymbol{k}}_0} = 8\pi^2\alpha\hbar\omega\frac{k_0}{\pi}|S_0(\hbar\omega)|^2\left|\sum_{i,j}\sum_{L,L'}\tilde{M}_L^{vo}(\boldsymbol{k}_{\mathrm{BZ}})\mathrm{e}^{-\mathrm{i}\boldsymbol{k}_{\mathrm{BZ}}\cdot\boldsymbol{R}_{io}}\tau_{LL'}^{ij}\mathrm{i}^{l'}Y_{L'}(\hat{\boldsymbol{k}}_0)\mathrm{e}^{\mathrm{i}\boldsymbol{k}_0\cdot\boldsymbol{R}_{jo}}\right|^2 \tag{85}$$

which is to be compared with the analogous expression for LEED/MEED to be derived below.

Of particular importance is the high energy case in which one integrates over the BZ at fixed direction of escape of the photoelectron. Taking into account the relation

$$\frac{1}{N}\sum_{\boldsymbol{k}_{\mathrm{BZ}}}\mathrm{e}^{-\mathrm{i}\boldsymbol{k}_{\mathrm{BZ}}\cdot\boldsymbol{R}_{io}} = \delta_{io}$$

where N is the total number of unit cells in the system and introducing the average matrix element

$$\overline{M}_L^{vo} = \frac{1}{N}\sum_{\boldsymbol{k}_{\mathrm{BZ}}}\tilde{M}_L^{vo}(\boldsymbol{k}_{\mathrm{BZ}})$$

one finds

$$\sum_{\boldsymbol{k}_{\mathrm{BZ}}}\frac{\mathrm{d}\sigma}{\mathrm{d}\hat{\boldsymbol{k}}_0} \approx 8\pi^2\alpha\overline{\hbar\omega}\frac{k_0}{\pi}|S(\overline{\hbar\omega})|^2\sum_i\left|\sum_{j,L,L'}\overline{M}_L^{vo}\tau_{LL'}^{ij}\mathrm{i}^{l'}Y_{L'}(\hat{\boldsymbol{k}}_0)\mathrm{e}^{\mathrm{i}\boldsymbol{k}_0\cdot\boldsymbol{R}_{ji}}\right|^2 \tag{86}$$

where $\overline{\hbar\omega}$ is an average photon energy over the valence band width and we have inserted in the formula an irrevelant factor $\mathrm{e}^{-\mathrm{i}\boldsymbol{k}_0\cdot\boldsymbol{R}_{io}}$ to be able to refer site j to site i instead of o.

In other words, if one integrates over the energy of the initial valence state in the BZ, the amplitudes of photoemission originating from the various unit cells do not interfere any more and the resulting intensity is interpretable in terms of a localized source. There is still a difference between this case and the inner shell case though, since the valence state contains more L components in the wavefunction than the core state so that different combinations of final L components of the scattering path operator τ interfere to give the photoemitted intensity.

4.3. The Auger electron diffraction

The case of Auger diffraction is quite similar to photoelectron diffraction as only the excitation process differs. Kostroun *et al* [58], among others, have proposed an atomic theory of this effect. Here, we shall derive the cross-section for Auger electron diffraction, i.e. in the case where the scattering of the escaping Auger electron by the atoms of the surrounding cluster is fully taken into account.

The present calculation of the Auger process rests on the following assumptions.

(i) The effect is considered as a two-step process (ionization and decay). The ionization step is of no further interest, so the initial state has a core hole localized on one of the atoms of the cluster under investigation.
(ii) A non-relativistic first order treatment of the decay (Wentzel *ansatz* [59]) is used. Since our aim is the description of the diffraction process of the continuum Auger electron, we can adopt this kind of approximation without loss of generality, as apparent from the following assumption.
(iii) The ejected Auger electron is decoupled from the other electrons of the system, so that one has the option to treat the remaining electrons under more or less sophisticated approximations.

As is well known, the process originates from the de-excitation of an electron belonging to an upper orbital into the initial hole, with the concomitant transfer, via the Coulomb interaction, of the de-excitation energy to another electron (the Auger electron). Therefore, the problem we

have to treat here is a two-potential problem as we have to take the sample potential into account as well.

From section 2.3, and more particularly equation (26), we deduce that the Auger transistion probability per unit time can be written as

$$W_{i\to f} = \frac{2\pi}{\hbar}\left|\langle[\Psi_f^-]^{(N-1)}|V_c|\Psi_i^{(N-1)}\rangle\right|^2 \rho(E_f)$$

where $V_c = 1/2\sum_{i\neq j} e^2/r_{ij}$ is the Coulomb potential describing the interaction of the electrons involved in the transition with the other electrons of the system and $\rho(E_f)$ is the density of final states for the energy E_f that satisfies the conservation of energy.

The transition is between a state of $(N-1)$ electrons $|\Psi_i^{(N-1)}\rangle$ (if N is the number of electrons in the neutral cluster) containing a core hole described by the wavefunction $\phi_c(\boldsymbol{r})\chi_c \equiv \phi_c(\boldsymbol{x})$ (where χ is a spin state and $\boldsymbol{x}$ stands for a spin-space variable) and decoupled from the valence electrons, and a state $\langle[\Psi_f^-]^{(N-1)}|$ containing a continuum electron described by $\phi_{\boldsymbol{k}}^-(\boldsymbol{r})\Theta\chi_k \equiv \phi_{\boldsymbol{k}}^-(\boldsymbol{x})$ (Θ being the time-reversal operator) and two holes not necessarily localized onto the atom making the transition (they can both be valence or core electrons or one core and one valence electron). As in the photoemission case, the exponent $(-)$ indicates that the wavefunction of the escaping electron obeys a boundary condition that accounts for the fact that there is no electron in the continuum in the remote past.

The initial Auger state can be written in all generality as

$$\Psi_i^{N-1}(\boldsymbol{x}_1,\ldots,\boldsymbol{x}_{N-1}) \tag{87}$$

whereas under the assumptions described above and similarly to the photoemission case (32) we can write for the final state

$$\Psi_f^{N-1}(\boldsymbol{x}_1,\ldots,\boldsymbol{x}_{N-1}) = ((N-1)!)^{1/2}A\sum_\alpha \phi_{\alpha\boldsymbol{k}}^-(\boldsymbol{x}_1)\phi_c(\boldsymbol{x}_2)\tilde{\Psi}_\alpha^{N-3}(\boldsymbol{x}_3,\ldots,\boldsymbol{x}_{N-1}) \tag{88}$$

where A is the usual antisymmetrization operator and the state $|\tilde{\Psi}_\alpha^{N-3}\rangle$ contains a core hole in the initial orbital c and two holes in some upper orbitals.

The single-particle scheme adopted for the Auger transition now follows a reduction procedure from a many-body approach similar to the one sketched in section 3 for the photoemission case, whereby the Auger electron is to be considered as moving in an effective potential related to a particular chosen channel β.

By inserting equations (87) and (88) into the expression for the transition probability, introducing the effective initial state wavefunction as modified by the final channel β,

$$\Psi_{\text{eff}}^\beta(\boldsymbol{x}_1,\boldsymbol{x}_2) = \iint \tilde{\Psi}_\beta^{N-3}(\boldsymbol{x}_3,\ldots,\boldsymbol{x}_{N-1})^*\Psi_i^{N-1}(\boldsymbol{x}_1,\ldots,\boldsymbol{x}_{N-1})\,\mathrm{d}\boldsymbol{x}_3\cdots\mathrm{d}\boldsymbol{x}_{N-1} \tag{89}$$

and normalizing the continuum wavefunction to one state per Rydberg, one finds for the width Γ of the Auger β line

$$\Gamma = \frac{2k}{16\pi^2}|D_k \pm E_k|^2$$

where

$$D_k = \iint \left[\phi_c(\boldsymbol{x}_1)\phi_{\boldsymbol{k}}^-(\boldsymbol{x}_2)\right]^*\frac{1}{|\boldsymbol{r}_1-\boldsymbol{r}_2|}\Psi_{\text{eff}}^\beta(\boldsymbol{x}_1,\boldsymbol{x}_2)\,\mathrm{d}\boldsymbol{x}_1\,\mathrm{d}\boldsymbol{x}_2 \tag{90}$$

$$E_k = \iint \left[\phi_c(\boldsymbol{x}_2)\phi_{\boldsymbol{k}}^-(\boldsymbol{x}_1)\right]^*\frac{1}{|\boldsymbol{r}_1-\boldsymbol{r}_2|}\Psi_{\text{eff}}^\beta(\boldsymbol{x}_1,\boldsymbol{x}_2)\,\mathrm{d}\boldsymbol{x}_1\,\mathrm{d}\boldsymbol{x}_2 \tag{91}$$

are the direct and exchange transition matrix elements for the Auger process. The $+$ sign applies for singlet states, the $-$ sign for triplet states. Specialization to various approximations for the initial and/or final states can be found in [60].

As for photoemission from valence states, we partition the muffin-tin space in cells around the spheres covering the whole space. Assuming that the core electron ϕ_c is localized in the cell at the origin, we can write $D = \sum_i D^i$, where D^i are the same integrals as defined above in which the second integration is extended to the space contained in the ith cell, the first being always extended to the cell at the origin. If we now insert for $[\phi_{\boldsymbol{k}}^-(\boldsymbol{r})]^*$ the expression of equation (49) in the ith cell we obtain for Γ

$$\Gamma = 2k \left| \sum_i \sum_L A_L^i B_L^i(\boldsymbol{k}) \right|^2 . \tag{92}$$

which can be rewritten according to (51) as

$$\Gamma = 2k \left| \sum_{i,j} \sum_{L,L'} A_L^i \tau_{LL'}^{ij} \mathrm{i}^{l'} Y_{L'}(\hat{\boldsymbol{k}}) \mathrm{e}^{\mathrm{i}\boldsymbol{k}\cdot\boldsymbol{R}_{ji}} \right|^2 . \tag{93}$$

where $A_L^i = D_L^i - E_L^i$ and the amplitudes D_L^i and E_L^i are obtained from those of equations (90) and (91) by replacing $\phi_{\boldsymbol{k}}$ by $\tilde{\Phi}_L^i$ of equation (49).

Regarding the cell dependence of the amplitude A_L^i we can distinguish three cases. Either the two final holes are in core states (in which case $A_L^i = A_L^o \delta_{io}$) or both are in valence delocalized states (full dependence on site i) or only one is in a core state (in which case either $A_L^i = D_L^i - E_L^i \delta_{io}$ or $A_L^i = D_L^i \delta_{io} - E_L^i$).

In the case of periodic systems, neglecting surface effects, one has the further relation

$$A_L^i = A_L^o \mathrm{e}^{\mathrm{i}\boldsymbol{k}_{\mathrm{BZ}}\cdot\boldsymbol{R}_{io}} .$$

The similarity of equation (93) to equation (82) is striking. In the case where the final two-hole states are localized onto the atom at the origin the formula is practically the same; only the amplitude for producing the final state photoelectron is different. Moreover, the photoelectron energy is fixed in the Auger process, whereas in photoelectron diffraction it can be tuned by varying that of the impinging photon. Notice also the further interference process in the case of a CVV Auger process, which is the same as in the photoemission process from a valence state.

4.4. The Auger–photoemission coincidence spectroscopy (APECS), and angle-resolved (AR) APECS

Auger and core-level photoelectron spectroscopies are strongly correlated, as the core hole filled during the Auger decay is just the one created by the photoemission process. Such a connection has been more clearly explored only recently, with the development of Auger–photoelectron coincidence spectroscopy (APECS), where the core photoelectron is measured in time coincidence with its associated Auger electron. The important features of this spectroscopic technique were underlined more than 15 years ago by Sawatzky [62].

(a) *Increased surface sensitivity.* In a coincidence event, the two electrons must originate from the same atom, and, thus, the effective escape depth in solids is reduced to: $\lambda_{\mathrm{eff}} = \lambda_P \lambda_A / (\lambda_P + \lambda_A)$ (P labels the photoelectron and A the Auger). Here λ, through the relation $I = I_0 \mathrm{e}^{-x/\lambda}$, measures the probability that an electron emitted by an atom at a distance x from the surface escapes from the solid. The fact that λ_{eff} is always smaller than the escape depth of the two single events reveals the increased surface sensitivity for this technique.

(b) *Precise identification of overlapping multiplet structures.* The kinetic energies of the photoelectron and Auger electron are related by the expression

$$E_k^P + E_k^A = \hbar\omega - (\mathsf{E}_{N-2} - \mathsf{E}_N) \tag{94}$$

where $\hbar\omega$ is the energy of the incoming photon and $\mathsf{E}_{N-2} - \mathsf{E}_N$ is the energy difference of the two-hole final state and the initial state. Thus, for a given process, the sum of Auger and photoelectron kinetic energies is constant, and this allows the separation of the various multiplet contributions (or satellite lines) to the total photoelectron spectrum by selecting the energy of the Auger electron and vice versa.

(c) *Elimination of the lifetime broadening due to the decay of the intermediate one-hole state.* This property comes directly from equation (94). The sum of the Auger plus the photoelectron kinetic energy has a width which is only determined by the lifetime of the two-hole state ($N-2$): thus, if we measure the photoelectron spectrum in coincidence with an Auger electron of a particular kinetic energy, the intermediate state lifetime broadening is removed.

A further level of discrimination is obtained when the angular dependence of the two emitted electrons is also resolved (AR-APECS). In this case, the detection of escape directions gives an insight into the orbital occupancy of the two-hole residual ion, due to angular momentum conservation [63]. It is the aim of this section to extend the MS formalism to cover also this kind of spectroscopy.

In order to deal with AR-APECS, we should start from equation (29), with V_{I1} given by the photoionization potential and V_{I2} by the Coulomb repulsion. In this way, Auger–photoelectron angular correlations can be correctly described and the total amplitude for the process can be written as

$$A \propto \sum_n \frac{\langle \Phi_f | \frac{e^2}{|r_1 - r_2|} | \Phi_n \rangle \langle \Phi_n | \hat{e}_{q_i} \cdot \boldsymbol{p} \mathrm{e}^{\mathrm{i}q_i \cdot r} | \Phi_i \rangle}{\mathcal{E}_i - \mathcal{E}_n + \mathrm{i}\Gamma_n} \delta(\mathcal{E}_i - \mathcal{E}_n). \tag{95}$$

In the following we deal with core–core–core spectroscopies, as the introduction of valence-shell spectroscopies is a more formidable task and it will be attacked in the near future. Thus equation (95) can be labelled in terms of core-angular-momentum quantum numbers. Moreover, as we are interested in angular correlations at fixed energy for Auger electrons and photoelectrons, in the following we drop the energy dependence in the delta function and the denominator. If, moreover, we restrict ourselves to the dipole approximation and do not consider spin–orbit splitting (jj-coupling can be dealt with in a similar way), we finally get

$$\begin{aligned} A^{l_1 l_2 LMSS_z}_{l_c m_c \sigma_c}(k_P, \sigma_P, k_A, \sigma_A) &= \langle (l_c, m_c, \sigma_c); \phi^-(k_A, \overline{\sigma}_A) \Big| \frac{e^2}{|\boldsymbol{r}_1 - \boldsymbol{r}_2|} \Big| (l_1, l_2) LM, SS_z \rangle \\ &\times \langle \phi^-(k_P, \overline{\sigma}_P) | \hat{e}_{q_i} \cdot \boldsymbol{r} | (l_c, m_c, \sigma_c) \rangle \equiv F^{l_1 l_2 LMSS_z}_{l_c m_c \sigma_c}(k_A, \sigma_A) D_{l_c m_c \sigma_c}(k_P, \sigma_P). \end{aligned} \tag{96}$$

Here subscripts P and A refer to the photoelectron or Auger electron, and k and σ are their outgoing wavevector and spin. The overline indicates time reversal. The dipole amplitude $D_{l_c m_c \sigma_c}(k_P, \sigma_P)$ depends on the core–shell quantum numbers l_c, m_c and σ_c. In the Coulomb matrix element $F^{l_1 l_2 LMSS_z}_{l_c m_c \sigma_c}(k_A, \sigma_A)$ we represent the final two-hole state in terms of its global angular momentum as

$$|((l_1, l_2)L, M, S, S_z\rangle = R_{l_1} R_{l_2} [Y_{l_1} \otimes Y_{l_2}]_{L,M} [\chi^{(1)} \otimes \chi^{(2)}]_{S,S_z}. \tag{97}$$

Here $[Y_{l_1} \otimes Y_{l_2}]_{L,M} \equiv \sum_{m_1,m_2} C^{L,M}_{l_1,m_1,l_2,m_2} Y_{l_1,m_1} Y_{l_2,m_2}$ is a tensor spherical harmonic, where C is the usual Clebsch–Gordan coefficient and R_{l_1} and R_{l_2} are the radial parts of the single-particle wavefunctions.

If we adopt the usual expansion for the scattering wavefunction inside the muffin-tin sphere I_0

$$\phi^-(\boldsymbol{r}_i, \boldsymbol{k}, \sigma) = \sum_L B^0_L(\boldsymbol{k}) R_l(\boldsymbol{r}_i) Y_L(\hat{\boldsymbol{r}}_i) \chi_\sigma \tag{98}$$

where the amplitudes $B^i_L(\boldsymbol{k})$ are defined by equation (51), it becomes possible to express dipole and Coulomb matrix elements as

$$D^{l_c m_c \sigma_c}(k_P, \sigma_P) = \sum_{l_p m_p} \sqrt{\frac{3(2l_c+1)}{4\pi(2l_p+1)}} R_{l_p,l_c} C^{l_p,0}_{l_c,0,1,0} C^{l_p,m_p}_{l_c,m_c,1,0} \delta_{\sigma_P,\sigma_c} B^0_{L_p}(\boldsymbol{k}) \tag{99}$$

and

$$F^{l_1 l_2 L M S S_z}_{l_c m_c \sigma_c}(k_A, \sigma_A) = \sum_{l_A, l} g(l_A, l, l_1, l_2, l_c, L) \times \sum_{m_A, m_c,} C^{L,M}_{l_c,m_c,l_A,m_A} C^{S,S_z}_{1/2,\sigma_c,1/2,\sigma_A} B^0_{L_A}(\boldsymbol{k}_A) - Ex \tag{100}$$

where Ex is the exchange term, with l_1 and l_2 interchanged, $R_{l_p,l_c} \equiv \int R_{l_p}(r) r R_{l_c}(r)\,\mathrm{d}r$ is the radial dipole matrix element and $g(l_A, l, l_1, l_2, l_c, L)$ takes into account the radial matrix element for the Coulomb process. Its explicit expression is

$$g(l_A, l, l_1, l_2, l_c, L) = \sin\delta_{l_A} \mathrm{e}^{i\delta_{l_A}} \int r_1^2 r_2^2 R_{l_c}(r_1) R_{l_A}(r_2) \frac{r_<^l}{r_>^{l+1}} R_{l_1}(r_1) R_{l_2}(r_2) \frac{\mathrm{d}r_1 \mathrm{d}r_2}{2l+1} \times (-1)^{(l+l_2+l_c+L)} \sqrt{(2l+1)(2l_1+1)(2l_c+1)} C^{l_c,0}_{l,0,l_1,0} C^{l_A,0}_{l,0,l_2,0} \begin{Bmatrix} l_A & l_2 & l \\ l_1 & l_c & L \end{Bmatrix} \tag{101}$$

where the phase shifts $\sin\delta_{l_A}\mathrm{e}^{\mathrm{i}\delta_{l_A}}$ are explicitly indicated. Of course, when the two electrons are equivalent the exchange term disappears: however, in this case, particular care must be taken for the normalization procedure of coupled wavefunctions, as detailed, e.g., in [66].

The total intensity is obtained by summing up the square modulus of the amplitude incoherently over the initial and final states and coherently over the intermediate states, following equation (29). We find, for the spin-unpolarized case,

$$\begin{aligned} I_{l_c,l_1,l_2,L,S}(k_A, k_P) &= \sum_{\sigma_A,\sigma_P,M,S_z} \Bigg| \sum_{l_A,l,l_P} f_{l_P} g(l_A, l, l_1, l_2, l_c, L) \\ &\quad \times \sum_{m_A,m_p,m_c,\sigma_c} C^{l_p,m_p}_{l_c,m_c,1,0} \delta_{\sigma_P,\sigma_c} C^{L,M}_{l_c,m_c,l_A,m_A} C^{S,S_z}_{1/2,\sigma_c,1/2,\sigma_A} B^0_{l_P}(\boldsymbol{k}_P) B^0_{l_A}(\boldsymbol{k}_A) \Bigg|^2 \\ &= \sum_{l_A,l,l_P} \sum_{l'_A,l',l'_P} f_{l_P} f^*_{l'_P} g(l_A, l, l_1, l_2, l_c, L) g^*(l'_A, l', l_1, l_2, l_c, L) \\ &\quad \times (-1)^{l_A+l'_A+l_P+l'_P} (2L+1) \sqrt{(2l_P+1)(2l'_P+1)} \\ &\quad \times \sum_{L_1,L_2} \begin{Bmatrix} l_c & l_A & L \\ L_1 & 1 & l_P \end{Bmatrix} \begin{Bmatrix} l_c & l'_A & L \\ L_2 & 1 & l'_P \end{Bmatrix} \\ &\quad \times \sum_M C^{L_1,M}_{L,M,1,0} C^{L_2,M}_{L,M,1,0} [B^0_{l_P} \otimes B^0_{l_A}]_{L_1,M} [B^{0*}_{l_P} \otimes B^{0*}_{l_A}]_{L_2,M} \end{aligned} \tag{102}$$

with $f_{l_P} \equiv \sin\delta_{l_P}\mathrm{e}^{\mathrm{i}\delta_{l_P}} \left[3(2l_c+1)/4\pi(2l_p+1)\right]^{\frac{1}{2}} R_{l_p,l_c} C^{l_p,0}_{l_c,0,1,0}$. In contrast to the atomic case (see, e.g., [64, 65]), equation (102) cannot be simplified further in analytical terms, because the B^0_L do not allow an addition theorem like for spherical harmonics. Thus, equation (102) is our final result to be evaluated numerically. However, in order to show a simple example of Auger–photoelectron angular correlation, it is convenient to describe the atomic case, where the B^0_{lm} coefficients are substituted by the spherical harmonics Y_{lm}. In this case the addition theorem can be applied and the two products of double spherical harmonics can be simplified with the help

of the expression $Y_{lm}(\Omega)Y_{l'm'}(\Omega) = \sum_{m,m'} C^{L,M}_{l,m,l',m'} Y_{LM}(\Omega)$. Then after straightforward, but lengthy, calculations to sum up all azimuthal dependences in the Clebsch–Gordan coefficients, it is possible to derive the final expression

$$I_{l_c,l_1,l_2,L,S}(k_A, k_P) = \sum_{L_A,L_P,L} c(l_c, l_1, l_2, L, S, L_A, L_P, L)[Y_{L_P}(k_P) \otimes Y_{L_A}(K_A)]_{L,0} \tag{103}$$

where $c(l_c, l_1, l_2, L, S, L_A, L_P, L)$ is a coefficient depending, among other things, on the radial matrix elements. In equation (103), $L = 0, 1, 2$ (for the purely dipole incoming radiation) and $M = 0$, because we suppose the incoming radiation to be directed along z. One can generalize this result to the case where the polarization is expressed by a density matrix operator, which turns out to be scalarly coupled to the double spherical harmonics (in this case we recover the results of [64, 65]). However, expression (103) is enough to discuss a simple example of angular correlation on an atomic system. In [67] coincident experiments were performed between an Ar 2p photoelectron of 5 keV kinetic energy and each of the 3p Auger electrons. Amongst all possible decay channels, one is suitable for an immediate interpretation, $\mathrm{Ar} + h\nu \rightarrow \mathrm{Ar}^{2+}3\mathrm{p}^4(^1\mathrm{S}^e) + e_A$ ($l = 1$), as it involves only one possible value for l_A, so that we do not need Coulomb radial matrix elements. We have also assumed that the radial matrix element of the $l - 1$ channel of the photoelectron process is strongly suppressed with respect to the $l + 1$. In this case, the angular correlation expressed by equation (103) can be calculated analytically and provides the observed angular correlation, as given by the expression $(\cos\theta_A + 3\cos(\theta_A - 2\theta_P))^2$. Here it is clear that the angular position of the maximum intensity in the revealed Auger electron strongly depends on the angular position of the revealed photoelectron. Moreover, it is immediate to check that integrating this analytical expression over θ_A leaves the usual angular dependence for atomic photoelectrons, which is given by $(1 + \beta P_2(\cos\theta_P))$.

All the other cases, as well as the possibility to describe theoretically the extension of the correlation techniques to solid state physics, require the implementation of a computer code, which is currently in progress.

4.5. Other coincidence spectroscopies

The APECS is probably one of the best known coincidence spectroscopies but there are some other such spectroscopies which have proved equally useful and informative in the last decade. Those spectroscopies that are among the scope of this review article (i.e. for which the incoming beam of particles is composed either of photons or of electrons) can be divided into two groups, respectively called $(\gamma, 2e)$ and $(e, 2e)$. The first term in the doublet represents the incoming beam and the second the outgoing particles. Therefore, these two families of spectroscopies can be viewed as the coincidental detection of a second electron in photoemission, Auger or EELS. In all cases, as we have already seen for APECS, coincidence spectroscopies provide a unique way to select a subset of transitions in order to disentangle the complex cascade of effects that contribute to a given single-electron spectroscopy peak.

APECS, which we have discussed in detail, is not the only $(\gamma, 2e)$ coincidence spectroscopy. Recently, two-electron photoemission has been developed both experimentally [68] and theoretically [27, 28]. Two competing effects can contribute to its cross-section. In one case, an electron excited by a photon in the ultraviolet range ejects a second (valence) electron through an inelastic collision. In the second case, the photon excites a quasiparticle formed by an electron pair [27]. The former contribution however should dominate in solids in contrast to atomic targets because of the high number of valence electrons. Its potentialities have not been assessed yet, but it will certainly prove useful in the study of the physics of correlations.

Like APECS, $(e, 2e)$ coincidence techniques are in a rather advanced stage now, although their application to solids took some time because of the difficulties linked to the short mean free path of electrons in the solid matter. Indeed, in a standard $(e, 2e)$ experiment, which consists generally in the collision of the incoming electrons with valence electrons of the sample, most of the primary electrons and those excited are lost in the bulk. For this reason, only two experimental configurations are possible:

(i) a high energy ($\sim$10 keV) primary beam in transmission through a thin film;
(ii) a low energy beam in a back-reflection geometry.

In the first case, the cross-section reflects the spectral momentum density of the target electron while in the second case, because of multiple scattering and only 2D momentum conservation, no such direct information on the electronic structure can be obtained [69], which means in particular that a theoretical modelling is necessary in order to extract this type of information. Nevertheless, the information that can be extracted with these coincidence spectroscopies, both on electronic structure and scattering dynamics, is more detailed than that to be obtained from the corresponding one-electron techniques. Moreover, some specific information on electron–electron correlations can be obtained, including some visualization of the exchange–correlation hole [70, 71].

It should be noted that spin-polarized $(e, 2e)$ spectroscopies are now currently used to study the corresponding spin-related quantities both for ferromagnetic surfaces [72–74] (through the exchange interaction) and for non-magnetic heavy targets [75, 76] (through the spin–orbit interaction).

The starting point of all these coincidence spectroscopies is the expression (29) of the doubly differential ionization cross-section, as for APECS. The importance of the multiple-scattering effect in these spectroscopies has been stressed by Feder *et al* [69] and by Fominykh and co-workers [70]. The present framework allows a proper treatment of the multiple scattering for all the $(\gamma, 2e)$ and $(e, 2e)$ coincidence spectroscopies.

4.6. The LEED/MEED case

The cross-section for electron scattering off a finite cluster of atoms, however big, located at sites $\boldsymbol{R}_j$ is obtained in terms of the T-matrix, which is defined on the basis of the behaviour of the scattering wavefunction in the asymptotic region. Following appendix A, we write this wavefunction as

$$\phi^+_{\boldsymbol{k}}(\boldsymbol{r}_o) = \sum_L \underline{A}^o_L(k) \left[J_L(\boldsymbol{r}_o) + \sum_{L'} \tilde{H}^+_{L'}(\boldsymbol{r}_o) T_{L'L} \right]. \tag{104}$$

In the same appendix, we demonstate that the T-matrix elements for the cluster can be expressed as

$$T_{LL'} = \sum_{i,j} \sum_{\Lambda,\Lambda'} J^{oi}_{L\Lambda} \tau^{ij}_{\Lambda\Lambda'} J^{jo}_{\Lambda' L'}. \tag{105}$$

Notice that with the definitions given in section 3.1 the scattering path operator τ is proportional to $1/k$. Therefore, recalling the expression (25) of the cross-section for electron scattering off a sample, and making use of the fact that the element $\langle \boldsymbol{k}|L\rangle = \sqrt{2/(\pi k)}\mathrm{i}^{-l} Y_L(\hat{\boldsymbol{k}})$ with our normalization conditions, we obtain for the scattering cross-section into the direction $\hat{\boldsymbol{k}}_s$ for electrons impinging on the cluster with wavevector $\boldsymbol{k}_i$

$$\frac{\mathrm{d}\sigma}{\mathrm{d}\hat{\boldsymbol{k}}_s} = (4\pi)^2 \left| \sum_{\Lambda,\Lambda'} \mathrm{i}^{-\lambda'} Y_{\Lambda'}(\hat{\boldsymbol{k}}_s) T_{\Lambda'\Lambda} \mathrm{i}^{\lambda} Y_{\Lambda}(\hat{\boldsymbol{k}}_i) \right|^2$$

$$= (4\pi)^2 \left| \sum_{\Lambda',\Lambda} \mathrm{i}^{-\lambda'} Y_{\Lambda'}(\hat{\boldsymbol{k}}_s) \sum_{j,L'} J^{oj}_{\Lambda' L'} \sum_{i,L''} \tau^{ji}_{L' L''} J^{io}_{L''\Lambda} \mathrm{i}^{\lambda} Y_{\Lambda}(\hat{\boldsymbol{k}}_i) \right|^2 . \tag{106}$$

Moreover using the relation derived in appendix A

$$\sum_{L} \mathrm{i}^{l} Y_L(\hat{\boldsymbol{k}}) J^{jo}_{LL'} = \mathrm{i}^{l'} Y_{L'}(\hat{\boldsymbol{k}}) \mathrm{e}^{\mathrm{i}\boldsymbol{k}\cdot\boldsymbol{R}_{jo}} \tag{107}$$

we finally find for the cross-section

$$\frac{\mathrm{d}\sigma}{\mathrm{d}\hat{\boldsymbol{k}}_s} = (4\pi)^2 \left| \sum_{i,L} \sum_{j,L'} \mathrm{i}^{-l'} Y_{L'}(\hat{\boldsymbol{k}}_s) \mathrm{e}^{-\mathrm{i}\boldsymbol{k}_s\cdot\boldsymbol{R}_{jo}} \tau^{ji}_{L'L} \mathrm{i}^{l} Y_L(\hat{\boldsymbol{k}}_i) \mathrm{e}^{\mathrm{i}\boldsymbol{k}_i\cdot\boldsymbol{R}_{io}} \right|^2$$

$$= (4\pi)^2 \left| \sum_{i,L} \sum_{j,L'} \mathrm{i}^{-l'} Y_{L'}(\hat{\boldsymbol{k}}_s) \mathrm{e}^{-\mathrm{i}\boldsymbol{q}\cdot\boldsymbol{R}_{jo}} \tau^{ji}_{L'L} \mathrm{i}^{l} Y_L(\hat{\boldsymbol{k}}_i) \mathrm{e}^{\mathrm{i}\boldsymbol{k}_i\cdot\boldsymbol{R}_{ij}} \right|^2$$

$$= (4\pi)^2 \left| \sum_{i,L} \sum_{j,L'} \mathrm{i}^{-l'} Y_{L'}(\hat{\boldsymbol{k}}_s) \mathrm{e}^{\mathrm{i}\boldsymbol{k}_s\cdot\boldsymbol{R}_{ij}} \tau^{ji}_{L'L} \mathrm{i}^{l} Y_L(\hat{\boldsymbol{k}}_i) \mathrm{e}^{-\mathrm{i}\boldsymbol{q}\cdot\boldsymbol{R}_{io}} \right|^2 \tag{108}$$

where $\boldsymbol{q} = \boldsymbol{k}_s - \boldsymbol{k}_i$ is the momentum transfer.

The same formula can be derived in the case of an infinite system, which is obtained as the limiting case of a finite system of volume V which is enclosed in a larger volume V_0 such that $\lim V_0 \to \infty$ before $\lim V \to \infty$ and $\lim V_0/V \to \infty$ [61].

It is interesting to note at this point that these equations are also valid in the presence of electron damping. In fact, we already noted in section 3.3 that the elastic cross-section for electron scattering in a complex potential is given by the squared modulus of the scattering amplitude calculated in the same way as for real potential [50].

Equation (108) is valid whatever the spatial arrangement of the atomic sites. It has the appearence of a linear combination of photoelectron diffraction amplitudes emanating from any initial site i, with the coefficients given by $\mathrm{i}^{l} Y_L(\hat{\boldsymbol{k}}_i) \mathrm{e}^{-\mathrm{i}\boldsymbol{q}\cdot\boldsymbol{R}_{io}}$. This is in keeping with the physical fact that the incoming electronic wave can be scattered by any center i so that there is no localized source. In this respect equation (108) is very similar to the analogous expression for the photoemission process from a valence state equations (83) and (85) although the linear combination in the angular momentum variables has different coefficients. Moreover, the scattering amplitude in (108) is very reminiscent of the Thomson amplitude for x-ray diffraction, with a complex form factor given by a photoelectron diffraction amplitude. This obviously leads to a Bragg condition for scattering in periodic structures.

In this last case it would be very useful to see how the various expressions specialize in the case of periodic systems, e.g. a stack of a certain number N of Bravais-lattice planes with the same unit cell, but possibly different atoms in each plane. We shall neglect for a moment the electron damping to take full advantage of the periodicity and shall indicate at the end how the result is modified in presence of damping.

If we fix an arbitrary origin in the mth plane ($m = 1, N$) by the vector $\boldsymbol{r}_{mo}$ and indicate the plane lattice vectors by $\boldsymbol{P}_n$, then the general site position is given by

$$\boldsymbol{R}_{io} = \boldsymbol{r}_{mo} + \boldsymbol{P}_n .$$

In order to exploit the translational invariance of the system within the planes we take the Fourier transform of the defining equation (52) for the scattering path operator τ, which can

also be written as

$$\tau_{LL'}^{ij} = t^i \delta_{ij} \delta_{LL'} - t^i \sum_{k \neq i} \sum_{L''} G_{LL''}^{ik} \tau_{L''L'}^{kj} \tag{109}$$

introducing the quantities

$$T_{LL'}^{m}(\boldsymbol{k}) = \sum_{m', \boldsymbol{P}_n} \mathrm{e}^{\mathrm{i}\boldsymbol{k}\cdot(\boldsymbol{r}_{mo} - \boldsymbol{r}_{m'o} - \boldsymbol{P}_n)} \tau_{LL'}^{\boldsymbol{r}_{mo},\, \boldsymbol{r}_{m'o} + \boldsymbol{P}_n} \tag{110}$$

together with

$$\tilde{G}_{LL'}^{mm'} = \sum_{\boldsymbol{P}_n} \mathrm{e}^{\mathrm{i}\boldsymbol{k}\cdot(\boldsymbol{r}_{mo} - \boldsymbol{r}_{m'o} - \boldsymbol{P}_n)} G_{LL'}^{\boldsymbol{r}_{mo}, \boldsymbol{r}_{m'o} + \boldsymbol{P}_n} \tag{111}$$

and the quantity that describes multiple scattering within each plane m

$$\tau_{LL'}^{m}(\boldsymbol{k}) = [(t^{-1} + \tilde{G}^{mm}(\boldsymbol{k}))^{-1}]_{LL'} \tag{112}$$

where t denotes the matrix $t_l^m \delta_{LL'}$ in the angular momentum indices. We find in this way

$$T_{LL'}^{m}(\boldsymbol{k}) = \tau_{LL'}^{m}(\boldsymbol{k}) - \sum_{m'=1}^{N} \sum_{\Lambda, \Lambda'} \tau_{L\Lambda}^{m}(\boldsymbol{k}) \tilde{G}_{\Lambda\Lambda'}^{mm'} T_{\Lambda'L'}^{m'}(\boldsymbol{k}). \tag{113}$$

We thus recover equations (5.22) of [12] (see also references therein) for a stack of periodic planes. The only difference with the no damping case, apart for the complex phase shifts used in the calculation of the atomic t matrices, is that the quantities $\tilde{G}_{LL'}^{mm'}$ depend now on the origin chosen on the various planes. It is easy to convince oneself that the correct choice in this case is to take all the origins on the various planes as close as possible to the z-axis, assumed perpendicular to the surface, and perform the lattice sum in equation (110) by including all the lattice points within a circle of radius between two and three times the electron mean free path up to convergence.

5. Probe electron not detected

In this section, we will consider spectroscopies where the probe electron is not detected.

5.1. Photoabsorption

Even though the case of x-ray absorption has already been treated in some details in section 3.2, we would like to present in this section two applications of the new method of fitting the XANES energy region of the absoprtion spectrum. The first application analyses the Fe K-edge polarized XANES of a single crystal of the iron protein carbonmonoxy-myoglobin (MbCO) and its cryogenic photoproduct Mb*CO, with the purpose of deriving the structural parameters (angles and bond lengths) around the metal ion. The fitting procedure allows us to discriminate among three (in the case of MbCO) and two (in the case of Mb*CO) conflicting sets of parameters derived from diffraction analysis of the crystal proteins. The technique is simple and is illustrated in figure 2. As soon as a best fit is achieved between the simulated and the experimental signal, the electronic parameters (such as potential and energy-dependent damping) are left unchanged, while the fitted atomic positions are replaced by the diffraction sets under scrutiny. The set that gives the smallest R-factor is considered the best candidate. More details are given in [49]. The second example concerns the fitting of electronic properties, in particular electron population analysis. The idea is that in systems where the absorption process can be reasonably well described in terms of one electron moving in an effective optical potential of the local density type (like the H-L potential), then, assuming a known structure,

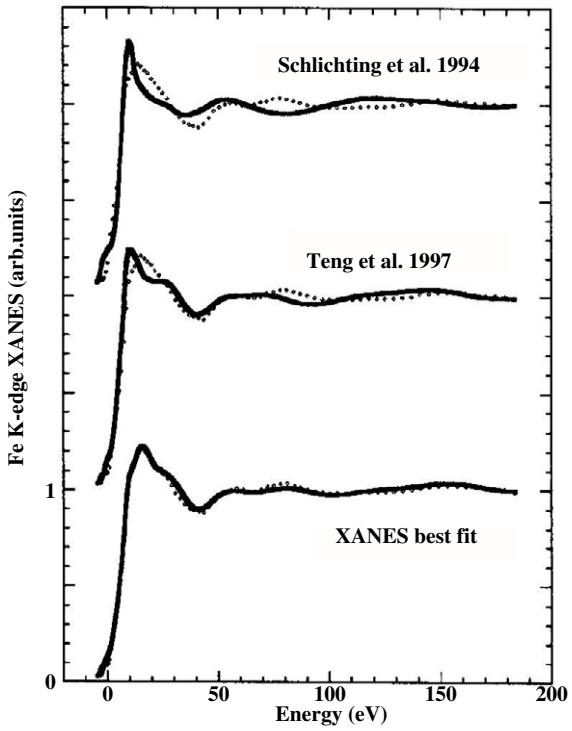

Figure 2. Comparison between polarized ($\hat{e}_q$ perpendicular to the haem plane) experimental (· · · · · ·) and calculated (——) Fe K-edge spectra derived from two different reported structures for Mb*CO protein. The bottom theoretical curve is the MXAN best fit [49].

one can try to fit the total charge density onto the experimental spectrum. This procedure has been followed to obtain the 3d and 2p occupation numbers on Ti and O respectively in TiO_2. On Ti atoms, different from the photoabsorber, one finds $n_d = 1.00$, $n_p = 6 - n_d/2 = 5.50$ on the oxygen atoms and $n_d^* = 1.91$ on the Ti photoabsorber, pointing to an incomplete screening of the core-hole charge. This is in keeping with other evidence from Ca compounds [37] and seems to be a general feature of absorption. Figure 3 describes the fitting procedure and shows that the most sensitive part of the spectrum for this kind of analysis is the pre-edge structure. More details are found in [77].

5.2. EELS

The basic idea that presided over the development of the study of the fine structure in EELS (EELFS) was the strong similarity observed in many cases with EXAFS spectra. This led people to think that it might be possible to perform EXAFS-like analysis without the need for synchrotron radiation, as EELS is a typical laboratory technique.

In an EELS experiment, a primary beam of electrons is focused onto the sample under study. The scattered beam, at an energy lower than that of the incoming beam, in contrast to LEED, is then measured. The difference in energy between the two beams results from the promotion of an electron, generally from a core state, to an excited state (bound or continuum) through a Coulomb interaction.

The similarity of core EELS to EXAFS is clear, as only the type of excitation of the core electron (Coulomb versus dipole) varies and gives the same chemical sensitivity. We

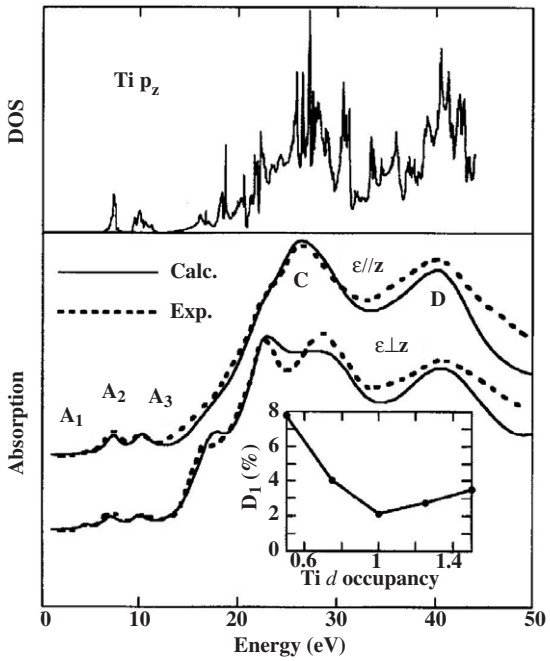

Figure 3. Lower panel: comparison between experimental (· · · · · ·) and calculated (——) Ti K-edge XANES spectra of a single crystal of TiO_2 for two orientations of the electric field and wavevectors. Inset: variation of the *R*-factor with the Ti 3d occupancy. Upper panel: p-projected density of states on a Ti atom calculated by the FLAPW band structure method [77].

see therefore why similar modulations are expected and have been found very often in practice. Let us look in more detail at the differences we can expect on the basis on the experimental environment. First, the ingoing and outgoing particles in EELS are electrons, while they are photons in EXAFS. This means that both beams will undergo multiple scattering and this will interfere with the multiple scattering of the lost (excited) electron to complicate the experimental pattern. Then, we know that the dipole approximation usually holds for EXAFS. Coulomb selection rules are more involved. However, as hinted by Saldin [78], if the ratio of the energy of the loss electron to that of the incoming beam is very small with respect to unity, there should be a dominance of the dipole-allowed channel in the excitation process. This condition is not always fulfilled however in experiments.

Nevertheless, the similarity with EXAFS, and the fact that only electrons are involved in the various processes, indicates that it must be possible to treat EELS within the same theoretical framework. Such an approach has been developed by De Crescenzi *et al* [79] within a scattering path operator approach in a mixed spherical wave/plane wave representation and by Sébilleau [80] from a basis-independent point of view. We will outline the derivation of the former here and refer the reader to the corresponding reference for further details.

The starting point of the derivation is provided by equation (27), which gives the cross-section for a particle energy involved in inelastic scattering, within the distorted wave Born approximation, in terms of the matrix element of the loss potential. In the case of EELS, the initial and final states of the system in the presence of the sample potential V_S are many-particle states which can be written as $|\Phi_i^+\rangle = |\varphi_o\rangle|\phi_i^+\rangle$ and $\langle\Phi_f^-| = \langle\phi_f^-|\langle\varphi_n|$, where, as before, $|\phi_{i,f}^{\pm}\rangle$ is an electron state with the appropriate boundary condition, the eigenstate of $H_S = H_o + V_S$,

and $|\varphi_o\rangle$, $|\varphi_n\rangle$ are respectively the ground state and an excited state of the system. A sum over all the possible excited states n should be added outside the square modulus in (27) with the corresponding energy conservation rule $\delta(\mathsf{E}_o + E_i - \mathsf{E}_n - E_f)$. The Coulomb potential being a two-particle operator, exchange processes must also be taken into account, leading to

$$\frac{\mathrm{d}\sigma}{\mathrm{d}\hat{\boldsymbol{k}}_f} = 4\pi^4 \frac{k_f}{k_i} \sum_n \Big| \langle\varphi_n|\langle\phi_f^-|V_C|\varphi_o\rangle|\phi_i^+\rangle_d \pm \times \langle\phi_f^-|\langle\varphi_n|V_C|\varphi_o\rangle|\phi_i^+\rangle_e \Big|^2 \delta(\mathsf{E}_o + E_i - \mathsf{E}_n - E_f) \tag{114}$$

where the indices d and e refer respectively to the direct and exchange integrals and the $-$ sign is for triplet states, the $+$ for singlet. Rydberg units have been assumed here.

If N is the total number of electrons in the system, then the direct and exchange terms can be written as

$$\langle\varphi_n|\langle\phi_f^-|V_C|\varphi_o\rangle|\phi_i^+\rangle_d = \frac{1}{N}\sum_{m=1}^{N} \int\int \varphi_n^*(\boldsymbol{r}_1, \ldots, \boldsymbol{r}_m, \ldots, \boldsymbol{r}_N) \times \varphi_o(\boldsymbol{r}_1, \ldots, \boldsymbol{r}_m, \ldots, \boldsymbol{r}_N)\phi_f^{-*}(\boldsymbol{r}) \frac{1}{|\boldsymbol{r} - \boldsymbol{r}_m|}\phi_i^+(\boldsymbol{r})\,\mathrm{d}\boldsymbol{r}\,\mathrm{d}\tau \tag{115}$$

$$\langle\phi_f^-|\langle\varphi_n|V_C|\varphi_o\rangle|\phi_i^+\rangle_e = \frac{1}{N}\sum_{m=1}^{N} \int\int \varphi_n^*(\boldsymbol{r}_1, \ldots, \boldsymbol{r}_{m-1}, \boldsymbol{r}, \boldsymbol{r}_{m+1}, \ldots, \boldsymbol{r}_N) \times \varphi_o(\boldsymbol{r}_1, \ldots, \boldsymbol{r}_m, \ldots, \boldsymbol{r}_N)\phi_f^{-*}(\boldsymbol{r}_m) \frac{1}{|\boldsymbol{r} - \boldsymbol{r}_m|}\phi_i^+(\boldsymbol{r})\,\mathrm{d}\boldsymbol{r}\,\mathrm{d}\tau \tag{116}$$

where $\mathrm{d}\tau = \prod_{m=1}^{N} \mathrm{d}\boldsymbol{r}_m$.

Using the approximation described in [79] to calculate the exchange term in (116) we can define an effective transition operator for the process as

$$T^{\pm}(\boldsymbol{r}) = \int \phi_f^{-*}(\boldsymbol{r}') \left(\frac{1}{|\boldsymbol{r} - \boldsymbol{r}'|} \pm \frac{4\pi}{|\boldsymbol{k}_i - \boldsymbol{k}|}\delta(\boldsymbol{r} - \boldsymbol{r}') \right) \phi_i^+(\boldsymbol{r}')\,\mathrm{d}\boldsymbol{r}' \tag{117}$$

where $\boldsymbol{k}$ is the wavevector of the excited electron.

By partitioning the volume in non-overlapping cells Ω_j with no interstitials, and using equation (49), we can calculate the cell integrals in terms of the local solutions $\phi_i^+(\boldsymbol{r}_j, \boldsymbol{k}_i)$ and the scattering amplitudes $B_L^j(\boldsymbol{k})$. For a finite cluster this poses no particular computational problems.

In the case of periodic systems we assume that the sample under investigation can be decomposed into long-range ordered planes so that LEED-type states can be used for $|\phi_i^+\rangle$ and $\langle\phi_f^-|$, following the usual behaviour of Bloch functions. When the energies of the incoming and scattered beams are large enough, the surface does not contribute much and we can use the lattice vectors of the crystal rather than those of the individual planes (including the surface plane) to describe the LEED-type states. In this case the scattering amplitudes in equation (49) satisfy the relation

$$B_L^j(\boldsymbol{k}_i) = B_L^0(\boldsymbol{k}_i)\mathrm{e}^{\mathrm{i}\boldsymbol{k}_i \cdot \boldsymbol{R}_{j0}} \tag{118}$$

so that the effective transition operator takes the form

$$T^{\pm}(\boldsymbol{r}) = 4\pi \sum_n \mathrm{e}^{\mathrm{i}(\boldsymbol{q}_{\mathrm{BZ}} + \boldsymbol{G}_n)\cdot\boldsymbol{r}} \left[\frac{1}{|\boldsymbol{q}_{\mathrm{BZ}} + \boldsymbol{G}_n|^2} \pm \frac{1}{|\boldsymbol{k}_i - \boldsymbol{k}|} \right] \rho(\boldsymbol{G}_n).$$

Here, $\boldsymbol{G}_n$ is a reciprocal lattice vector of the system and $\boldsymbol{q} = \boldsymbol{k}_i - \boldsymbol{k}_f$ is the momentum transfer. Moreover $\rho(\boldsymbol{G}_n)$ is the Fourier transform of the quantity $\phi_i^+(\boldsymbol{r})\phi_f^{-*}(\boldsymbol{r})$.

In both cases therefore, the sum (difference) $M^+(M^-)$ of the direct and exchange matrix elements takes the form

$$M^{\pm} = \frac{1}{N}\sum_{m=1}^{N}\int \varphi_n^*(\boldsymbol{r}_1,\ldots,\boldsymbol{r}_m,\ldots,\boldsymbol{r}_N)\varphi_o(\boldsymbol{r}_1,\ldots,\boldsymbol{r}_m,\ldots,\boldsymbol{r}_N)T^{\pm}(\boldsymbol{r}_m)\,\mathrm{d}\tau. \tag{119}$$

If we assume that, apart from the core electron undergoing the transition, all other electrons in the system are merely spectators, the determinantal approximation applies to the many-electron states $|\varphi_n\rangle$ and $|\varphi_o\rangle$, namely $|\varphi_o\rangle = |\psi\rangle|\phi_{L_o}\rangle$ and $|\varphi_n\rangle = |\psi\rangle|\phi_{\boldsymbol{k}}\rangle$, where $|\psi\rangle$ is a $(N-1)$-electron state, $|\phi_{L_o}\rangle$ is the initial core state of the excited electron and $\phi_{\boldsymbol{k}}$ its scattering wavefunction with energy k^2. As a consequence expression (119) reduces to

$$M^{\pm} = \int \phi_{\boldsymbol{k}}^*(\boldsymbol{r})T^{\pm}(\boldsymbol{r})\phi_{L_o}(\boldsymbol{r})\,\mathrm{d}\boldsymbol{r}$$

which, when replaced into the expression (114) of the cross-section, leads to

$$\begin{aligned}\frac{\mathrm{d}\sigma}{\mathrm{d}\hat{\boldsymbol{k}}_f} &= 4\pi^4\frac{k_f}{k_i}\sum_{\boldsymbol{k}}\sum_{m_o}\left|\langle\phi_{\boldsymbol{k}}|T^{\pm}|\phi_{L_o}\rangle\right|^2\delta(E_o+E_i-E_{\boldsymbol{k}}-E_f)\\ &= -4\pi^3\frac{k_f}{k_i}\sum_{m_o}\int \phi_{L_o}(\boldsymbol{r})\left[T^{\pm}\right]^*(\boldsymbol{r})\,\mathrm{Im}\left[G(\boldsymbol{r},\boldsymbol{r}')\right]T^{\pm}(\boldsymbol{r}')\phi_{L_o}(\boldsymbol{r}')\,\mathrm{d}\boldsymbol{r}\,\mathrm{d}\boldsymbol{r}'\end{aligned}$$

where the Green function $G(\boldsymbol{r},\boldsymbol{r}')$ is given by equation (60).

As before, for real potentials the cross-section reduces to

$$\frac{\mathrm{d}\sigma}{\mathrm{d}\hat{\boldsymbol{k}}_f} = -4\pi^3\frac{k_f}{k_i}\sum_{m_o}\sum_{L,L'}\mathrm{Im}\left[M^*_{L_oL}\tau^{00}_{LL'}M_{L'L_o}\right] \tag{120}$$

with the coupling matrix elements given by

$$M_{LL_o} = \int \tilde{\Phi}_L(\boldsymbol{r})T(\boldsymbol{r})\phi_{L_o}(\boldsymbol{r})\,\mathrm{d}\boldsymbol{r} \tag{121}$$

dropping for simplicity the $\pm$ sign on M and T.

This is indeed an expression similar to that found in x-ray absorption with the difference that the coupling elements M_{LL_o} lead in principle to more complex selection rules and that the effective transition operator $T(\boldsymbol{r})$ contains the effect of the multiple scattering of the incoming and outgoing electron. It is indeed clear from the form of the transition operator T that the expression (121) describes processes like diffraction of the incoming beam prior to loss or loss followed by diffraction of the outgoing beam.

The predominance of the dipole term has been demonstrated in the case of the excitation of an s core level ($l_o = 0$) in crystalline silicon, where De Crescenzi *et al* [79] showed that most of the cross-section could be obtained by restraining the sum over l and l' to the value unity, but monopole transitions were also important. However, for other core levels, the situation is more complex and there is no clear demonstration of the validity of the dipole approximation.

5.3. The anomalous resonant x-ray diffraction

Anomalous resonant x-ray diffraction is a very powerful experimental technique to analyse structural and electronic properties of matter in a ordered phase. This spectroscopic technique measures the elastic Bragg reflection intensities versus incident photon energy. As apparent from expression (22), the resonant x-ray scattering process may be described as the virtual absorption of a photon by a core electron that is promoted to an unoccupied level. The excited electron decays to the initial state, thereby emitting the outgoing photon without loss of energy. The unoccupied states are sensitive to the electronic configuration, such as the population of

the highest occupied orbitals, their magnetic moment and the surrounding atomic distribution. If the decay process of the excited photoelectron happens to be toward a state different from the initial state, the initial photon will be inelastically scattered, so that in this case one can resolve the energy of the final outgoing photon in order to study the low energy excitations of the system (e.g. charge transfer and orbital excitations in strongly correlated electron systems). The former technique is referred to as resonant elastic x-ray scattering (REXS) or resonant x-ray diffraction (RXD); the latter instead goes under the name of resonant inelastic x-ray scattering (RIXS). In this review however we shall only deal with REXS.

When measured at Bragg-allowed peaks, REXS is more often called diffraction anomalous fine structure (DAFS) and combines the long range sensitivities of x-ray diffraction with the short range sensitivities of x-ray absorption techniques. In the extended fine structure region, DAFS provides the same short range structural information as EXAFS: the bond lengths, coordination numbers, neighbour types, and bond disorders for the atoms surrounding the resonantly scattering atoms. In the near edge region, DAFS provides the same structural and spectroscopic sensitivities as XANES: the valence, empty orbital and bonding information for the resonant atoms. Therefore, DAFS can provide EXAFS- and XANES-like information for the specific subset of atoms selected by the diffraction condition and site-specific absorption-like spectroscopic and structural information for the inequivalent sites of a single atomic species within the unit cell.

At Bragg-forbidden peaks, REXS becomes a probe sensitive to the electronic configuration of the resonant element, which includes the surrounding structural arrangement of the neighbouring atoms and its symmetries, the highest occupied orbitals, their ordering and their magnetic moments. This technique has found natural application in several 3d systems such as high T_c cuprates, the magneto-resistive manganites and other electron correlated systems like transition metal oxides. Since the excitation and the subsequent decay processes are mainly dipolar in character (but we shall also report on dipole–quadrupole interference effects), one might think that REXS performed near the transition metal L edge is the best way to probe directly the chemical and magnetic environment of the important 3d electrons. However, their 2p edges lie at around 650 eV, which corresponds to $\approx$19 Å for photon wavelengths and the minimum dimensions of the periodic unit cell. Moreover, at these photon energies all the experimental set-up, including the spectrometer, the detector and the cold finger of the cooling system, needs to be in vacuum. Faced with these difficulties, an alternative approach has been to study the 3d properties indirectly with K-edge REXS. Even though delocalized, the intermediate conduction band states of p symmetry reached in K-edge spectroscopies are sensitive enough to the electronic properties of the underlying states of d symmetry. This technique has therefore been used to indirectly probe the orbital [84, 85] and magnetic [82, 83] correlations present in the ground state of many correlated electron systems.

In this review we shall limit ourselves to charge scattering, in which only time-reversal even properties of the system are probed, like orbital ordering in manganites and a subtle dipole–quadrupole interference effect, present in many corundum geometries, that allows the determination of a quantity related to the local rotatory power in V_2O_3 and α-Fe_2O_3 [88].

With this in mind, the elastic scattering amplitude of the process, $A(\boldsymbol{k}, \omega)$, can be written in terms of the atomic scattering factors (ASFs), $f_j(\omega)$, of the atoms at positions $\boldsymbol{R}_j$ in the unit cell as

$$A(\boldsymbol{k}, \omega) = \sum_j \mathrm{e}^{\mathrm{i}\boldsymbol{k}\cdot\boldsymbol{R}_j} f_j(\omega) \tag{122}$$

where $\hbar\boldsymbol{k}$ is the momentum transfer in the scattering process, $\hbar\omega$ the incoming and outgoing photon energy and the sum is over all atoms in the unit cell. The ASF is given by the resonant

term of equation (21)

$$f_j(\omega) = \frac{r_0}{m} \sum_n \frac{\langle \phi_i^{(j)} | \hat{e}_{q_s}^* \cdot \boldsymbol{p} \mathrm{e}^{-\mathrm{i}\boldsymbol{q}_s \cdot \boldsymbol{r}} | \phi_n \rangle \langle \phi_n | \hat{e}_{q_i} \cdot \boldsymbol{p} \mathrm{e}^{\mathrm{i}\boldsymbol{q}_i \cdot \boldsymbol{r}} | \phi_i^{(j)} \rangle}{\hbar\omega - (E_n - E_i) - \mathrm{i}\Gamma_n} \tag{123}$$

where we have explicitly indicated that the origin for the initial state ϕ_i is taken on the jth scattering atom. Here Γ_n is a damping term that takes into account the core hole and the finite lifetime of the excited states ϕ_n and the index $i(s)$ refers to the incident (scattered) properties of the photon field. In the multiple-scattering approach, $\phi_n \equiv \phi_k$ is the scattering wavefunction of equation (98). In this case the intermediate sum $\sum_n$ becomes an integral over the kinetic energy $E = k^2$ of the excited photoelectron above the Fermi level and over the direction of $\hat{\boldsymbol{k}}$ [82]. In this case, using the generalized optical theorem (55) for the scattering amplitude $B_L^j(\boldsymbol{k})$, writing for short $R_L(E) = R_l(E; r)Y_L(\hat{\boldsymbol{r}})$ and defining

$$f_j''(E) = \frac{r_0}{m} \sum_{LL'} \langle \phi_i^{(j)} | \hat{e}_{q_s}^* \cdot \boldsymbol{p} \mathrm{e}^{-\mathrm{i}\boldsymbol{q}_s \cdot \boldsymbol{r}} | R_L(E) \rangle \langle R_{L'}(E) | \hat{e}_{q_i} \cdot \boldsymbol{p} \mathrm{e}^{\mathrm{i}\boldsymbol{q}_i \cdot \boldsymbol{r}} | \phi_i^{(j)} \rangle \left(-\frac{1}{\pi} \right) \mathrm{Im} \left[\tau_{LL'}^{jj}(E) \right] \tag{124}$$

we can write equation (123) as

$$f_j(\omega) = \int_0^\infty \mathrm{d}E \frac{f_j''(E)}{\hbar\omega - (E + I_c) - \mathrm{i}\Gamma(E)} \tag{125}$$

writing $E + I_c = E_n - E_i$, where E is the photoelectron kinetic energy and I_c is the core ionization energy referred to the Fermi level. Alternatively, one can use the real space representation (60) of the Green's function of the system [89] to calculate $f_j''(E)$.

Neglecting the electric dipole–magnetic dipole terms, which are usually negligible in the x-ray range, we can write the matrix elements of the transition operator in the coordinate form up to the electric quadrupole contribution as [90]

$$\langle \phi_f | \hat{e}_{\boldsymbol{q}} \cdot \boldsymbol{p} \mathrm{e}^{\mathrm{i}\boldsymbol{q}\cdot\boldsymbol{r}} | \phi_i \rangle \propto \langle \phi_f | \hat{e}_{\boldsymbol{q}} \cdot \boldsymbol{r} \left(1 + \frac{\mathrm{i}}{2} \boldsymbol{q} \cdot \boldsymbol{r} \right) | \phi_i \rangle. \tag{126}$$

The matrix element in equation (123) depends only on the electronic part of equation (126), in such a way that the radiation parameters, $\hat{e}_{\boldsymbol{q}_{i(s)}}$ and $\boldsymbol{q}_{i(s)}$, can be factorized. After some algebra equation (123) can be written as a scalar product of two irreducible tensors [91]

$$f_j(\omega) = \sum_{p,q} (-1)^q T_q^{(p)} F_{-q}^{(p)}(j; \omega) \tag{127}$$

where $T_q^{(p)}$ depends on the incident and scattered polarizations and wavevectors and $F_q^{(p)}$ is the tensor representing the properties of the system. It is important to note that $F_q^{(p)}(j; \omega) \equiv \langle \phi_i^{(j)} | \hat{F}_q^{(p)}(\omega) | \phi_i^{(j)} \rangle$ is such that it must belong to the totally symmetric representation of the local point group of the scattering atom (the A_{1g} representation, in Bethe's notation). In fact it is easy to check that if $\hat{R}$ is a symmetry operation for $|\phi_i^{(j)}\rangle$ (i.e., $\hat{R}|\phi_i^{(j)}\rangle = |\phi_i^{(j)}\rangle$) then

$$\langle \phi_i^{(j)} | \hat{F}^{(p)}(\omega) | \phi_i^{(j)} \rangle = \langle \phi_i^{(j)} | \hat{R}^{-1} \hat{F}^{(p)}(\omega) \hat{R} | \phi_i^{(j)} \rangle. \tag{128}$$

Thus, the only allowed matrix elements are those of the components of $\hat{F}^{(p)}(\omega)$ that are invariant for any symmetry elements of the point group.

The link with the multiple-scattering theory is provided by the fact that the scattering amplitude expressed by the ASF turns out to be proportional to mean value in the scattering functions of some multipolar operator (magnetic dipole, electric quadrupole, etc according to the kind of reflection and local symmetry), as detailed, e.g., in [82, 85, 92–94].

In the following we consider some examples where the previous ideas are applied and it is shown how a multiple scattering calculation can provide quantitative information about REXS experiments in the case of manganites (e.g., $LaMnO_3$ and $LaSr_2Mn_2O_7$) and for corundum systems like V_2O_3 or α-Fe_2O_3.

5.3.1. The case of manganites. In 1998, two experimental works [95, 96], using the REXS technique at the Mn K-edge around a forbidden reflection in $La_{0.5}Sr_{1.5}MnO_4$ and $LaMnO_3$ perovskite compounds, have reported observation of scattered intensity in the rotated polarization channel ($\sigma\pi$), which has been presented as providing direct experimental evidence of the theoretically predicted orbital ordering in these materials.

In the particular case under consideration, the excitation of the Mn 1s electron to empty 4p states (split in their y and x, z components by an energy Δ due to some interaction with the surroundings) gives rise to nonzero resonant scattered intensity proportional to Δ^2 at the forbidden reflections (300), which is sensitive to the difference between the ASF of the two orbitally ordered sublattices. The origin of the splitting Δ is not specified in the model proposed in [95, 96], but the authors clearly stated that one possible source is the Coulomb interaction between the 4p conduction band states and the ordered 3d orbitals. An alternative mechanism, they suggested, comes from the coherent Jahn–Teller distortion (JTD) of the oxygen octahedra surrounding the Mn atoms that accompanies the orbital ordering, with the long axis always along the occupied 3d e_g orbital.

It was finally demonstrated in [84] for $La_{0.5}Sr_{1.5}MnO_4$ and $LaMnO_3$ and in [85] for $LaSr_2Mn_2O_7$ that the main signal comes from the oxygen distortion, i.e., it is a consequence of the Jahn–Teller and not of the orbital ordering, which plays a minor role. Such an analysis was performed with the help of *ab initio* calculations, and the anomalous signal of the forbidden reflections was perfectly understood both qualitatively and quantitatively, simply invoking the Jahn–Teller effect, as an ordered geometrical distortion around the resonant ions.

For example, in the case of $LaSr_2Mn_2O_7$, below $T_C = 210$ K, a series of superlattice reflections corresponding to an orthorhombic distortion of the high-temperature tetragonal lattice $I4/mmm$ is found [85]. The total anomalous scattering factor depends on the difference between the local amplitudes of the two Mn ions connected by the $(0\frac{1}{2}0)$ translation in orthorhombic units. Since the two Mn^{3+} ions connected by the $(0\frac{1}{2}0)$ translation have different local symmetries, they contribute to the scattering amplitude. In order to write their contribution explicitly, we make use of the following relations, describing the symmetry operations that connect the 8e Mn^{3+} sites to one another: $F_2 = \hat{I}F_1$, $F_5 = \hat{\sigma}_{x(y)}F_1$, $F_6 = \hat{I}\hat{\sigma}_{x(y)}F_1$, $F_3 = F_1$, $F_4 = F_2$, $F_7 = F_5$, $F_8 = F_6$, where F_i indicates the ith ion, $\hat{I}$ is the inversion, and $\hat{\sigma}_{x(y)}$ the mirror operator with respect to the $x(y)$ plane. These relations can be derived from the International Tables for Crystallography, No 63 (rotated) [86]. In this way the Bragg condition can be rewritten as (f_j is the ASF)

$$\begin{aligned} A &= e^{2\pi z_0}(f_1 - f_5 + f_3 - f_7) + e^{-2\pi z_0}(f_2 - f_6 + f_4 - f_8) \\ &= 2[e^{2\pi z_0} + \hat{I}e^{-2\pi z_0}][1 - \hat{\sigma}_{x(y)}]f_1 \end{aligned} \tag{129}$$

where $z_0 = 0.096\,96$. The atomic scattering factor is scalar with respect to rotoinversion operations: it can be written as the scalar product between two tensors, one representing the properties of the system, the other the properties of the light. When we write equation (129) the inversion or mirror operators are intended to act only on one of the previous two tensors, leaving the other unaltered. Since we are dealing with nonmagnetic properties in the dipole approximation, the two tensors can only have rank zero or two. The scalar is forbidden because of the mirror symmetry of equation (129), thus recovering the extinction rule for the usual Thomson scattering. Of the five components of the rank-two tensor, only the

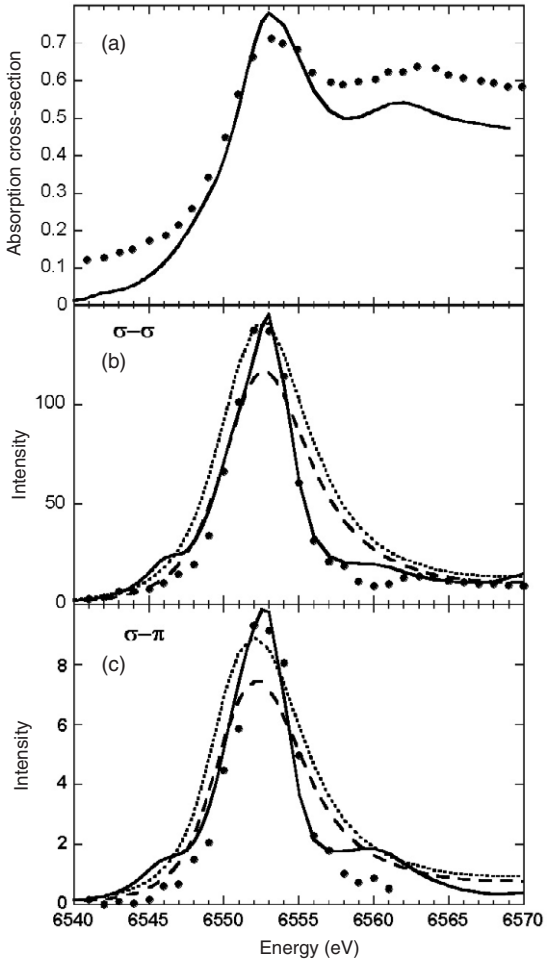

Figure 4. (a) Energy dependence (experiment and theory) of the fluorescence intensity from the $LaSr_2Mn_2O_7$ single crystal at $T = 170$ K close to the Mn K absorption edge. (b) Energy dependence (experiment and theory) of the superlattice reflection $(-1/4, 1/4, 10)$ in the $\sigma\sigma$ channel at $T = 170$ K. (c) The same as (b) in the $\sigma\pi$ channel. R is the radius of the cluster used in the calculations. ●●●, experimental points; ——, theory, with cluster radius $R = 5$ Å; — — — and · · · · · · (with finite difference method), cluster radius $R = 3$ Å, with and without orbital order, respectively [85].

symmetric combination $F_{xy} + F_{yx}$ survives, since it changes sign under the action of both mirror symmetries $\sigma_{x(y)}$. In contrast, all the other four components ($F_{xz} + F_{zx}$, $F_{yz} + F_{zy}$, $F_{x^2-y^2}$, and $F_{3z^2-r^2}$) are invariant with respect to at least one of the two mirror symmetries $\sigma_{x(y)}$ and their contribution in equation (129) vanishes. This tensor is coupled to the similar linear combination $e^i_x e^o_y + e^i_y e^o_x$. In this way it is possible to calculate the resonant signal by means of an MS calculation. The results, shown in figure 4, in excellent agreement with the experiment, demonstrate that the main peak is due to the effect on 4p states of the Jahn–Teller oxygen distortion.

5.3.2. The case of V_2O_3 and α-Fe_2O_3. Third generation radiation sources have made possible the detection of relatively small effects in crystal electronic structure due either to magnetic anisotropy or to interference between dipole and quadrupole (E1–E2) transition

matrix elements. For example, it is now well established that K-edge circular dichroism in absorption is sensitive to the angular orbital moment L_z in magnetic spectroscopies such as XMCD (x-ray magnetic circular dichroism), or to the peculiar physical quantity $L_z\Omega_z$ (Ω is the toroidal moment) in nonmagnetic spectroscopies such as XNCD (x-ray natural circular dichroism). However, if a paramagnetic system has a global inversion symmetry, even though at a local level this symmetry is broken, the resulting XNCD signal vanishes. A similar situation arises, *mutatis mutandis*, for XMCD in many antiferromagnets, where the locally broken time-reversal symmetry can be globally restored, making the total dichroic signal zero. A common way to circumvent this limitation is to use anomalous x-ray diffraction, where the local transition amplitudes are added with a phase factor that can compensate the vanishing effect due to the global symmetry. This technique has been widely used for antiferromagnets to study local magnetic effects. The same technique can be used to measure the quantity $L_z\Omega_z$ for systems with a global inversion symmetry (see [87] for further details). To show how this is possible, we analyse the measured Bragg-forbidden $(00.3)_h$ Finkelstein reflection, in systems belonging to the corundum crystal class having a global inversion symmetry, namely, V_2O_3 and α-Fe_2O_3.

If we focus our theoretical analysis on the paramagnetic corundum phase of V_2O_3 (space group $R\bar{3}c$), then we can neglect magnetic contributions. In the corundum systems the local symmetry on each scattering atom is $\hat{C}_3$. Thus equation (128) imposes the following restriction: only the irreducible tensors whose azimuthal numbers with respect to the threefold axis are 0 or ± 3 are allowed. If we choose the quantization axis coincident with the threefold axis, for $\boldsymbol{q} = (00.3)_h$, equation (122) becomes

$$A(\boldsymbol{k},\omega) = \mathrm{e}^{2\pi \mathrm{i}t} f_1 + \mathrm{e}^{-2\pi \mathrm{i}t} f_2 + \mathrm{e}^{\mathrm{i}\pi}\mathrm{e}^{2\pi \mathrm{i}t} f_3 + \mathrm{e}^{\mathrm{i}\pi}\mathrm{e}^{-2\pi \mathrm{i}t} f_4 = (\mathrm{e}^{2\pi \mathrm{i}t} + \mathrm{e}^{-2\pi \mathrm{i}t}\hat{I})(1-\hat{m}_x) f_1$$
$$= \begin{cases} 2\cos(2\pi t)(1-\hat{m}_x) f_1 & \text{(E1–E1 and E2–E2)} \\ 2\mathrm{i}\sin(2\pi t)(1-\hat{m}_x) f_1 & \text{(E1–E2)} \end{cases} \tag{130}$$

where we used the symmetry operations of the space group $R\bar{3}c$ and $t = 0.1537$. The mirror $\hat{m}_x$ is such that $(x, y, z) \to (-x, y, z)$. For the chosen reference frame its action on spherical tensors is given by [97] $\hat{m}_x F_q^{(p)} = (-1)^{P+p} F_{-q}^{(p)}$, where P is the parity of the tensor ($+1$ for E1–E1 and E2–E2 tensors and -1 for E1–E2 tensors). The combined action of glide-plane and C_3 symmetry forbids any E1–E1 contributions, as expected, and leaves us with only three possible terms: two come from the E1–E2 channel ($F_0^{(2)}$ and $F_3^{(3)} - F_{-3}^{(3)}$) and the other is of E2–E2 origin: $F_3^{(4)} - F_{-3}^{(4)}$, the one recognized in [91].

Their polarization and wavevector dependence shows that the signal is different from zero only in the $\sigma\pi$ channel and only for $T_0^{(2)}$ and $T_3^{(4)} - T_{-3}^{(4)}$. In fact, the $T_3^{(3)} - T_{-3}^{(3)}$ term is proportional to $k_x - k'_x$ or $k_y - k'_y$, where $\boldsymbol{k}$ and $\boldsymbol{k}'$ are the incident and scattered wavevectors and x and y are orthogonal to the trigonal axis. In the geometry of the $(00.3)_h$, $k_x = k'_x$ and $k_y = k'_y$ at any azimuthal angle.

It is now easy to compare the theoretical azimuthal dependence around the momentum transfer $\hbar\boldsymbol{q}$ with the experimental one [83]: the contribution of $T_0^{(2)}$ is constant with respect to the azimuthal angle ϕ around the $\boldsymbol{q}$-vector, while that of $T_3^{(4)} - T_{-3}^{(4)}$ is threefold periodical in the amplitude [91]. Note that time-reversal even quantities are real in the E2–E2 channel and imaginary in the E1–E2 channel [94]. Because of the imaginary unit in the E1–E2 term of equation (130), both amplitudes are real and interfere. Thus, the global dependence in the scattered intensity is proportional to $(\alpha + \sin(3\phi))^2$, i.e., a threefold modulation of the sixfold periodic intensity. The constant α is the ratio of the $F_0^{(2)}$ and the $F_3^{(4)} - F_{-3}^{(4)}$ matrix elements and incorporates the relative weight of the radial matrix elements together with the geometrical factors of the corresponding tensors $T_q^{(p)}$.

In order to estimate such a constant, we have performed a numerical simulation with a multiple-scattering program implemented in the FDMNES package [98]. The results support our previous theoretical considerations. The energy scan shows no features at E1–E1 energies, as experimentally detected while a structure exists around the 3d energies (5465 eV). Also, the azimuthal scan of this structure is compatible with the experimental data and makes clear its double-component origin. The possibility to evaluate separately the two contributions in the FDMNES program allows us to estimate the ratio between the constant E1–E2 signal and the maximum of E2–E2: $\alpha = 0.05$.

6. Discussion on the convergence of the MS series

As illustrated in the previous sections, both photoelectron diffraction and photoabsorption are most sensitive to structural details for low photoelectron kinetic energies, say below 100–150 eV, as measured from the Fermi level. This is due to the fact that the angular behaviour of the electron–atom scattering factor ranges from being nearly isotropic at very low photoelectron energies to being strongly forward peaked at very high energies (>1000 eV). The need to use the low energy part of these spectroscopies to extract the maximum of structural information justifies the efforts to devise new methods for analysing the spectra and to improve the theory. The elimination of the MT approximation for the potential and the extension of the theory to many channels to describe local correlations [37] go in this direction. Another strategy has been to use the full MS approach in calculating the low energy signals and a fitting procedure that fits at the same time the structural parameters and the photoelectron damping, so as to account for the inelastic processes which are insufficiently well described by the present theory. This approach has met with some success, as we have tried to show, especially for these two spectroscopies.

Moreover, the use of full MS approach avoids problems connected with the convergence of the MS series, as given by expression (70). Indeed, as discussed by Natoli and Benfatto [10], the MS series does not converge at all energies. Actually, its convergence depends on the value of the spectral radius $\rho(GT_c)$, which is defined as the largest modulus of the eigenvalues of the corresponding operator. When the kinetic energy of the electron is decreased, this spectral radius will increase and will eventually become larger than unity, therefore preventing any convergence. This usually happens around 50 eV of photoelectron kinetic energy. Note however that any process that will affect either the propagator matrix G or the transition matrix T_c of the sample will change this spectral value and hence the convergence properties of the multiple-scattering series. This is typically the case when including a damping to account for the vibrations of the atoms (which changes T_c) or a damping of the wavefunction to account for inelastic losses (which changes both T_c and G). In both cases, it will have the effect of decreasing the spectral radius, thereby extending the convergence domain of the series.

In figure 5 we present a comparison between a full multiple-scattering calculation, obtained by numerically inverting the multiple-scattering matrix, and the series expansion approach truncated at the first, second, third, fourth and fifth orders respectively, where the order is the value of the exponent n in the series (70). These calculations correspond to simulations of the P 2p core level azimuthal modulations from an InP(110) surface, where the surface component was isolated from the bulk contribution by making use of the surface core level shift. Here, the kinetic energy of the 2p electrons was set to the measured value of 34 eV and the internal polar emission angle to 36° according to experimental conditions. The structure used for the simulations corresponds to the rigid rotation type of relaxation, the P and In pairs in the first layer rotating by a relaxation angle $\omega_1 = 23°$ and those in the second layer counterrotating by $\omega_2 = -5°$, as described by Gota *et al* [102]. The calculations were performed for a cluster of 59

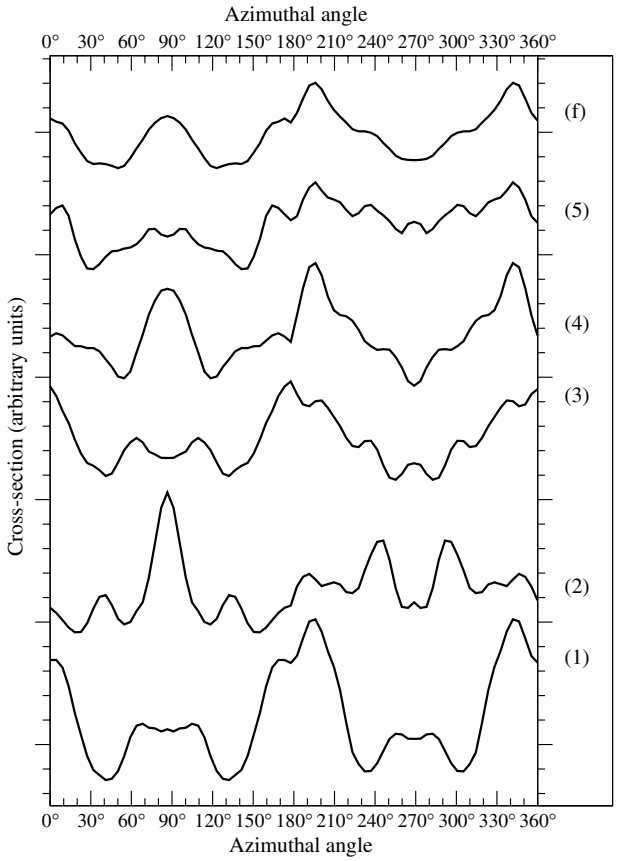

Figure 5. Comparison of the full multiple-scattering calculation with the series expansion approach up to order five for low energies. Calculations have been performed for P 2p core levels at a kinetic energy of 34 eV in the case of an InP(110) cluster. (f) The full multiple-scattering calculation while (n) for $n = 1, 5$ gives the result for the nth scattering order.

atoms lying within a sphere of 8.44 Å centred on the photoabsorber. Check calculations with 85 atoms lying within 9.53 Å of the emitter did not show any appreciable difference, demonstrating thereby that convergence of the cluster size had been achieved. Therefore, the size of the cluster used cannot account for the discrepancies observed. Comparison between the full multiple-scattering calculation and the series expansion results up to order five shows clearly here that for such a low kinetic energy the multiple-scattering series does not converge. As shown by Gota *et al* [102], the full multiple-scattering calculation does give a very good agreement with the experimental results. None of the series expansion calculations can give such an agreement, and the lack of convergence is very clear here, signalled by the rapid variations in the shape of the modulations as a function of the scattering order. Actually, we checked in this case that among the eigenvalues of the GT_c operator at least one had modulus larger than unity.

It is also worth noticing that the rate of convergence of the MS series can be different in PED and XAFS. As illustrated above, if we neglect inelastic losses, the integral of the PED signal over all directions of space should give the XAS modulations, as stated by the optical theorem that ensures the conservation of flux. This was recognized more than 30 years ago by Lee [99] in the early days of PED and EXAFS in an approximate way and shown to be valid

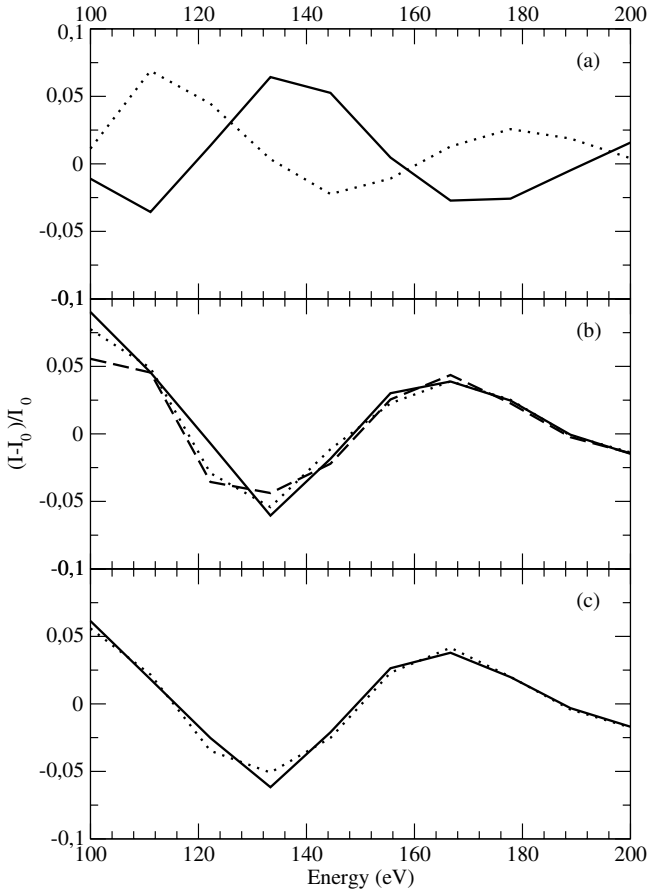

Figure 6. EXAFS versus PED summed over all directions. The calculations have been made with a nine-atom MgO cluster without any damping. (a) Single-scattering PED (——) and double-scattering PED (· · · · · ·); (b) PED truncated to order 3 (——), order 4 (· · · · · ·) and order 5 (— — —); (c) EXAFS with contributions up to order 2 (——) and order 4 (· · · · · ·).

to all orders of perturbation theory by Mustre de Leon *et al* [100]. For sake of completeness, this equivalence has been rederived at the end of section 3.1 and is illustrated numerically in figure 6. Here, the PED and EXAFS signals have been calculated using a multiple-scattering series expansion approach, such as defined by the expression (70) of the scattering path operator τ, on a nine-atom MgO cluster. No damping of any sort was included. The integration of the PED signal over the 4π steradian was performed using a Gaussian quadrature formula with 1202 weighted points, as derived by Lebedev and Laikov [101]. The series expansion was carried out up to the fourth scattering order for EXAFS and to the fifth for PED (because of the strong forward peaking of the scattering factor when the energy increases, PED does not converge as fast as EXAFS). The agreement between the EXAFS and the PED signal is clearly excellent once the MS series has converged (which corresponds to the third order of PED here). It thereby provides a numerical demonstration of the optical theorem. Small discrepancies arise at the low energies (between 100 and 140 eV). They are due to an insufficient convergence of the multiple-scattering series in this energy range (below 50 eV, the multiple-scattering series can even diverge [10], as illustrated above), and it is a consequence of the fact that the

optical theorem is only valid on fully converged signals. This is seen very clearly here as first and second order PED do no match even the second order EXAFS signal. This demonstates unambiguously that the optical theorem is valid for fully converged scattering path operators.

7. Conclusion

We have presented a unitary cluster approach for the description of many spectroscopies which have the common feature that the measured spectrum contains information collected by an electron excited within the material under study. This does not put restrictions on the type of particles used as a probe or detected by the analyser, as we have reviewed it. It should be noted that other techniques involving an electron as the probe particle and not presented here for lack of space can also be described within the same framework. This is the case for instance of Bremsstrahlung isochromat spectroscopy (BIS) or scanning tunnelling microscopy (STM) and many others.

Starting from a many-body description within the multichannel scattering theory, we have reduced the system to one described by an effective one-electron Schrödinger equation that can be handled easily with the standard multiple-scattering tools, and in particular within the scattering path operator framework. This framework is particularly convenient for numerical calculations as it disconnects the numerically demanding scattering part from the electron excitation part and, when electrons are detected, the electron escape part, thereby allowing us to compute the multiple-scattering problem independently of the angular positionning of the incoming and outgoing beams, whatever their nature.

This derivation, making use of a Hedin–Lundqvist type of optical potential, allowed us to give clear physical grounds to the phenomenological concept of mean free path and make an unambiguous link to the size of the cluster needed, which actually depends on whether the probe electron is detected or not.

This unitary approach allowed us to make a direct comparison of the various spectroscopies we have derived here. As a by-product, it shows that once we have a reliable multiple scattering code to compute the scattering path operator, or equivalently the scattered wavefield amplitudes $B_L^i(\boldsymbol{k}_0)$ given by equation (51), we can model many spectroscopies.

Acknowledgments

DS acknowledges financial support from the SRRT network and from INFN. Z-YW acknowledges the financial support of the Outstanding Youth Fund (10125523), the Key Important Project (90206032, 10490191) of the National Natural Science Foundation of China and also the Pilot Project of the Knowledge Innovation Programme of the Chinese Academy of Sciences (KJCX2-SW-N11).

Appendix A. Derivation of the MS equations

For the convenience of the reader we derive here the solution of the Dyson-like equation

$$\left[\nabla^2 + k^2 - V_c(\boldsymbol{r})\right]\phi(\boldsymbol{r}) = \int \Sigma^{\mathrm{opt}}(\boldsymbol{r}, \boldsymbol{r}'; \hbar\omega)\phi(\boldsymbol{r}')\,\mathrm{d}\boldsymbol{r}' \tag{A.1}$$

subject to the asymptotic scattering boundary conditions

$$\phi(\boldsymbol{r}) \simeq \left(\frac{k}{16\pi^3}\right)^{\frac{1}{2}}\left[\mathrm{e}^{\mathrm{i}\boldsymbol{k}\cdot\boldsymbol{r}} + f(\hat{\boldsymbol{r}}; \boldsymbol{k})\frac{\mathrm{e}^{\mathrm{i}kr}}{r}\right] \tag{A.2}$$

in the framework of multiple-scattering theory and in the non-muffin-tin case. Unless explicitly stated we shall use real spherical harmonics.

The main ingredients for this derivation are the single- and two-centre expansions of the free Green function with outgoing wave boundary conditions. They are given by

(a) around one centre located at the origin,

$$G_o^+(\boldsymbol{r}-\boldsymbol{r}';E)=-\frac{\mathrm{e}^{\mathrm{i}k|\boldsymbol{r}-\boldsymbol{r}'|}}{4\pi|\boldsymbol{r}-\boldsymbol{r}'|}=\sum_L J_L(\boldsymbol{r}_<)\tilde{H}_L^+(\boldsymbol{r}_>) \tag{A.3}$$

with $\tilde{H}_L^+(\boldsymbol{r})=-\mathrm{i}kH_L^+(\boldsymbol{r})$ and the same definitions as in section 3,

(b) around two centres located at $\boldsymbol{R}_i$ and $\boldsymbol{R}_j$, defining $\boldsymbol{r}_i=\boldsymbol{r}-\boldsymbol{R}_i$ and $\boldsymbol{R}_{ij}=\boldsymbol{R}_i-\boldsymbol{R}_j$, and provided that $R_{ij}>r_i+r_j$,

$$G_o^+(\boldsymbol{r}-\boldsymbol{r}';E)=\sum_{L,L'} J_L(\boldsymbol{r}_i)G_{LL'}^{ij}(E)J_{L'}(\boldsymbol{r}_j') \tag{A.4}$$

where

$$G_{LL'}^{ij}(E)=4\pi\sum_{L''}\mathrm{i}^{l-l'+l''}C_{LL'}^{L''}\tilde{H}_{L''}^+(\boldsymbol{R}_{ij}) \tag{A.5}$$

are the real space KKR structure factors already introduced by (47) in section 3 and

(c) when the two centres are such that $r_o>R_{io}+r_i$, where o is the origin of coordinates,

$$G_o^+(\boldsymbol{r}-\boldsymbol{r}';E)=\sum_{L,L'} J_L(\boldsymbol{r}_i)J_{LL'}^{io}(E)\tilde{H}_{L'}^+(\boldsymbol{r}_o') \tag{A.6}$$

with

$$J_{LL'}^{io}(E)=4\pi\sum_{L''}\mathrm{i}^{l-l'+l''}C_{LL'}^{L''}J_{L''}(\boldsymbol{R}_{io}). \tag{A.7}$$

We assume here that $E>0$ in order to treat scattering states; however, the above relations still hold for $E<0$, provided we take the analytic continuation of the functions of energy appearing in the above equations and in (A.2) we put to zero the incoming plane wave. In this way within the same formalism we can also treat bound states. For simplicity we consider only short range potentials (the extension to long range ones is however straightforward as will be apparent from the following). Then there exists a volume Ω_o enclosing all the atoms of our system so big that in $\complement\Omega_o$, the complement of Ω_o in the whole space, the solution of (A.1) is of the form (A.2). We partition this 'molecular' volume in N non-overlapping cells Ω_j with centres at $\boldsymbol{r}_j$ (they might even be empty, i.e. not enclosing a physical atom), filling completely Ω_o (i.e. without interstices, so that $\Omega_o=\sum_{j=1}^N\Omega_j$) in such a way that

(a) there is a finite, however small, neighbourhood around the origin of each cell lying completely in the cell (if there is an atom inside the cell, its nucleus should coincide with the origin) and

(b) the shortest inter-cell vector, joining the origins of nearest neighbours cells, is larger than any intra-cell vector.

We then start from the obvious equality involving surface integrals

$$\sum_{j=1}^N\int_{S_j}\left[G_o^+(\boldsymbol{r}-\boldsymbol{r}')\nabla\phi(\boldsymbol{r}')-\phi(\boldsymbol{r}')\nabla G_o^+(\boldsymbol{r}-\boldsymbol{r}')\right]\cdot\boldsymbol{n}_j\,\mathrm{d}\sigma_j'$$
$$-\int_{S_o}\left[G_o^+(\boldsymbol{r}-\boldsymbol{r}')\nabla\phi(\boldsymbol{r}')-\phi(\boldsymbol{r}')\nabla G_o^+(\boldsymbol{r}-\boldsymbol{r}')\right]\cdot\boldsymbol{n}_o\,\mathrm{d}\sigma_o'=0 \tag{A.8}$$

valid for all $\boldsymbol{r}$ and with obvious meaning of the symbols, provided $\phi(\boldsymbol{r})$ is continuous with its first derivatives, as required by the solution of the Schrödinger-like equation.

By taking $\boldsymbol{r}$ inside Ω_i such that $r_i \longrightarrow 0$, we use (A.3) in the surface integral over S_i, (A.4) in the integral over S_j and (A.6) in the one over S_o. We then find

$$\sum_L J_L(\boldsymbol{r}_i)\Bigg\{\int_{S_i}\left[\tilde{H}_L^+(\boldsymbol{r}_i')\nabla\phi(\boldsymbol{r}_i') - \phi(\boldsymbol{r}_i')\nabla\tilde{H}_L^+(\boldsymbol{r}_i')\right]\cdot\boldsymbol{n}_i\,\mathrm{d}\sigma_i' + \sum_{j\neq i}\sum_{L'} G_{LL'}^{ij}\int_{S_j}\left[J_{L'}(\boldsymbol{r}_j')\nabla\phi(\boldsymbol{r}_j') - \phi(\boldsymbol{r}_j')\nabla J_{L'}(\boldsymbol{r}_j')\right]\cdot\boldsymbol{n}_j\,\mathrm{d}\sigma_j' - \sum_{L'} J_{LL'}^{io}\int_{S_o}\left[\tilde{H}_{L'}^+(\boldsymbol{r}_o')\nabla\phi(\boldsymbol{r}_o') - \phi(\boldsymbol{r}_o')\nabla\tilde{H}_{L'}^+(\boldsymbol{r}_o')\right]\cdot\boldsymbol{n}_o\,\mathrm{d}\sigma_o'\Bigg\} = 0 \tag{A.9}$$

so that, due to the angular completeness of the set $J_L(\boldsymbol{r})$, the expression inside the brackets { } should be zero for each L.

Similarly, if we take $\boldsymbol{r}\in\complement\Omega_0$ with $\boldsymbol{r}'$ inside Ω_i, we obtain the equation

$$\sum_L \tilde{H}_L^+(\boldsymbol{r}_0)\Bigg\{\sum_{j=1}^N\sum_{L'} J_{LL'}^{0j}\int_{S_j}\left[J_{L'}(\boldsymbol{r}_j')\nabla\phi(\boldsymbol{r}_j') - \phi(\boldsymbol{r}_j')\nabla J_{L'}(\boldsymbol{r}_j')\right]\cdot\boldsymbol{n}_j\,\mathrm{d}\sigma_j' - \int_{S_o}\left[J_L(\boldsymbol{r}_o')\nabla\phi(\boldsymbol{r}_o') - \phi(\boldsymbol{r}_o')\nabla J_L(\boldsymbol{r}_o')\right]\cdot\boldsymbol{n}_o\,\mathrm{d}\sigma_o'\Bigg\} = 0. \tag{A.10}$$

We now introduce inside each cell Ω_j basis functions $\Phi_L^j(\boldsymbol{r}_j)$ which are solutions of the Dyson-like equation (A.1) and behave at the origin like $J_L(\boldsymbol{r}_j)$. They constitute a complete set so that the general solution $\phi(\boldsymbol{r})$ can be locally expanded as

$$\phi(\boldsymbol{r}_j) = \sum_L A_L^j(k)\Phi_L^j(\boldsymbol{r}_j).$$

Likewise, in the outer domain $\complement\Omega_o$, in order to impose the boundary conditions (A.2), we can take

$$\phi(\boldsymbol{r}_o) = \sum_L \underline{A}_L^o(k)\left[J_L(\boldsymbol{r}_o) + \sum_{L'}\tilde{H}_{L'}^+(\boldsymbol{r}_o)T_{L'L}\right] \tag{A.11}$$

where $\underline{A}_L^o(k) = \mathrm{i}^l Y_L(\hat{\boldsymbol{k}})(k/\pi)^{1/2}$, due to the well known decomposition of a plane wave. Inserting these expressions into (A.9), using the relation

$$\int_{S_0}\left[\tilde{H}_{L'}^+(\boldsymbol{r}_o)\nabla J_L(\boldsymbol{r}_o) - J_L(\boldsymbol{r}_o)\nabla\tilde{H}_{L'}^+(\boldsymbol{r}_o)\right]\cdot\boldsymbol{n}_o\,\mathrm{d}\sigma_o = \delta_{LL'}$$

and the identity

$$\sum_{L'} J_{LL'}^{io}\mathrm{i}^{l'}Y_{L'}(\hat{\boldsymbol{k}}) = \mathrm{i}^l Y_L(\hat{\boldsymbol{k}})\mathrm{e}^{\mathrm{i}\boldsymbol{k}\cdot\boldsymbol{r}_{io}} \tag{A.12}$$

which is obtained from (A.7) by observing that

$$\sum_{L'} C_{LL'}^{L''}Y_{L'}(\hat{\boldsymbol{k}}) = Y_L(\hat{\boldsymbol{k}})Y_{L''}(\hat{\boldsymbol{k}})$$

we derive directly equation (43) of section 3

$$\sum_{L'} C_{LL'}^i A_L^i(\boldsymbol{k}) = A_L^o(\boldsymbol{k}) - \sum_j\sum_{L',L''}(1-\delta_{ij})G_{LL'}^{ij}S_{L'L''}^j A_{L''}^j(\boldsymbol{k}) \tag{A.13}$$

with the definitions (46) for the surface integrals $C_{LL'}^i$ and $S_{LL'}^i$.

We can use a similar approach to solve equation (A.10). The counterpart of (A.13) is written then as

$$\sum_{L''}\left[\sum_{j}\sum_{L'} J^{0j}_{LL'} S^{j}_{L'L''} A^{j}_{L''}(\boldsymbol{k}) - T_{LL''}\underline{A}^{o}_{L''}(k)\right] = 0. \tag{A.14}$$

Making use of the definition (48) of the coefficients $B^i_L(\boldsymbol{k})$, the previous equation can be rewritten as

$$\sum_{i}\sum_{L'}\left[J^{0i}_{LL'} B^{i}_{L}(\boldsymbol{k}) - T_{LL'}\underline{A}^{o}_{L'}(k)\right] = 0. \tag{A.15}$$

From the expressions (51) of $B^i_L(\boldsymbol{k})$ and (44) of $A^i_L(\boldsymbol{k})$, we deduce, using the identity (A.12) and the definition of $\underline{A}^o_L(k)$, that

$$B^{i}_{L}(\boldsymbol{k}) = \sum_{j}\sum_{L',L''} \tau^{ij}_{LL'} J^{j0}_{LL''}\underline{A}^{o}_{L''}(k).$$

Replacing into the expression (A.15) eventually leads to

$$T_{LL'} = \sum_{i,j}\sum_{\Lambda,\Lambda'} J^{0i}_{L\Lambda}\tau^{ij}_{\Lambda\Lambda'} J^{j0}_{\Lambda' L'}. \tag{A.16}$$

In the case of long range potentials (or if the short range potential is substantially different from zero in the outer region) we have to supplement this equation with a similar one obtained from (A.8) by taking $\boldsymbol{r} \in \complement\Omega_o$, describing the effect of the scattering by the external potential. However, the solution inside the central cell is very often rather insensitive to the potential in the external region, provided the radius of the cluster is greater than the mean free path of the photoelectron at the energy considered. Clearly the above formalism can be easily extended to treat bound states.

The solution of (A.13) proceeds via the calculations of the surface integrals $C^i_{LL'}$ and $S^i_{LL'}$ and the structure factors $G^{ij}_{LL'}$. These latter are routinely calculated and in principle there should be no problem in also calculating the surface integrals $C^i_{LL'}$ and $S^i_{LL'}$. However, their practical calculation for polyhedral cells of general shape, though feasible, has turned out to be rather complicated. Recently, however, a practical method for generating basis functions for truncated potentials inside their bounding sphere has led to a considerable advance for the calculation of the cell T-matrices $T^i_{LL'} = \sum_{L''} S^i_{LL''}(C^i)^{-1}_{L''L'}$ introduced in section 3 and the implementation of a computer code for non-MT potentials [103]. In the meantime, the usual approach is to use cells of spherical shape, inscribed in the polyhedrons. The filling of space in this case leaves the problem of the interstitial region (IR), which can be minimized by increasing the number of empty spheres. However, in order to treat the irregular shape of the remaining IR one is obliged to approximate the potential by a constant (e.g. its volume average). By absorbing this constant into the definition of energy the interstitial potential becomes zero, so that the surface integrals $C^i_{LL'}$ and $S^i_{LL'}$ and (A.13) remain unchanged, by application of the Green's theorem. A further simplification, though not necessary, is achieved by replacing the potential inside each sphere by its angular average, so that one has to deal with spherically symmetric potentials. In this case the basis functions $\Phi^i_L(\boldsymbol{r}_i)$ can be written as $R^i_L(r_i)Y_L(\hat{\boldsymbol{r}}_i)$, where $R^i_L(r_i)$ is the solution of the radial Schrödinger equation inside sphere i. Consequently the surface integrals $C^i_{LL'}$ and $S^i_{LL'}$ reduce to

$$C^{i}_{LL'} = k\delta_{LL'} R_s^2 W\left[-\mathrm{i}h^{+}_{l}, R^{i}_{l}\right]\big|_{r=R_s}$$

and

$$S^{i}_{LL'} = \delta_{LL'} R_s^2 W\left[j_l, R^{i}_{l}\right]\big|_{r=R_s}$$

where we have introduced the Wronskian of two functions $f(r)$ and $g(r)$ as $W[f, g] = fg' - gf'$ calculated at the sphere radius R_s. Then the atomic scattering amplitude $T^i_{LL'} = \sum_{L''} S^i_{LL''}(C^i)^{-1}_{L''L'}$, also known as the atomic T-matrix, takes the form

$$T^i_{LL'} = \delta_{LL'} t^i_l = \delta_{LL'} k^{-1} \frac{W\left[j_l, R^i_l\right]\big|_{r=R_s}}{W\left[-\mathrm{i}h^+_l, R^i_l\right]\big|_{r=R_s}} \tag{A.17}$$

which is the expression one would find by solving the scattering problem for a spherical wave of angular momentum l impinging on a spherical potential truncated at radius $r = R_s$. From scattering theory one also has that $t^i_l = k^{-1}\exp(\mathrm{i}\delta_l)\sin\delta_l$, where δ_l is the phase shift of the radial solution $R_l(r)$. It is the shift caused by the potential to $R_l(r)$ with respect to the free solution $j_l(r)$. If the potential is real, conservation of flux requires that $k|t_l|^2 = \mathrm{Im}[t_l]$ (this is the optical theorem), so that δ_l is real; otherwise, $k|t_l|^2 < \mathrm{Im}[t_l]$, implying that δ_l is complex and the difference $\mathrm{Im}[t_l] - k|t_l|^2$ is related to the loss of flux due to the absorptive part of the potential, which becomes the source of the damping of the electronic wave (see section 3.3).

References

[1] Natoli C R, Benfatto M, Della Longa S and Hatada K 2003 *J. Synchrotron Radiat.* **10** 26
[2] Filipponi A, Di Cicco A and Natoli C R 1995 *Phys. Rev.* B **52** 15122
[3] Filipponi A and Di Cicco A 1995 *Phys. Rev.* B **52** 15135
[4] Binsted N and Hasnain S S 1996 *J. Synchrotron Radiat.* **3** 185
[5] Rehr J J and Albers R C 2000 *Rev. Mod. Phys.* **72** 621
[6] Hedin L and Lundqvist S 1969 *Solid State Physics* vol 23, ed F Seitz, D Turnbull and H Ehrenreich (New York: Academic) p 1
[7] Hedin L and Lundqvist B I 1971 *J. Phys. C: Solid State Phys.* **4** 2064
[8] Fujikawa T, Hatada K and Hedin L 2000 *Phys. Rev.* B **62** 5387 and references therein
[9] Schaich W L 1973 *Phys. Rev.* B **8** 4028
[10] Natoli C R and Benfatto M 1986 *J. Phys. C: Solid State Phys.* **8** 11
[11] Osterwalder J, Stuck A, Friedman D J, Kaduwela A, Fadley C S, Mustre de Leon J and Rehr J J 1990 *Phys. Scr.* **41** 990
[12] Van Hove M A, Weinberg W H and Chan C-M 1986 *Low Energy Electron Diffraction* (*Springer Series in Surface Science* vol 6) (Berlin: Springer)
[13] Natoli C R, Benfatto M, Brouder C, Ruiz Lopez M F and Foulis D L 1990 *Phys. Rev.* B **42** 1944
[14] Wood J H and Boring A M 1978 *Phys. Rev.* B **18** 2701
[15] Strange P 1998 *Relativistic Quantum Mechanics* (Cambridge: Cambridge University Press)
[16] Gonis A and Butler W H 2000 *Multiple Scattering in Solids* (New York: Springer) p 185
[17] Osterwalder J, Greber T, Hüfner S and Schlapbach L 1990 *Phys. Rev.* B **41** 12495
[18] Schiff L I 1968 *Quantum Mechanics* (Tokyo: McGraw-Hill/Kogakusha) p 314
[19] Cohen-Tannoudji C, Dupont-Roc J and Grynberg G 1988 *Processus D'interaction Entre Photons et Atomes* (Paris: InterEditions Editions du CNRS) p 220
[20] Schiff L I 1968 *Quantum Mechanics* (Tokyo: McGraw-Hill/Kogakusha) p 336
[21] Cohen-Tannoudji C, Dupont-Roc J and Grynberg G 1988 *Processus D'interaction Entre Photons et Atomes* (Paris: InterEditions Editions du CNRS) p 36
[22] Holstein B R 1992 *Topics in Advanced Quantum Mechanics* (Redwood City, CA: Addison-Wesley) p 157
[23] Louisell W H 1973 *Quantum Statistical Properties of Radiation* (New York: Wiley) p 296
[24] Scadron M D 1979 *Advanced Quantum Theory* (New York: Springer) p 168
[25] Newton R G 1982 *Scattering Theory of Waves and Particles* 2nd edn (Heidelberg: Springer) p 177
[26] Bethe H A and Jackiw R 1986 *Intermediate Quantum Mechanics* 3rd edn (Menlo Park: Benjamin Cummings) p 310
[27] Berakdar J 1998 *Phys. Rev.* B **58** 9808
[28] Fominykh N, Henk J, Berakdar J, Bruno P, Gollisch H and Feder R 2000 *Solid State Commun.* **113** 665
[29] Stefani G, Iacobucci S, Ruocco A and Gotter R 2002 *J. Electron Spectrosc. Relat. Phenom.* **127** 1
[30] Breit G and Bethe H A 1954 *Phys. Rev.* **93** 888
[31] Mustre de Leon J, Rehr J J, Zabinsky S I and Albers R C 1991 *Phys. Rev.* B **44** 4146
[32] Natoli C R, Benfatto M and Doniach S 1986 *Phys. Rev.* A **34** 4682

[33] Gunnella R, Bullock E L, Patthey L, Natoli C R, Abukawa T, Kono S and Johannson L S 1998 *Phys. Rev.* B **57** 14739
[34] Gunnella R, Solal F, Sébilleau D and Natoli C R 2000 *Comput. Phys. Commun.* **132** 251
[35] Dreiner S, Schürmann M and Westphal C 2004 *Phys. Rev. Lett.* **93** 126101
[36] Wu Z-Y, Benfatto M and Natoli C R 1996 *Phys. Rev.* B **54** 13409
[37] Krüger P and Natoli C R 2004 *Phys. Rev.* B **70** 245120
[38] Filipponi A 1995 *J. Phys.: Condens. Matter* **7** 9343
[39] Filipponi A 1995 *Physica* B **208/209** 29
[40] Fujikawa T 1999 *J. Phys. Soc. Japan* **68** 2444
[41] Campbell L, Hedin L, Rehr J J and Bardyszewski W 2002 *Phys. Rev.* B **65** 064107
[42] Müller J E and Wilkins J W 1982 *Phys. Rev.* B **29** 365
[43] Müller J E, Jepsen O and Wilkins J W 1984 *Solid State Commun.* **42** 4331
[44] Penn D R 1987 *Phys. Rev.* B **35** 482
[45] Lee P A and Beni G 1977 *Phys. Rev.* B **15** 2862
[46] Benfatto M, Natoli C R, Bianconi A, Garcia J, Marcelli A, Fanfoni M and Davoli I 1986 *Phys. Rev.* B **34** 5774
[47] Tyson T A, Hodgson K, Natoli C R and Benfatto M 1992 *Phys. Rev.* B **46** 5997
[48] Chen Y, Garcia de Abajo F J, Chassé A, Ynzunza R X, Kaduwela A P, Van Hove M A and Fadley C S 1998 *Phys. Rev.* B **58** 13121
[49] Benfatto M, Della Longa S and Natoli C R 2003 *J. Synchrotron Radiat.* **10** 51
[50] Landau L D and Lifshitz E M 1966 *Mécanique Quantique. Théorie non Relativiste* (Moscow: MIR) p 632
[51] Hara S 1967 *J. Phys. Soc. Japan* **22** 710
[52] Quinn J J and Ferrell R A 1958 *Phys. Rev.* **112** 812
[53] Ferrari L, Pedio M, Barrett N, Gunnella R, Capozi M, Ottaviani C and Perfetti P 2001 *Surf. Sci.* **482–485** 1287
[54] Gunnella R, Bullock E L, Natoli C R, Uhrberg R I G and Johansson L S O 1996 *Surf. Sci.* **352–354** 332
[55] Gunnella R, Yeom H M, Bullock E L, Johansson L S O, Kono S and Solal F 2002 *Surf. Sci.* **499** 244
[56] Bullock E L, Gunnella R, Patthey L, Abukawa T, Kono S, Natoli C R and Johansson L S O 1995 *Phys. Rev. Lett.* **74** 2756
[57] Gunnella R, Shimomura M, Munakata M, Takano T, Yamazaki T, Abukawa T and Kono S 2004 *Surf. Sci.* **566–568** 618
[58] Kostroun V O, Chen M H and Crasemann B 1971 *Phys. Rev.* A **3** 533
[59] Wentzel Z 1927 *Z. Phys.* **43** 521
[60] Zåhringer K, Meyer H-D and Cederbaum L S 1992 *Phys. Rev.* A **45** 318
Zåhringer K, Meyer H-D and Cederbaum L S 1992 *Phys. Rev.* A **46** 5643
[61] Lloyd P and Smith P V 1972 *Adv. Phys.* **21** 69
[62] Sawatzky G 1988 *Treatise of Materials Science and Technology* vol 30, ed C L Briant and R P Messmer (New York: Academic) pp 167–243
[63] Gotter R, Ruocco A, Butterfield M T, Iacobucci S, Stefani G and Bartynski R A 2003 *Phys. Rev.* B **67** 033303
[64] Kabachnik N M 1992 *J. Phys. B: At. Mol. Opt. Phys.* **25** L389
[65] Kabachnik N M, Lohmann B and Mehlorn W 1991 *J. Phys. B: At. Mol. Opt. Phys.* **24** 2249
[66] Cowan R 1981 *The Theory of Atomic Structure and Spectra* (Berkeley, CA: University of California Press) p 250
[67] Bolognesi P, Coreno M, De Fanis A and Avaldi A 2004 *Phys. Rev.* A **70** 022701
[68] Herrmann R, Samarin S N, Schwabe H and Kirschner J 1998 *Phys. Rev. Lett.* **81** 2148
[69] Feder R, Gollisch H, Meinert D, Scheunemann T, Artamonov O M, Samarin S N and Kirschner J 1998 *Phys. Rev.* B **58** 16418
[70] Fominykh N, Berakdar J, Henk J and Bruno P 2002 *Phys. Rev. Lett.* **89** 086402
[71] Schumann F O, Kirschner J and Berakdar J 2005 *Phys. Rev. Lett.* **95** 117601
[72] Berakdar J 1999 *Phys. Rev. Lett.* **83** 5150
[73] Samarin S N, Berakdar J, Artamonov O M and Kirschner J 2000 *Phys. Rev. Lett.* **85** 1746
[74] Gollisch H and Feder R 2004 *J. Phys.: Condens. Matter* **16** 2207
[75] Gollisch H, Yi X, Scheunemann T and Feder R 1999 *J. Phys.: Condens. Matter* **11** 9555
[76] Samarin S N, Artamonov O M, Sergeant A D, Kirschner J, Morozov A and Williams J F 2004 *Phys. Rev.* B **70** 073403
[77] Joly Y, Cabaret D, Renevier H and Natoli C R 1999 *Phys. Rev. Lett.* **82** 2398
[78] Saldin D K 1988 *Phys. Rev. Lett.* **60** 1197
[79] De Crescenzi M, Lozzi L, Picozzi P, Santucci S, Benfatto M and Natoli C R 1989 *Phys. Rev.* B **39** 8409
[80] Sébilleau D 2001 *Surf. Sci.* **482–485** 729
[81] Faulkner J S and Stocks G M 1980 *Phys. Rev.* B **21** 3222
[82] Joly Y, Di Matteo S and Natoli C R 2004 *Phys. Rev.* B **69** 224401

[83] Paolasini L, Di Matteo S, Vettier C, de Bergevin F, Sollier A, Neubeck W, Yakhou F, Metcalf P A and Honig J M 2001 *J. Electron Spectrosc. Relat. Phenom.* **120** 1
[84] Benfatto M, Joly Y and Natoli C R 1999 *Phys. Rev. Lett.* **83** 636
[85] Di Matteo S, Chatterjee T, Joly Y, Stunault A, Paixao J A, Suryanaryanan R, Dhalenne G and Revcolevschi A 2003 *Phys. Rev.* B **68** 024414
[86] Hahn T (ed) 2002 *International Tables for Crystallography* 5th edn (Dordrecht: Kluwer)
[87] Di Matteo S, Joly Y and Natoli C R 2005 *Phys. Rev.* B **72** 144406
[88] Di Matteo S, Joly Y, Bombardi A, Paolasini L, de Bergevin F and Natoli C R 2003 *Phys. Rev. Lett.* **91** 257402
[89] Ankudinov L L and Rehr J J 2000 *Phys. Rev.* B **62** 2437
[90] Blume M 1994 *Resonant Anomalous X-ray Scattering* ed G Materlik, J Sparks and K Fisher (Amsterdam: Elsevier) p 495
[91] Carra P and Thole B T 1994 *Rev. Mod. Phys.* **66** 1509
[92] Di Matteo S and Natoli C R 2002 *J. Synchrotron Radiat.* **9** 9
[93] Di Matteo S 2004 *Phys. Rev.* B **70** 165115
[94] Di Matteo S and Varma C M 2003 *Phys. Rev.* B **67** 134502
[95] Murakami Y, Kawada H, Kawata H, Tanaka M, Arima T, Moritomo Y and Tokura Y 1998 *Phys. Rev. Lett.* **80** 1932
[96] Murakami Y, Hill J P, Gibbs D, Blume M, Koyama I, Tanaka M, Kawata H, Arima T, Tokura Y, Hirota K and Endoh Y 1998 *Phys. Rev. Lett.* **81** 582
[97] Ballhausen C J 1962 *Introduction to Ligand Field Theory* (New York: McGraw-Hill)
[98] Joly Y 2001 *Phys. Rev.* B **63** 125120
[99] Lee P A 1971 *Phys. Rev.* B **13** 5261
[100] Mustre de Leon J, Rehr J J, Natoli C R, Fadley C S and Osterwalder J 1989 *Phys. Rev.* B **39** 5632
[101] Lebedev V I and Laikov D N 1999 *Dokl. Math.* **59** 477
[102] Gota S, Gunnella R, Wu Z-Y, Jézéquel G, Natoli C R, Sébilleau D, Bullock E L, Proix F, Guillot C and Quémerais A 1993 *Phys. Rev. Lett.* **71** 3387
[103] Hatada K, Hayakawa K, Benfatto M and Natoli C R 2006 to be published